UNIVERSITY OF CALIFORNIA
SANTA CRUZ

COSMOLOGICAL, TERRESTRIAL, AND ASTROPHYSICAL PROBES OF PARTICLE DARK MATTER THEORIES

A dissertation submitted in partial satisfaction of the
requirements for the degree of

DOCTOR OF PHILOSOPHY

in

PHYSICS

by

Jonathan M. Cornell

June 2015

The Dissertation of Jonathan M. Cornell
is approved:

Professor Stefano Profumo, Chair

Professor Michael Dine

Professor Joel Primack

Dean Tyrus Miller
Vice Provost and Dean of Graduate Studies

Table of Contents

List of Figures

Abstract

Cosmological, Terrestrial, and Astrophysical Probes of Particle Dark Matter Theories

by

Jonathan M. Cornell

It has been shown through multiple observations that there is approximately five times as much dark matter as normal matter in the universe. Understanding the nature of this dark matter is currently one of the major goals of particle physics. In this dissertation, I examine the relationship between the different ways that dark matter can be detected – including direct detection, indirect detection in cosmic rays, and direct production at colliders – and its cosmological properties. In particular, I focus on the relationship between the different detection avenues and two cosmological observables: the thermal relic density of dark matter and cutoff to the matter power spectrum, which corresponds to the smallest dark matter halo that can form in the early universe.

I begin with a relatively model independent study, in which the interactions between dark matter and standard model particles are described by an effective operator. Using constraints from direct detection and collider searches, I come to conclusions about what values are allowed for the matter power spectrum cutoff for each operator. I then turn my attention to particular dark matter candidates: the neutralino and gravitino of supersymmetry and the Kaluza-Klein photon of universal extra dimensions (UED). For these models, I show that there exists a tight correlation between direct detection rates, the

flux of neutrinos from dark matter annihilation in the sun, and the matter power spectrum cutoff. I also re-evaluate the relic density for Kaluza-Klein photons in light of the recent measurement of the Higgs boson mass, taking into account previously unconsidered co-annihilation channels. This result is compared against limits on UED from direct detection and collider searches to make statements about the continued viability of the minimal UED model. Finally, I consider how null observations of cosmic anti-deuterons constrain theories of decaying gravitino dark matter that are compatible with the observed relic density.

Acknowledgments

This thesis would not have been possible without the help of many people. First and foremost, I would like to thank my Ph.D. advisor, Stefano Profumo, for his support over the past four years. I have learned much from Stefano about both the science in this thesis as well how to present it. I have also benefitted from the expertise of my two other committee members, Michael Dine and Joel Primack, both by taking courses from them and through informal conversations.

I have been very lucky to have three excellent collaborators for the work described herein: William Shepherd, Angelo Monteux, and Eric Carlson. I could never have completed the research presented in this dissertation without their help. Angelo deserves particular recognition for leading the antideuteron studies, as well as for being an excellent conference buddy.

During my Ph.D. I spent a year visiting the Oskar Klein Centre for Cosmoparticle Physics at Stockholm University. My supervisor there was Joakim Edsjö, and he deserves many thanks for making my visit an extremely enjoyable and scientifically rewarding one. During my time at Stockholm, I became involved in two projects which are still in progress and so are not included in this thesis. One of these is an attempt to constrain neutralino dark matter through searches for cosmic antideuterons from its annihilation. The other is a large scale collaboration building the GAMBIT global fitting code, which has allowed me to meet and collaborate with too many talented scientists to list here. However, I would like thank the ones with whom have I worked most closely (many of whom are also collaborators on the antideuteron project). These include Joakim, Pat Scott, Christoph Weniger, Torsten

Bringmann, Chris Savage, and Antje Putze.

Early in my graduate career at UC Santa Cruz, I was involved in research on the properties of silicon particle detectors that were to be used in the ATLAS upgrade. Vitaliy Fadeyev and Patrick Maddock deserve recognition here for getting me started in the laboratory, which allowed me to ease back into physics after my three year absence from the field. I was also involved in a project with the Fermi-LAT collaboration looking for gamma ray emission from dark matter annihilation in the galactic halo. In this project I worked closely with Brandon Anderson, and I greatly appreciate his patience and the knowledge he shared with me.

Throughout my graduate career, I have been very lucky to have shared offices with a great bunch of fellow graduate students. During my first three years at UC Santa Cruz, these included Eddie Santos, T.J. Torres, Hal Cambier, Milton Bose, and Emma Storm. All of them made our rather bleak looking office an enjoyable place to work, with many interesting conversations about physics and beyond. Emma and Lauren Porter deserve particular recognition for being thoughtful and hardworking collaborators in a project to redesign a lab for the lower division physics courses. I also would like to thank Matt Wittmann and Amalie Christensen for their friendship. Amalie deserves special thanks for her hospitality and skills as a tour guide during my visits to Copenhagen.

During my visit to Stockholm, I made friends amongst the postdocs and graduate students of the Oskar Klein Centre. I would especially like to thank Brandon Anderson (again), Natasha Karkpenka, Johannes Bergström, Angnis Schmidt-May, and Tanja Petrusevska, who made great traveling companions during trips to Abisko to see the northern

lights and Gotland for Midsommar. Upon my return to Santa Cruz, I was again fortunate to have excellent officemates, including Laurel Stephenson Haskins, Adam Coogan, Laura Fava, and Eric Carlson. I greatly appreciate their support during the job search process and the finishing of this thesis. Thanks are also due to Patrick Draper and Farinaldo Queiroz, two former UC Santa Cruz postdocs who I am happy to see are continuing in promising careers in theoretical physics. I had many great conversations with the two of them on physics, the job market, and life in general.

Finally, I would like to thank all of my family for their constant well wishes and encouragement. Special thanks goes to my parents, Lois and Michael Cornell. They have both been very supportive during this process. I also appreciate my father's honesty about his own graduate school experience.

I am extremely grateful to the National Science Foundation for supporting my graduate career through the NSF Graduate Research Fellowship under Grant No. (DGE-1339067). In addition, I appreciate the support of both the Swedish Research Council (VR) and the NSF through the NSF Nordic Research Opportunity.

The text of this dissertation includes excerpts from the following previously published material in which I have collaborated with people listed above. For each article, I describe my particular contribution to the work:

1. *Jonathan M. Cornell and Stefano Profumo. "Earthly probes of the smallest dark matter halos".* JCAP *1206 (2012), 011.* DOI*: 10.1088/1475-7516/2012/06/011. arXiv: 1203.1100 [hep-ph].* For this article I wrote the code for the parameter space scans and did the analytic calculations of the kinetic decoupling temperature.

I made all of the plots and wrote the majority of the text.

2. *Jonathan M. Cornell, Stefano Profumo, and William Shepherd. "Kinetic Decoupling and Small-Scale Structure in Effective Theories of Dark Matter".* Phys.Rev. *D88.1 (2013), 015027.* DOI: *10.1103/PhysRevD.88.015027. arXiv: 1305.4676 [hep-ph].* In this work I was responsible for the calculation of the kinetic decoupling temperature, relic density, and halo cutoff mass for all of the operators. I made all of the plots and contributed heavily to the text.

3. *Jonathan M. Cornell, Stefano Profumo, and William Shepherd. "Dark matter in minimal universal extra dimensions with a stable vacuum and the 'right' Higgs boson".* Phys.Rev. *D89.5 (2014), 056005.* DOI: *10.1103/PhysRevD.89.056005. arXiv: 1401.7050 [hep-ph].* Here I was responsible for the calculation of the relic density and direct detection limits, as well as determining how future collider sensativities mapped into the mUED parameter space. I again made all of the figures and wrote a substantial portion of the text.

4. *Angelo Monteux, Eric Carlson, and Jonathan Cornell. "Gravitino Dark Matter and Flavor Symmetries".* JHEP *1408 (2014), 047.* DOI: *10.1007/JHEP08(2014)047. arXiv: 1404.5952 [hep-ph].* In this work, I contributed to the design of the study, the calculation of expected anti-deuteron production rates, the calculation of present limits on the various operators, and the prediction of sensitivities of future searches. I also wrote some of the text.

Chapter 1

Introduction: Gravitational Evidence for Dark Matter

The evidence for the existence of "dark matter" (DM), a form of matter that does not interact directly with electromagnetic radiation, is overwhelming. A multitude of observations of the universe, on scales from the size of a galaxy to the entire cosmic microwave background, point to the conclusion that approximately 85% of the matter in the universe is a particle which appears to interact solely gravitationally with visible matter[5].[1] The standard model (SM) contains two types of particles that do not interact directly with photons: neutrinos and the Higgs boson. However, the Higgs cannot be the dark matter because it decays extremely quickly, and neutrinos are not produced in the early universe in the necessary large abundances to make up all of the dark matter. Furthermore, neutrinos are produced with too much kinetic energy (making them "hot") for the observed

[1] This figure only includes matter. The dark energy is by far the largest component of the universe's energy density today

cosmic structure on smaller scales to form. Therefore, dark matter must be some new particle, and much of the work in particle physics over the past 40 years has been devoted to understanding what this particle is. This thesis contains my incremental contributions to this effort. In the next few pages I will give in more detail the evidence for dark matter. This treatment is standard and relies heavily on existing reviews, in particular [6] and [7].

One of the most compelling pieces of evidence for dark matter is the fact that the rotation curves of spiral galaxies are flat, i.e. that the matter in galaxies is moving at a constant rate, even at radii beyond the visible disk of the galaxy. From simple Newtonian dynamics, it would be expected that the velocity of the gas outside of the disk should fall off as $\sim 1/\sqrt{r}$. However, this is not what is observed – the velocity of the gas is measured to remain constant far beyond the disk. This points to the presence of a halo of dark matter that extends beyond the visible stars. This is vividly illustrated in the plot of the rotation curve of NGC 6503 in Figure 1.1.

On larger scales, observations of galaxy clusters also contain evidence of dark matter. The mass of clusters is measured in three independent ways. First, the measured velocity dispersion of the galaxies in the cluster is used to infer the mass distribution in the cluster using the virial theorem. Also, the temperature of the gas in the cluster can be determined from X-ray observations, which can then be used to estimate the mass in the cluster. Treating the gas in a typical cluster as an ideal gas in hydrostatic equilibrium, it can be shown [6] that its temperature follows the relation

$$T \approx (1.3 - 1.8)\,\mathrm{keV} \left(\frac{M_r}{10^{14} M_\odot}\right) \left(\frac{1\,\mathrm{Mpc}}{r}\right) . \tag{1.1}$$

In the above equation, M_r is the mass contained within a radius r. The correlation of

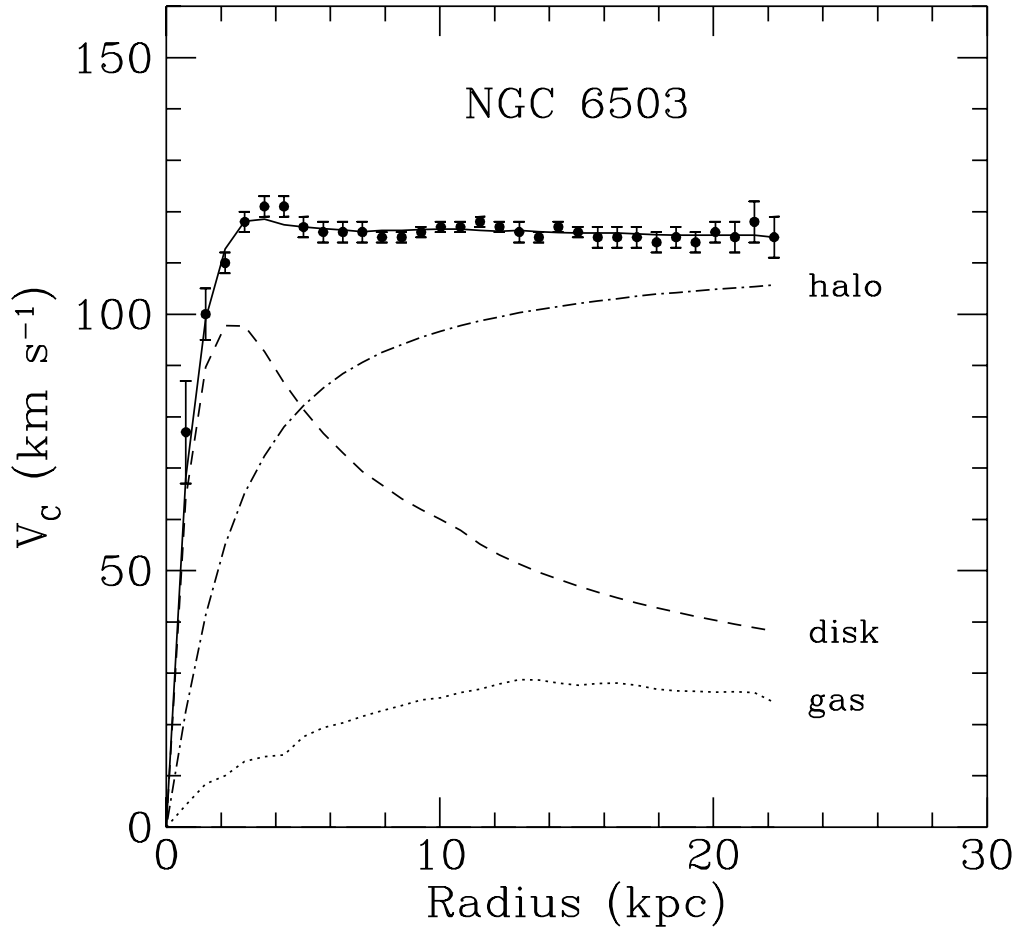

Figure 1.1: *Rotation curve for the spiral galaxy NGC 6503. The data points are the measured circular rotation velocities as a function of distance and the solid line is the best fit curve to the points. The dashed and dotted lines represent the expected rotation curve based on considerations of the mass in the observed disk and gas respectively. The dashed-dotted line is the necessary contribution from the dark matter halo in order for the rotation curve to take the observed form. Taken from [8].*

temperature with cluster mass is what allows an inference of the mass from X-ray data. Finally, gravitational lensing signatures are used to determine the mass contained in the cluster. All of these observations agree rather remarkably that the total mass of an average cluster is about five times the mass contained in the cluster gas and the stars that make up the galaxies of the cluster. (For a compendium of all of these measurements for the Coma cluster, see [9]).

On cosmological scales, dark matter is in evidence as well. The cosmic microwave background, or CMB, is made up of photons that have been traveling toward us ever since the universe became opaque to radiation, at the period of recombination. While the radiation is nearly completely isotropic and fits extremely well the spectrum expected from a black body with a temperature of 2.7 K, there are minuscule anisotropies of order 30 μK. These anisotropies are expanded in spherical harmonics, and the magnitude of each mode tells us much about the cosmology of the early universe [5].

In particular, the form of the CMB angular power spectrum is one of our most accurate probes of the dark matter density. This is because the anisotropy in the CMB is caused by two competing forces, radiation pressure and the gravitational force. These two forces work against each other, causing oscillations in the primordial baryon-photon plasma. Baryonic matter experiences both forces, whereas dark matter is only affected by gravity. Increasing the dark matter density leads to effects on specific peaks in the power spectrum, all well as to an overall decline in the height of all of the peaks [10].

All of the evidence that has been presented above for the existence of dark matter is based solely on its gravitational interactions. However, there is a major question about

dark matter that is very difficult to be explained through gravitational interactions: how is it produced? In nearly all of the compelling answers the theoretical particle physics community has come up with for this question, it is necessary for the dark matter to interact non-gravitationally.

The existence of interactions between dark matter and standard model particles beyond the gravitational often gives dark matter the ability to annihilate or decay, leading to model dependent signatures from astrophysical sources. There can also be scattering interactions between dark and standard model particles with a force much stronger than the gravitational, which leads to significant effects on cosmological structure and avenues for DM direct detection. In the following chapters, I describe the results of my investigations into how particular particle physics models for DM lead to distinct predictions for signals in astrophysical and terrestrial searches as well as effects on cosmological observables. By combining these three types of probes, we can make stronger statements about dark matter's particle nature than by considering one type of search alone.

The structure of the thesis is as follows. In chapter 2, I give background on the behavior of dark matter candidates in the early universe, as well as introduce the particle physics models for dark matter which will be explored in the subsequent chapters. In chapter 3, I consider how the particle physics model of dark matter can affect the formation of small scale structure in the early universe for the case in which the interaction between DM and SM fermions can be described by an effective four-point interaction. Constraints on these operators from direct detection experiments and collider searches are included to constrain the smallest possible dark matter halo that can form in the early universe. Moving

on to specific models for dark matter interactions, in chapter 4 I present investigations into how the size of this smallest possible halo correlates with both direct detection constraints and the flux of neutrinos expected from dark matter annihilations in the sun. I explore these correlations for two specific DM candidates: the neutralino of supersymmetry and the Kaluza-Klein (KK) photon of minimal universal extra dimensions (UED). Continuing with my study of Kaluza-Klein photons, in chapter 5 I present a study in which previously unconsidered annihilation channels are included in the calculation of the KK photon relic density. Constraints on the theory from direct detection experiments and the Large Hadron Collider (LHC) are also considered to give the most up to date limits on minimal UED. Returning to supersymmetry, in chapter 6, I explore limits on theories of gravitino DM in which the gravitino decays through R-parity violating operators. The astrophysical constraint I consider here is null searches for cosmic anti-deuterons. Finally, in chapter 7, I summarize my findings.

Chapter 2

WIMP and SuperWIMP Dark Matter

By far the most commonly studied class of candidates for dark matter are the Weakly Interacting Massive Particle (WIMPs), which are compelling because of their production mechanism and the multiple avenues they present for detection. A fair amount of attention has also been given to so called superWIMPs. In this chapter, I discuss the behavior of these two types of particles in the early universe and discuss the specific particle models for each that will be studied in more detail in this thesis.

2.1 The early universe

The first minute that the universe exists after the big bang has to be the most exciting minute in all of its history. During this period, the universe likely underwent exponential expansion, developed an asymmetry between baryons and anti-baryons, underwent

electroweak symmetry breaking, and saw the formation of hadrons. During this period, the abundance of dark matter (assuming it is a WIMP or superWIMP), was also set. For a few minutes after this point, the dark matter likely remained in thermal equilibrium with standard model particles, and the longer it remained in thermal equilibrium, the more small scale structure was suppressed.

One of the most important things to understand about a dark matter model is how much dark matter it produces. In particular, it is important that dark matter not be *overproduced*. In the next sections, I discuss the two production mechanisms for the candidates discussed in this thesis. I also discuss kinetic decoupling and its effect on small scale structure, which could be a complimentary probe of dark matter's particle properties.

2.1.1 WIMP freeze out

The standard method that is discussed in the literature for setting the relic abundance of WIMP dark matter is thermal freeze out. This method is particularly compelling because it generally requires a dark matter particle to annihilate with a velocity averaged cross section of $\langle \sigma v \rangle \approx 3 \times 10^{-26}\,\mathrm{cm}^2/\mathrm{s}$, a cross section on the order of the weak scale. Since this seems like a natural energy scale to find new physics, many in the dark matter community have taken to referring to this as the "WIMP miracle". It is this "miracle", along with the large number of detection possibilities which it leads to, which makes WIMPs by far the most common dark matter candidate studied.

To find the number density of WIMPs, one uses the integrated form of the Boltzmann equation with an appropriate collision term for WIMP annihilations [11]. This takes

the form

$$\frac{dn_\chi}{dt} + 3Hn_\chi = -\langle\sigma v\rangle \left[n_\chi^2 - \left(n_\chi^{\rm EQ}\right)^2\right] . \tag{2.1}$$

In this equation $H = \dot{a}/a$ is the Hubble expansion rate, $\langle\sigma v\rangle$ is the WIMP self-annihilation cross section, and n_χ is the *actual* number density of WIMPs, while $n_\chi^{\rm EQ}$ is the number of density of WIMPs if they are in thermal equilibrium. Solving this differential equation gives the behavior displayed by the solid lines in figure 2.1. There are two things to note in this plot. First, when temperature of the thermal photon bath is equal to the mass of the WIMP (i.e. when $x = m_\chi/T \approx 1$), the comoving number density begins to drop significantly, due to the fact that the energy of the WIMP is approximately equal to its mass at the point, leading to the number density to be suppressed by a factor of $\exp(-m_\chi/T)$. This continues until $x \sim 1/20$, after which the comoving number density becomes approximately constant. This point in time is when the Hubble rate is approximately equal to the WIMP annihilation rate (i.e. when $H \approx \langle\sigma v\rangle n_\chi$). After this, the WIMPs can no longer annihilate efficiently enough to stay in chemical equilibrium with the standard model particles, so we say that their number density has "frozen out". Note that in this picture, the WIMP is assumed to have a lifetime on the order of multiple times the age of the universe, if it is not completely stable.

$\langle\sigma v\rangle$ in Equation 2.1 is the WIMP self annihilation cross section. However it is also possible for a WIMP to annihilate with a particle other than itself, or for particles that will eventually decay to a stable WIMP to annihilate with each other. Such processes are called co-annihilations, and they are extremely important in setting the relic density for the models considered in this thesis. When such processes exist, the form of the Boltzmann

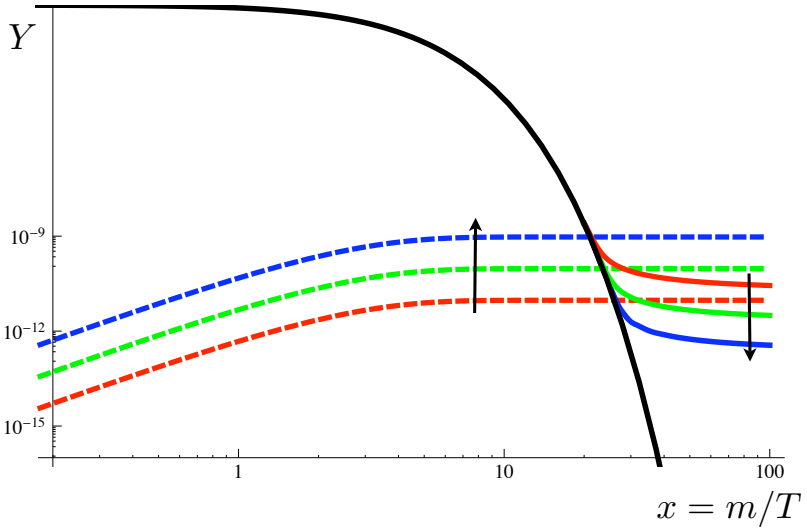

Figure 2.1: *The number density of dark matter in the early universe for the freeze out and freeze in cases.* $Y = n_\chi/S$*, where* n_χ *is the DM number density and* S *is the entropy density of the plasma. The solid black line is the equilibrium number density* n^{EQ}*. The solid colored lines show the behavior of the number density for the freeze out case while the dashed colored lines show the same for freeze in. The curves represent different couplings between the DM and thermal bath particles, with blue representing the strongest couplings and red representing the weakest. Taken from [12].*

equation that one needs to consider is [13]

$$\frac{dn}{dt} + 3Hn = -\langle \sigma_{\text{eff}} v \rangle \left[n^2 - \left(n^{\text{EQ}} \right)^2 \right] . \tag{2.2}$$

In this equation, n is the sum of the number density of all species that will decay to the WIMP and the WIMP itself. Also,

$$\sigma_{\text{eff}} = \sum_{ij}^{N} \sigma_{ij} r_i r_j \qquad \text{with} \qquad r_i \equiv \frac{n_i^{\text{EQ}}}{n^{\text{EQ}}} . \tag{2.3}$$

The indices i and j refer to the species that make up the total number density n. All of these species at WIMP freeze out are no longer relativistic and their equilibrium number density is suppressed by a factor of $\exp(-m_i/T)$. Therefore, co-annihilations are only important when there are such species with approximately the same mass as the WIMP.

2.1.2 SuperWIMP freeze in

As is evident from figure 2.1, as the WIMP interaction cross section becomes less and less, the thermal relic density becomes greater and greater. Eventually, it becomes so great to exceed the measured total amount of DM in the universe, invalidating a particular theory of dark matter. However, If we move to extremely small cross sections, an alternative method for producing DM called "freeze-in" [12] becomes viable. The particles that undergo such processes are referred to as either FIMPs (Feebly Interacting Massive Particles) or superWIMPs.

The idea here, as would be expected by the name of the process, is for the most part the opposite of freeze-out. Here the abundance of DM is expected to be negligible at high temperatures. This contrasts to freeze-out, where the DM number density is at its

largest at high temperatures due to the fact that at those temperatures the DM is in thermal equilibrium with the photon bath. In the freeze-in case, SM particles can interact to give superWIMPs, and so the number density grows as the temperature decreases (slowly, due to the extremely weak interactions) and moves toward the thermal equilibrium value. This behavior is shown by the dashed lines in figure 2.1.

The differential equations that describe the freeze-in scenario are slightly different from that presented in the last section. In particular, a different type of interaction leads to a different form of the right hand side of equation 2.1. There are two processes I consider which are relevant to freeze-in: decay of a thermal bath particle to another thermal bath particle and a superWIMP ($B_1 \to B_2 + \chi$) and annihilation of two thermal bath particles to a superWIMP and a thermal bath particle ($B_1 + B_2 \to B_3 + \chi$). For the first process, the differential equation which describes the process is:

$$\frac{dn_\chi}{dt} + 3Hn_\chi = g_{B_1} m_{B_1} \int \frac{d^3 p_{B_1}}{(2\pi)^3 E_{B_1}} f_{B_1} \Gamma_{B_1} \,. \tag{2.4}$$

In this equation, g_{B_1} is the number of degrees of freedom for the thermal bath particle, f_{B_1} is its kinetic energy distribution function, and Γ_{B_1} is its decay rate. For the case in which two the thermal bath particles annihilate the relevant equation is:

$$\frac{dn_\chi}{dt} + 3Hn_\chi = \langle \sigma v \rangle n_{B_1} n_{B_2} \,. \tag{2.5}$$

Here $\langle \sigma v \rangle$ is the velocity averaged cross section for this process. Notice that in equations 2.4 and 2.5 the right hand side of the equation is always positive, corresponding to a steadily increasing number density. This contrasts with equation 2.1, in which the sign of the right hand side of the equation is such that it adjusts the number density back towards the equilibrium value.

2.1.3 Kinetic decoupling and small scale structure[1]

What is described in the previous two sections pertains to the so-called *chemical* decoupling of WIMPs and superWIMPs: for WIMPs, the number density n_χ ceases to follow the equilibrium distribution once the pair-annihilation and pair-creation rates go out of equilibrium (i.e. annihilations occur less frequently than once per Hubble time), whereas for superWIMPs the production rate is no longer sufficient for the number density to continue to grow. After chemical decoupling, these particles do not entirely forget about the surrounding thermal environment: elastic scattering processes where dark matter scatters off of, for example, a light lepton l ($\chi l \leftrightarrow \chi l$) keep it in *kinetic* equilibrium. Dark matter particles continue to trace the thermal background kinetically, and structures cannot start to form via gravitational collapse. When the rate for elastic scattering processes also falls out of equilibrium, structures eventually start forming, and a small-scale cutoff is imprinted in the power-spectrum of density fluctuations in the universe. This cutoff scale also defines the size of the smallest possible dark matter halos ("protohalos"), some of which might survive and populate the late universe, with potentially important implications [14].

Kinetic decoupling of WIMPs was first discussed in Ref. [15] for heavy neutrinos as dark matter candidates, and for supersymmetric neutralinos, first in Ref. [16] some time later. It was subsequently argued in Ref. [17] that the typical kinetic freeze-out temperature could be as low as a keV, a value that would yield a cutoff scale on the same order of the

[1] Contains excerpts from Jonathan M. Cornell and Stefano Profumo. "Earthly probes of the smallest dark matter halos". *JCAP* 1206 (2012), 011. DOI: 10.1088/1475-7516/2012/06/011. arXiv: 1203.1100 [hep-ph] and Jonathan M. Cornell, Stefano Profumo, and William Shepherd. "Kinetic Decoupling and Small-Scale Structure in Effective Theories of Dark Matter". *Phys.Rev.* D88.1 (2013), 015027. DOI: 10.1103/PhysRevD.88.015027. arXiv: 1305.4676 [hep-ph]

mass of dwarf galaxies – the smallest observed dark matter halos. This would have been a profound result, potentially impacting our understanding of the mismatch between the predicted and observed number of small-scale dark matter halos in cold dark matter cosmology [18]. Unfortunately, Ref. [19] pointed out important kinematic effects that were neglected in [17], leading the latter analysis to vastly overestimate the cross sections relevant for kinetic decoupling. The kinetic decoupling temperature calculated in [19] pointed, instead, to the MeV to GeV range, with a resulting cutoff scale significantly smaller than dwarf galaxies halos, and on the order of the Sun's mass or small fractions of it.

A number of more recent studies addressed the question of calculating the kinetic decoupling temperature with increasingly finer detail, see e.g. Ref. [20], including WIMP models beyond supersymmetric neutralinos [21] as well as addressing the question of how to connect the kinetic decoupling temperature to the scale at which the matter power spectrum is effectively cut off [25, 22, 23, 24]. These studies were paralleled by a series of N-body simulations that targeted the nature and fate of the smallest dark matter halos, starting with Ref. [26] and continuing in [27, 28, 29]. Further analyses studied the question of whether the smallest-scale halos would survive tidal stripping and stellar encounters, and whether they would then be potentially hovering around in today's galaxies [29], with potentially important implications for indirect [30] as well as for direct [31] dark matter detection. Other work also targeted the direct detection of these primordial halos (alternately named protohalos, mini-halos or micro-halos: the latter two names allude to the size of the halos, which strongly depends on the particle physics model, see e.g. [21]) via gravitational lensing (e.g. [32, 33]).

Kinetic decoupling and the cutoff scale have also been the subject of much recent interest due to the fact that, if large enough, the scale could affect significantly how many "visible" small-scale structures, such as dwarf galaxies, form, perhaps being relevant to the question of the "missing satellite problem" [18] or to other issues associated with small scales in cold dark matter cosmologies [34]. It is also highly relevant to the question of the so-called "boost factor", as it literally sets the integration cutoff in the calculation of this factor (in practice, the enhancement to the annihilation rate from a given dark matter halo from sub-structure within the halo).

Temperature of kinetic decoupling

Kinetic decoupling approximately occurs when

$$H(T_{\rm kd}) = \tau^{-1}(T_{\rm kd}) = \sum_f n_f(T_{\rm kd})\sigma_{f\chi}(T_{\rm kd})(T_{\rm kd}/m_\chi)\,. \tag{2.6}$$

In the above equation, $T_{\rm kd}$ is the kinetic decoupling temperature, τ^{-1} is the DM thermal relaxation rate, and $\sigma_{f\chi}$ is dark matter-SM fermion scattering cross section. The factor T/m_χ counts the number of scatters needed to keep the dark matter in kinetic equilibrium. The main reason why this kinetic decoupling occurs after chemical decoupling for WIMPs can be easily understood by the number density that occurs in the above equation – it is that of SM particles, which are relativistic and therefore extremely abundant, whereas in the similar expression for WIMP chemical decoupling, the number density is that of the Boltzmann suppressed dark matter.

While the above approximation is widely used in the literature, the most thorough and comprehensive method to calculate the temperature of kinetic decoupling $T_{\rm kd}$ is a

numerical one described in Ref. [14]. This treatment begins with the Boltzmann equation in a flat Friedmann-Robertson-Walker spacetime:

$$E(\partial_t - H\mathbf{p}\cdot\nabla_{\mathbf{p}})f = C[f]. \tag{2.7}$$

Here f is the WIMP phase-space density, E and $\mathbf{p}$ are the WIMP energy and comoving momenta respectively, and H is the Hubble parameter. $C[f]$ is the collision term, and to find $T_{\rm kd}$ the necessary $C[f]$ is that of the scattering of a massive WIMP off of a standard model (SM) particle that is in thermal equilibrium with the plasma in the early universe. In [14], to lowest order in $\mathbf{p^2}/E^2$ and the SM particle momentum, this collision term is shown to be of the form

$$C[f] = c(T)M_\chi^2\left[M_\chi T\nabla_{\mathbf{p}}^2 + \mathbf{p}\cdot\nabla_{\mathbf{p}} + 3\right]f(\mathbf{p}). \tag{2.8}$$

where

$$c(T) = \sum_i \frac{g_{\rm SM}}{6(2\pi)^3 m_\chi^4 T}\int dk\, k^5\omega^{-1}\, g^{\pm}\left(1\mp g^{\pm}\right)\, \overline{|\mathcal{M}|}^2_{\substack{t=0\\ s=m_\chi^2+2m_\chi\omega+m_\ell^2}}. \tag{2.9}$$

In Equation (2.9), the sum is taken over all possible Standard Model scattering partners, $g_{\rm SM}$ is the number of associated spin degrees of freedom, ω is the energy of the Standard Model particle and k its momentum, and $g^{\pm}$ is the distribution for Fermi or Bose statistics, $g^{\pm}(\omega) = (e^{\omega/T}\pm 1)^{-1}$. In all expressions above, the upper sign is for fermions and the lower is for bosons. $\overline{|\mathcal{M}|}^2$ represents the scattering amplitude squared, summed over final and averaged over initial spin states.

We can define a temperature parameter

$$T_\chi \equiv \frac{2}{3}\left\langle\frac{\mathbf{p}^2}{2M_\chi}\right\rangle = \frac{1}{3M_\chi n_\chi}\int\frac{\mathrm{d}^3p}{(2\pi)^3}\mathbf{p}^2 f(\mathbf{p}). \tag{2.10}$$

Before kinetic decoupling, WIMPs are in thermal equilibrium with the heat bath, and

therefore $T_\chi = T$. After kinetic decoupling, the rate of WIMP scattering off SM particles drops below the level which is needed to keep them in thermal equilibrium, and so the WIMPs cool down due to Hubble expansion, with $T_\chi \propto T^2/M_\chi \propto a^{-2}$. The transition between these two asymptotic behaviors is rapid and corresponds to the temperature of kinetic decoupling, $T_{\rm kd}$. To find when this change occurs, Eq. 2.7 is multiplied by $\mathbf{p}^2/E$ and integrated over $\mathbf{p}$. Using integration by parts, this can be shown to give an equation describing the evolution of T_χ with the temperature of the universe:

$$(\partial_t + 5H)T_\chi = 2M_\chi c(T)(T - T_\chi). \tag{2.11}$$

The author of [14] has developed a routine which interfaces with the DarkSUSY code [35] and numerically solves this equation. By equating the limiting behavior of T_χ in the two regimes described above, when $T_\chi = T$ and when $T_\chi \propto T^2/M_\chi$, $T_{\rm kd}$ is found. It is important to note that kinetic decoupling can take place either before or after the QCD phase transition at $T_c \approx 170$ MeV, so one needs to consider carefully the effects of quark confinement on the sum in Eq. (2.9). At temperatures above $4\,T_c$, we follow the convention of Ref. [14], where the WIMPs scatter off leptons and, to be conservative, the three lightest quarks. After $4\,T_c$, we no longer consider scattering off quarks. However, for our calculations in chapter 3, we extend the treatment of Ref. [14] by including scattering of the dark matter off pions after the QCD phase transitions for the cases in which this process occurs at leading order, i.e. for the scalar, Eq. (3.1), and vector, Eq. (3.3), operator cases.

It is also important to note that in Eq. (2.9), the scattering amplitude is evaluated in the $t = 0$ limit, where t is the squared difference between the incoming and outgoing

4-momenta of a scattering particle. This limit is reasonable because the average momentum transfer in a scattering event between a relativistic particle and a heavy WIMP should be quite small. However, for the pseudoscalar operator considered in chapter 3, Eq. (3.2), the scattering amplitude vanishes for forward scattering, so we need to consider the scattering amplitude when the momentum transfer is not zero. Ref. [36] introduced a method to average over all possible values of t, in which $c(T)$ now takes the form:

$$c(T) = \sum_i \frac{g_{\rm SM}}{6(2\pi)^3 m_\chi^4 T} \int dk\, k^5 \omega^{-1}\, g^{\pm} \left(1 \mp g^{\pm}\right) \frac{1}{\left(4k^2\right)^2} \int_{-4k^2}^{0} dt(-t)\, \overline{|\mathcal{M}|}^2_{s=m_\chi^2+2m_\chi\omega+m_\ell^2}\,. \tag{2.12}$$

It was also shown in Ref. [24] that an analytic solution for $T_{\rm kd}$ can be found. For this to be possible, certain simplifying assumptions need to be made; namely, SM scattering partners are relativistic, variations in the universe equation of state are ignored (i.e. $g_{\rm eff}$, the number of relativistic degrees of freedom, is assumed to be constant), and the scattering amplitude is of the form $|\mathcal{M}|^2 \propto (\omega/M_\chi)^n$ where ω is the energy of the SM scattering partner. With these assumptions, the solution to Eq. 2.11 is

$$T_\chi = T \left\{ 1 - \frac{z^{1/(n+2)}}{n+2} \exp[z]\ \Gamma[-(n+2)^{-1}, z] \right\}_{z=(a/n+2)(T/M_\chi)^{n+2}}, \tag{2.13}$$

where n is the power of the leading term in $|\mathcal{M}|^2$ and a is a term that contains the leading coefficient of the scattering amplitude and $g_{\rm eff}$. In the limit $T \to 0$, this equation becomes

$$T_\chi = \left(\frac{a}{n+2}\right)^{1/(n+2)} \Gamma\left[\frac{n+1}{n+2}\right] \frac{T^2}{M_\chi}. \tag{2.14}$$

$T_{\rm kd}$ occurs when the above limiting behavior matches the high temperature behavior $T_\chi = T$. Therefore

$$T_{\rm kd} = M_\chi \left(\left(\frac{a}{n+2}\right)^{1/(n+2)} \Gamma\left[\frac{n+1}{n+2}\right] \right)^{-1}. \tag{2.15}$$

In our work we will use both the numerical code[2] and the analytic approximation of Eq. 2.15 to find $T_{\rm kd}$.

Protohalo size

In the period before kinetic decoupling, WIMPs behave as a fluid coupled to the cosmic heat bath via scattering interactions with standard model particles. This coupling leads to bulk and shear viscosity in the WIMP fluid which damps out the primordial structure in the fluid [37]. The amount of this damping has been shown to be given by a damping term of the form [20, 22]

$$D_{\rm d}(k) \equiv \frac{\Delta_{\rm wimp}(k,\eta_{\rm kd})}{\Delta_{\rm wimp}(k,\eta_{\rm i})} = \exp\left[-\left(\frac{k}{k_{\rm d}}\right)^2\right]. \tag{2.16}$$

In the equation above, η is the conformal time and $\Delta_{\rm wimp}$ a function which quantifies the amount of fluctuation in the WIMP density over an isotropic state, so $\Delta_{\rm wimp}(k,\eta_{\rm i})$ is the initial primordial value of the density perturbation function. The characteristic damping scale $k_{\rm d}$ is given by:

$$k_{\rm d} \approx 1.8\left(\frac{m_\chi}{T_{\rm kd}}\right)^{1/2}\frac{a_{\rm kd}}{a_0}H_{\rm kd} \approx \frac{3.76\times10^7}{1{\rm Mpc}}\left(\frac{m_\chi}{100\ {\rm GeV}}\right)\left(\frac{T_{\rm kd}}{30\ {\rm MeV}}\right)^{1/2}. \tag{2.17}$$

After kinetic decoupling, there are no longer interactions between the WIMPs and the cosmic heat bath, so damping no longer occurs due to viscosity in the fluid. However, in this epoch free streaming effects are found to significantly damp out density perturbations. In this process, the dark matter particles propagate from regions of high density to low density, smoothing out inhomogeneities. By considering the collisionless Boltzmann equation and using the results of the viscosity calculation as initial conditions, a characteristic scale

[2]We thank T. Bringmann for providing us with his routines.

for this damping process can be found, and this comoving scale approaches a constant value after matter-radiation equality [22]:

$$k_{\rm fs} \approx \left(\frac{m}{T_{\rm kd}}\right)^{1/2} \frac{a_{\rm eq}/a_{\rm kd}}{\ln(4a_{\rm eq}/a_{\rm kd})} \frac{a_{\rm eq}}{a_0} H_{\rm eq}, \tag{2.18}$$

where $a_{\rm eq}$ is the scale factor at matter radiation equality. The damping term for this free streaming $D_{\rm fs}$ is of a similar form as $D_{\rm d}$, and to find the total damping term, the two are multiplied together, i.e. $D(k) = D_{\rm d}(k) D_{\rm fs}(k)$:

$$D(k) \equiv \frac{\Delta_{\rm wimp}(k,\eta)}{\Delta_{\rm wimp}(k,\eta_{\rm i})} = \left[1 - \frac{2}{3}\left(\frac{k}{k_{\rm fs}}\right)^2\right] \exp\left[-\left(\frac{k}{k_{\rm fs}}\right)^2 - \left(\frac{k}{k_{\rm d}}\right)^2\right]. \tag{2.19}$$

Comparing $k_{\rm fs}$ and $k_{\rm d}$, one finds that $k_{\rm fs} \ll k_{\rm d}$; it is therefore $k_{\rm fs}$ that determines where the exponential cutoff in the mass spectrum is. Therefore, to find the mass of the smallest protohalo allowed by these processes, one just calculates the mass of WIMPs contained in a sphere of radius $\pi/k_{\rm fs}$, i.e. [14]:

$$M_{\rm fs} \approx \frac{4\pi}{3}\rho_\chi \left(\frac{\pi}{k_{\rm fs}}\right)^3 = 2.9\times10^{-6} M_\odot \left(\frac{1 + \ln\left(g_{\rm eff}^{1/4} T_{\rm kd}/30\ {\rm MeV}\right)/18.56}{(m_\chi/100\ {\rm GeV})^{1/2}\, g_{\rm eff}^{1/4}\, (T_{\rm kd}/50\ {\rm MeV})^{1/2}}\right)^3. \tag{2.20}$$

In later papers [25, 23], it was shown how an additional damping scale is set by acoustic oscillations in the cosmic heat bath itself. The calculation of this damping scale is independent of the other two, $k_{\rm d}$ and $k_{\rm fs}$, that we previously presented in equations 2.17 and 2.18 respectively. These oscillations, which are remnants of the inflationary epoch, couple to modes of oscillation in the WIMP fluid with k values large enough that they enter the horizon before kinetic decoupling. These modes in the WIMP fluid then oscillate with the acoustic modes in the heat bath and are damped out, while modes with k values corresponding to a distance larger than the horizon size at kinetic decoupling do not experience such a damping and grow logarithmically. The damping scale for this process is just the size of the horizon

at kinetic decoupling ($k_{\rm ao} \approx \pi H_{\rm kd}$), and therefore the cutoff mass for this process is the mass of WIMPs enclosed by the horizon at the kinetic decoupling time [14]:

$$M_{\rm ao} \approx \frac{4\pi}{3} \frac{\rho_\chi}{H^3}\bigg|_{T=T_{\rm kd}} = 3.4 \times 10^{-6} M_\odot \left(\frac{T_{\rm kd} g_{\rm eff}^{1/4}}{50 \text{ MeV}} \right)^{-3}. \tag{2.21}$$

Depending on the parameters of the WIMP model, either $M_{\rm ao}$ or $M_{\rm fs}$ can be larger, so to find a cutoff mass both are calculated and the larger one is used, i.e. $M_{\rm cut} = \max[M_{\rm fs}, M_{\rm ao}]$.

Probes of the mass cutoff scale

A comprehensive review on the detection of sub-solar-mass dark matter halos is given in Ref. [38]. Some of these detection methods might provide a more or less direct way to infer the value $M_{\rm cut}$, even if most of the studies mentioned here do not claim to probe cutoff masses as small as $M_{\rm cut}$. Dense, nearby protohalos could host enough dark matter pair-annihilation to be visible as gamma-ray sources, as envisioned in a number of studies, e.g. [39, 40, 41, 42, 43, 44, 45]. Small-scale subhalos could also contribute to the local cosmic-ray electron-positron population, potentially producing a sizable amount to be relevant for the reported anomalies in the abundances of these cosmic rays at 10-100 GeV energies [46, 47]. The possibility that gamma-ray data would be able to determine the proper motion of protohalos (not necessarily only the smallest protohalos, however) was first entertained in Ref. [48], but it was shown in [49] that the diffuse gamma ray background makes this idea unfeasible in practice. Rather than aiming to resolve individual substructures, Ref. [50] considered the anisotropy in the diffuse gamma ray emission, arguing that it could be possible to use a statistical analysis to measure the substructure mass function. Recently, direct observational constraints from the Fermi LAT Collaboration were

reported in Ref. [51] in the form of a search, leading to a null result, for unassociated gamma-ray sources with spectra that could be conducive to particle dark matter annihilation.

If the Earth were to pass through a dark matter clump, this would lead to an enhanced *direct* detection rate (which scales directly with the local dark matter density), although in [52] it was shown that the presence of substructure in the Milky Way halo is expected, on average, to *reduce* the direct detection rate relative to the rate with a smooth halo and no substructure. A long duration direct detection experiment might in principle detect variations in the rate due to intervening substrcture, as envisioned in [38].

It has been noted in [33] that substructure should affect pulsar timing measurements, with $M_{\rm cut}$ having an effect on the amount of the frequency shift. It has also been discussed in Ref. [32] that when there is a time-variable compact source that that is multiply imaged by strong gravitational lensing, small perturbations in the gravitational potential, such as those caused by protohalos, can lead to variations in the images which could be used to make statements about the size of the protohalos. Nanolensing from sub-solar-size dark matter halos was discussed in Ref. [53], together with the possibility of detecting events with much shorter durations and smaller amplitudes than the microlensing events due to stars with future surveys. Note that none of these studies would directly provide a probe of the size of the small-scale cutoff in the matter power spectrum.

2.2 Particle candidates

The number of particle physics models that have been proposed for dark matter can seem infinite. In this thesis, however, I focus on some of the most commonly studied ones,

the neutralino and gravitino of supersymmetry, and the Kaluza-Klein photon of minimal universal extra dimensions.

2.2.1 Supersymmetry

One of the most studied extensions of the standard model of particle physics is supersymmetry (SUSY). As such, there are many useful reviews on the subject, and in the following discussion, I follow [54], [7], and the conventions of [35]. One of the most well known and compelling reasons for the widespread interest in this theory is the infamous "hierarchy problem", which is a result of the fact that there is a large gap between the weak scale at approximately 10^2 GeV and the Planck scale at 10^{18} GeV. This is a "problem" when one considers the quantum corrections to the mass of the Higgs boson. The corrections to the the square of the Higgs mass due to fermion loops, such in the left diagram of figure 2.2, are proportional to the cutoff scale of the theory squared, and when the cutoff scale of the theory is at the Planck scale, these corrections can be enormous. However, these can be cancelled by mass corrections caused by scalar loops such as the one shown in the right side of figure 2.2, which also scale like the cutoff scale squared, but with an opposite sign. This happens naturally in supersymmetry, where every SM boson has a corresponding superpartner fermion and vice versa, leading to pairs of diagrams like the ones shown in figure 2.2 for every particle that can run in the loops.

The most minimal version of supersymmetry (which does not contain gravity) is called the minimal supersymmetric standard model (MSSM). In this model, the field content is that of the standard model plus superpartners of all of these fields, including so called gauginos and higgsinos of spin 1/2 and sleptons and squarks of spin 0. Also included

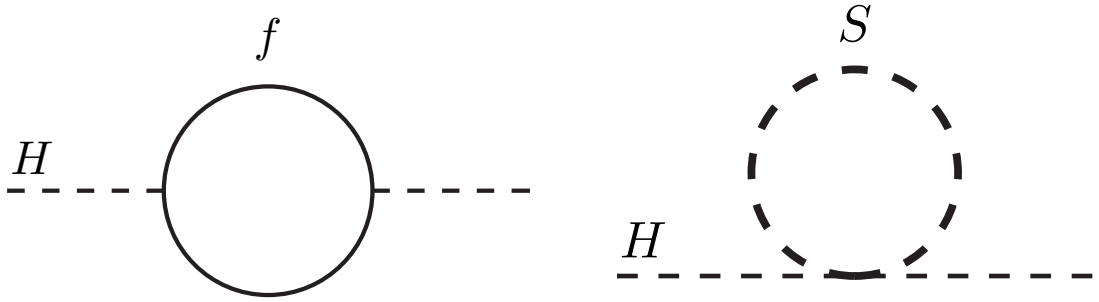

Figure 2.2: *One loop corrections to the Higgs mass due to a fermion (left) and a scalar particle (right).*

is a second Higgs doublet beyond that of the standard model with weak hypercharge $Y = -1/2$ and its corresponding superpartners. One reason for this extra doublet is to ensure the cancellation of gauge anomalies. For the anomaly diagrams to cancel, the condition $\mathrm{Tr}[T_3^2 Y] = \mathrm{Tr}[Y^3] = 0$ must be satisfied, where T_3 is the third component of weak isospin and the trace is taken over all fermions in the the anomaly loop diagram. In the MSSM, higgsinos can also run in these loops, so equal numbers of higgsinos with weak hypercharge $+1/2$ and $-1/2$ are needed for the continued anomaly cancellation, leading to the need for a second doublet.

If supersymmetry exists in an unbroken form, we would almost have certainly have observed it by now, as would lead to new particles with the same mass as those of the standard model. Therefore supersymmetry must be a broken symmetry, and it is the particular way that it is broken which leads to a plethora of phenomenological consequences. In this thesis, I do not consider particular schemes for the breaking of supersymmetry. Rather, I just make the assumption that supersymmetry is softly broken, i.e. that the supersymmetry breaking couplings all have positive mass dimension. This enforces the

requisite relationship between the couplings to scalar and fermion superpartners to prevent quadratic divergences from appearing when SUSY is broken.

If the MSSM is softly broken, the potential gains the following extra terms:

$$\begin{aligned} V_{\text{soft}} &= \epsilon_{ij}\left(-\tilde{\mathbf{e}}_R^*\mathbf{A}_E\mathbf{Y}_E\tilde{\mathbf{l}}_L^i H_d^j - \tilde{\mathbf{d}}_R^*\mathbf{A}_D\mathbf{Y}_D\tilde{\mathbf{q}}_L^i H_d^j + \tilde{\mathbf{u}}_R^*\mathbf{A}_U\mathbf{Y}_U\tilde{\mathbf{q}}_L^i H_u^j - B\mu H_u^i H_d^j + \text{h.c.}\right) \\ &\quad + H_u^{i*}m_{H_u}^2 H_u^i + H_d^{i*}m_{H_d}^2 H_d^i \\ &\quad + \tilde{\mathbf{q}}_L^{i*}\mathbf{M}_Q^2\tilde{\mathbf{q}}_L^i + \tilde{\mathbf{l}}_L^{i*}\mathbf{M}_L^2\tilde{\mathbf{l}}_L^i + \tilde{\mathbf{u}}_R^*\mathbf{M}_U^2\tilde{\mathbf{u}}_R + \tilde{\mathbf{d}}_R^*\mathbf{M}_D^2\tilde{\mathbf{d}}_R + \tilde{\mathbf{e}}_R^*\mathbf{M}_E^2\tilde{\mathbf{e}}_R \\ &\quad + \frac{1}{2}M_1\tilde{B}\tilde{B} + \frac{1}{2}M_2\left(\tilde{W}^3\tilde{W}^3 + 2\tilde{W}^+\tilde{W}^-\right) + \frac{1}{2}M_3\tilde{g}\tilde{g}. \end{aligned} \tag{2.22}$$

In 2.22 i and j are $SU(2)$ indices. A tilde represents a superpartner, and the R and L subscripts represent the chirality of the scalar field's fermionic superpartner. The Yukawa couplings $\mathbf{Y}$, the soft trilinear couplings $\mathbf{A}$, and the soft sfermion masses $\mathbf{M}$ are 3×3 matrices in generation space. The total number of new parameters that these new terms introduce to the theory is 105, a parameter space that is much too large to make any conclusive statement about. To reduce the number of parameters, it is often assumed that the squark and slepton mass matrices are diagonal to avoid flavor changing neutral currents. Furthermore, since the heaviest quarks have the largest Yukawa couplings, it is assumed that $\mathbf{A}_U = \text{diag}(0, 0, A_t)$, $\mathbf{A}_D = \text{diag}(0, 0, A_b)$ and $\mathbf{A}_E = 0$. These are the assumptions we will make when we consider this model in chapter 4.

Supersymmetry introduces terms into the Lagrangian that are invariant under the SM gauge group but do not conserve either baryon or lepton number. Combinations of these terms allow the proton to decay at an unacceptably high rate and so must be forbidden. To do so, R-parity is introduced. Every particle has a P_R value defined by the expression

$$P_R = (-1)^{3(B-L)+2s}. \tag{2.23}$$

B and L are baryon and lepton number respectively, and s is the spin of the particle. All of the standard model particles have even R-parity ($P_R = +1$) while all of the supersymmetric particle have odd R-parity ($P_R = -1$). Imposing the requirement that R-parity is exactly conserved leads to proton stability. It also has a very useful second consequence: it makes the lightest supersymmetric particle (LSP) stable, often making it an ideal dark matter candidate if it is also electrically neutral and colorless. In the next two subsections I will describe two such LSPs which could be the dark matter.

Neutralinos

In many regions of the parameter space of the MSSM, the LSP is a mixture of binos, winos, and higgsinos called the neutralino. To determine the mass of the neutralino eigenstates, one finds the eigenvalues of the neutralino mass matrix, which at tree level and with the choice of gauge-eigenstate basis $\tilde{\chi}^0 = (\tilde{B}, \tilde{W}^0, \tilde{H}_d^0, \tilde{H}_u^0)$ takes the following form:

$$\mathcal{M}_{\tilde{\chi}^0_{1,2,3,4}} = \begin{pmatrix} M_1 & 0 & -\frac{g' v_d}{\sqrt{2}} & +\frac{g' v_u}{\sqrt{2}} \\ 0 & M_2 & +\frac{g v_d}{\sqrt{2}} & -\frac{g v_u}{\sqrt{2}} \\ -\frac{g' v_d}{\sqrt{2}} & +\frac{g v_d}{\sqrt{2}} & 0 & -\mu \\ +\frac{g' v_u}{\sqrt{2}} & -\frac{g v_u}{\sqrt{2}} & -\mu & 0 \end{pmatrix} \tag{2.24}$$

The composition of the four neutralinos is therefore given by the corresponding eigenvector N to each eigenvalue, i.e.

$$\tilde{\chi}_i^0 = N_{i1}\tilde{B} + N_{i2}\tilde{W}^3 + N_{i3}\tilde{H}_d^0 + N_{i4}\tilde{H}_u^0, \tag{2.25}$$

In the equation above v_u and v_d are the vevs of the two Higgs doublets. As $\sqrt{v_u^2 + v_d^2} = v_{\mathrm{EW}}^2 \approx (246\,\mathrm{GeV})^2$, it is common to scan over the ratio of the two vevs, $\tan\beta \equiv v_u/v_d$.

The composition of the lightest neutralino is extremely important in determining its viability as a dark matter candidate. For example, if the neutralino is predominantly binolike, i.e. $N_{11} \approx 1$, then the neutralino annihilation cross section is extremely small due to the fact that the bino is a singlet under the standard model gauge groups. The neutralino is a WIMP and produced via the freeze out mechanism, so this small cross section leads to early chemical decoupling and too many relic neutralinos in the early universe, ruling out the binolike neutralino as a dark matter candidate.[3]

Gravitinos

We can also consider theories of supergravity, in which there exists a particle called the gravitino, which is the spin 3/2 partner of the graviton. The gravitino acquires a mass when supersymmetry is broken, and depending on the breaking mechanism, it can be the LSP. As it has odd R-parity, it is stable and is a dark matter candidate.

Three processes have been discussed in the literature that contribute to the gravitino abundance. These include gaugino scattering during reheating, direct gravitino freeze in, and the freeze out of the next to lightest supersymmetric particle (NLSP) and its subsequent decay to gravitinos [55]. It is often stated that there is a "gravitino problem", which consists of two parts. Gravitinos are often overproduced by the mechanisms described above, and they are produced slowly enough by NLSP decays (due to the fact that their coupling to other particles is suppressed by a factor of the Planck mass) that the decays continue in significant numbers during big bang nucleosynthesis (BBN). This leads to incorrect abundances of the elements that make up the universe [56].

[3]However, if the dark matter couples too strongly and is therefore underproduced, it is still possible for it to be the dark matter, as the "missing" dark matter could be some other species.

A method often proposed to avoid the gravitino problem, which we study in great detail in chapter 6, is to introduce a small amount of R-parity violation. While this is not significant enough to violate limits on the proton lifetime, it is sufficient to cause nearly all NLSP decays to be to standard model particles instead of the gravitino. This reduces the primordial gravitino abundance and resolves the issue of late time NLSP decays during BBN. It also solves another issue with gravitino DM – detecting it is extremely difficult. Because of their Planck mass suppressed couplings to other particles, gravitinos do not annihilate efficiently and would not produce any detectable signal in a direct detection experiment. However, introducing R-parity violation allows them to decay, and the gamma ray photons and charged cosmic rays that result from these decays could lead to detectable excesses.

2.2.2 Universal extra dimensions[4]

Other beyond the standard model theories contain dark matter candidates as well. One such type of theories are those with dimensions beyond the 3+1 of the standard version of general relativity. To explain our inability to observe them, these extra dimensions are often compactified. Such theories have been studied for many years, as early as 1919 with the attempt of Kaluza [57] and Klein [58] to unify gravity and electromagnetism. Universal extra dimensions (UED) is something of an outgrowth of this theory [59]. The minimal version of the theory, which is the only version we will consider in this thesis, has a five dimensional spacetime where the fifth dimension is compactified and orbifolded to give chiral

[4]Contains excerpts from Jonathan M. Cornell, Stefano Profumo, and William Shepherd. "Dark matter in minimal universal extra dimensions with a stable vacuum and the 'right' Higgs boson". *Phys.Rev.* D89.5 (2014), 056005. DOI: 10.1103/PhysRevD.89.056005. arXiv: 1401.7050 [hep-ph]

SM fermions, which will be discused below. The 3+1 dimensions we are familiar with are referred to as the brane, while any extra dimensions are referred to as the bulk. All of the standard model fields are allowed to propagate in the bulk (hence the term "universal"), in contrast to other recent extra dimensional theories such as the one by Arkani-Hamed, Dimopolous, and Divali, which was proposed to explain the weakness of the gravitational force and therefore allows only gravity to propagate in the bulk [60]. In the next few paragraphs I will introduce the properties of the minimal version of this theory, with a large debt to the review of Hooper and Profumo [61].

As in any model of small extra dimensions, the additional dimension manifests itself in four dimensions as a tower of Kaluza-Klein excitations of the fields allowed to propagate in the bulk. To reduce the theory down to an effective 4D theory, the fifth dimension is integrated over. This gives tree level masses of Kaluza-Klein (KK) excitations with the values

$$m^2_{X^{(n)}} = \frac{n^2}{R^2} + m^2_{X^{(0)}} \, . \tag{2.26}$$

In the above equation $X^{(n)}$ is the nth KK excitation of the SM field X and R is the radius of the extra dimension. R^{-1} is in general taken to be about a TeV, so the first term in equation 2.26 is much larger than the second. Therefore the masses of each of the KK particles with the same n value are approximately degenerate at tree level. As higher-dimensional theories are not renormalizable, it is necessary that additional new physics be invoked at some scale to restore good behavior at high energies; generically this cutoff scale is specified in the natural units of the extra dimension as the unitless number ΛR.

In principle, there remain many free parameters having to do with the exact nature

of the boundary conditions at the orbifold points in the extra dimensions, and these cannot be consistently set to zero as they are induced at loop level, but the framework of minimal UED [62] assumes that they are small enough not to significantly distort the spectrum or couplings of the theory, and neglects these parameters *tout-court*. With this assumption, the only remaining parameters needed to fully specify the model are the SM parameters, including of course the Higgs boson mass. The recent measurement of the Higgs mass [63] thus removes the last unconstrained parameter in the theory parameter space, leaving us with a treatable two-dimensional parameter space to consider. The compactness of the parameter space is one of the reasons this theory is compelling.

Because of the approximate tree level mass degeneracy of KK particles of a certain mode, loop corrections to the masses can be important, and have been calculated in detail [64]. The splittings grow logarithmically with the cutoff scale ΛR, as expected for a loop effect, with colored particles rising in mass more quickly than others, while the KK level-1 excitation of the hypercharge gauge boson $B^{(n)}$ drops slightly below the KK mass scale R^{-1}. These splittings have very important consequences for expected signals at colliders and for dark matter physics.

As it is impossible to construct a 5D chiral Lagrangian and the zero mode SM fermions must be chiral, it is necessary to introduce two 5D fermion fields: $\Psi(x^\mu, y)$ which has the quantum numbers of the left handed $\psi_{0L}(x^\mu)$ spinor and $\Psi'(x^\mu, y)$ which has the quantum numbers of the right handed $\psi_{0R}(x^\mu)$ spinor [65] (y refers to position in the fifth dimension). Using the periodicity of the fifth dimension, these fields can be Fourier

expanded in terms of KK modes in the form below

$$\Psi(x^\mu, y) = \frac{1}{\sqrt{2\pi R}}\left[\psi_0(x^\mu) + \sqrt{2}\sum_{n=1}^{\infty}\left(\psi_n^{(1)}(x^\mu)\cos\left(\frac{ny}{R}\right) + \psi_n^{(2)}(x^\mu)\sin\left(\frac{ny}{R}\right)\right)\right], \quad (2.27)$$

where the (1) and (2) indices represent different 4D fields. Ψ' takes the same form. The fermion fields are then just linear combinations of the two fields. This produces too many degrees of freedom, as the zero mode fermions should have a left handed component that comes only from Ψ and a right handed component that comes only from Ψ'. To get the desired form, Ψ is made to be odd under the S^1/Z_2 orbifold symmetry (under which the the spinor fields transform as $\Psi(x^\mu, y) \to \gamma_5\Psi(x^\mu, -y)$) while Ψ' is made to be even. With this condition, the fields have the following forms:

$$\begin{aligned}\Psi(x^\mu, y) &= \tfrac{1}{\sqrt{\pi R}}\left\{\psi_{0L}(x^\mu) + \sqrt{2}\textstyle\sum_{n=1}^{\infty}\left[\psi_{nL}^{(1)}(x^\mu)\cos\left(\frac{ny}{R}\right) + \psi_{nR}^{(2)}(x^\mu)\sin\left(\frac{ny}{R}\right)\right]\right\} \\ \Psi'(x^\mu, y) &= \tfrac{1}{\sqrt{\pi R}}\left\{\psi'_{0R}(x^\mu) + \sqrt{2}\textstyle\sum_{n=1}^{\infty}\left[\psi_{nR}^{\prime(1)}(x^\mu)\cos\left(\frac{ny}{R}\right) + \psi_{nL}^{\prime(2)}(x^\mu)\sin\left(\frac{ny}{R}\right)\right]\right\} \quad (2.28)\end{aligned}$$

Now we have what we want for the zero level mode, namely a 4 component fermion spinor whose left and right handed components have the correct quantum numbers. Note that for each of the KK modes, there are now two fields for each of the SM fields, one where both the left and right handed components have the SM left handed quantum numbers and one where both components have the SM right handed quantum numbers.

The n associated with a Kaluza-Klein mode can be associated with the momentum of the field in the fifth dimension. While usually such a quantity would be conserved, the introduction of the orbifolding breaks the translational symmetry, leading to this momentum (and the KK number) not being conserved. However, there remains a quantity called KK-parity (defined simply as $P = (-1)^n$) which must be conserved.

The existence of KK-parity serves to stabilize the lightest Kaluza-Klein particle (LKP). From equation 2.26, one can see that the LKP will nearly always be the first level excitation of the photon, which lacking electric and color charge is an excellent dark matter candidate. Since the photon mass eigenstate and the B hypercharge gauge boson interaction eigenstate are essentially degenerate for KK modes of 1 or greater, this candidate is referred to interchangeably as $\gamma^{(1)}$ or $B^{(1)}$. The KK photon is a standard WIMP whose relic density is set via the freeze-out mechanism. The mass degeneracy at each KK level leads to a large number of co-annihilations, and one of the main points of chapter 5 of this thesis is to explore the importance of co-annihilation processes which had previously unconsidered in the calculation of the freeze-out temperature.

Electroweak vacuum stability

The measured value for the Higgs mass presents an interesting conundrum, as it implies, at face value, that, at some very high energy, the potential for the Higgs boson develops a second minimum at very large field values, implying a second, lower-energy "true" vacuum that our universe could, in principle, decay into. The precise energy scale at which this takes place (and in fact the existence or absence of this vacuum state) depends very sensitively on the top quark mass as well as on the Higgs mass, but for all experimentally reasonable values the current universe is at least metastable. A viable model thus requires the lifetime of the universe's decay to be at least longer than the measured age of the universe itself.

In models with universal extra dimensions this problem becomes quite acute. The decrease in the Higgs quartic coupling which ultimately leads to this issue is driven largely

by the top quark Yukawa coupling, and in UED models there are additional fermions with strong coupling to the SM Higgs, namely the KK excitations of the top quark. As a result, the quartic coupling runs much faster as one introduces more "effective top quarks", and vacuum stability becomes a strong bound on the model parameters. Constraints of this nature can always be taken as defining a scale at which new physics must somehow stabilize the observed vacuum, so these constraints can be directly translated into an upper limit on ΛR for a given choice of R^{-1}. These constraints have been explored in detail [66], and allow maximal values of ΛR of about 5, relatively irrespective of the KK mass scale R^{-1}.

Chapter 3

Kinetic Decoupling and Small-Scale Structure in Effective Theories of Dark Matter

The calculation of the kinetic decoupling temperature $T_{\rm kd}$, and thus of the small-scale cutoff $M_{\rm cut}$ has been carried out in a variety of model-dependent contexts, including supersymmetry [37, 24, 21], universal extra-dimensions [21, 61], and models with Sommerfeld enhancement [67, 68]. It has become clear that WIMP models accommodate a broad variety of kinetic decoupling temperatures, with resulting cutoff scales ranging from $10^3\ M_\odot$ to much less than $10^{-6}\ M_\odot$ even only within the limited framework of the minimal supersymemtric extension of the Standard Model [21], where the symbol $M_\odot$ indicates the mass

Adapted from Jonathan M. Cornell, Stefano Profumo, and William Shepherd. "Kinetic Decoupling and Small-Scale Structure in Effective Theories of Dark Matter". *Phys.Rev.* D88.1 (2013), 015027. DOI: 10.1103/PhysRevD.88.015027. arXiv: 1305.4676 [hep-ph]

of the Sun. Particle physics details of the WIMP model affect in a highly model-dependent way the kinetic decoupling, producing a wide array of outcomes, but for many particle physics models there is still a strong correlation between certain experimentally accessible quantities such as the direct detection scattering cross section, as explored in Ref. [1], and $M_{\rm cut}$.

A possible model-independent route to evaluating ranges for the expected small-scale cutoff is to consider an effective theory description of interactions between Standard Model and dark matter particles, as pursued, recently, in Ref. [36, 69]. For example, assuming the dark matter is a spin 1/2 fermion, it is simple to write down the complete set of lowest dimensional operators that mediate such interactions. In turn, by assuming that only one single operator is dominating the relevant dark matter interactions, crossing symmetry allows to draw stringent constraints on the allowed effective energy scale associated with the operator, for example from direct dark matter detection or from collider searches. As a result we can robustly set *upper limits* to the size of the small-scale cutoff, for each class of operators, as a function of the relevant operator's effective energy scale. This upper limit is quite significant, as cosmologically relevant effects occur only for sufficiently large such cutoffs.

While rather sophisticated codes now exist to reliably calculate $T_{\rm kd}$ (see e.g. [14]), two potentially important ingredients have been only marginally studied thus far:

(i) scattering off of quarks only, for example in "lepto-phobic" theories with suppressed couplings to leptons (this was first partly addressed in Ref. [36]), and

(ii) the role of scattering off of pions, for the same class of theories, for kinetic

decoupling temperatures below the QCD confinement phase transition.

In addition, a third aspect that remains entirely unexplored to date is (iii) the relevance of loop-mediated scattering off of leptons, again notably in leptophobic theories.

In the present study, in addition to the general program of setting upper limits to the small-scale cutoff in the context of the mentioned effective theory description of interactions between Standard Model and dark matter particles, we address in detail the three novel issues listed above. We show that for leptophobic theories there exists an interesting interplay between loop-mediated scattering off of leptons and scattering off of pions, and that the two effects are generically comparable. We find that for WIMP models that can be described to a good approximation by an effective operator belonging to the class we consider here, there are stringent upper limits on the cut-off scale to the matter power spectrum, typically on the order of $10^{-3}\ M_{\odot}$. This scale hints at the fact that WIMP effective theories are not likely to have any impact on small-scale structure issues in cold dark matter cosmology. On the other hand, since the predicted protohalos are typically very small, sizable boost factors from substructure enhancements are a rather generic prediction of effective theories of dark matter.

The reminder of this chapter is organized as follows: we outline the class of effective operators we consider in the following section 3.1; section 3.2 presents all of our results; and the final section 3.3 summarizes our findings and concludes.

3.1 Classification of effective operators

The effective operator framework has been explored as a method for comparing experimental bounds coming from various types of experiments on dark matter couplings to Standard Model fields [71, 70]. Within this framework, one writes down higher-dimensional operators which couple dark matter to quarks, leptons, or Standard Model bosons, requiring that (i) the operator contain at least two dark matter particles to ensure stability, and that (ii) Standard Model gauge symmetries are respected. One operator from the list of possible operators is then assumed to be the dominant one for the physics being investigated, and its effects are explored assuming the other operators are suppressed and, thus, do not contribute to the observables in question. Each operator of interest is investigated separately in this way, and any interference effects from having multiple operators active simultaneously are assumed to be small. Generally these interference effects are equivalent to changing the assumed chirality structure of the operator in question, e.g. interfering a vector and an axial operator with equal suppression scales is equivalent to considering an operator which only couples to one chirality.

The basic assumption of this parametrization of dark matter interactions is that dark matter is the only new field light enough to be kinematically relevant, and these operators are suppressed by a mass scale which is related to the expected mass of the additional particles which mediate the interactions in some more complete model underlying the effective theory. Within the region of parameter space where this assumption is valid, a given complete model can be mapped into the space of these operators by integrating out the additional heavy fields. This assumption is a fairly weak one for elastic scattering of

dark matter off of Standard Model particles, where the momentum exchange is typically on the order of the MeV, but is a fairly strong assumption for LHC searches, where the center of mass energy of the created dark matter pair can be quite large compared to the dark matter mass. We therefore encourage caution when considering the collider bounds on these operators, but expect that the results for kinetic decoupling and the bounds arising from direct detection should be robust.

We also calculate the thermal relic density of WIMPs under the assumption that the same operator dominates dark matter interactions with Standard Model particles in the early as well as in the late universe. Of course, this is a rather strong assumption, as it entails for example the absence of processes such as coannihilation, the presence of thresholds or resonances that could exist at finite temperature but not in the late universe, and the absence of temperature-suppressed operators that might dominate the chemical freeze-out while being irrelevant at the later kinetic freeze-out. We note, however, that this assumption is largely equivalent to other assumptions discussed above, where it is presumed that dark matter is the only kinematically relevant new particle in the theory and that one operator is dominant in all of the observables being searched for.

We consider here a subset of all possible operators which conserve parity in addition

to the Standard Model gauge symmetries. The operators of interest are

$$\mathcal{O}_S = \frac{m_f}{\Lambda_S^3}\bar{\chi}\chi\bar{f}f \tag{3.1}$$

$$\mathcal{O}_P = \frac{m_f}{\Lambda_P^3}\bar{\chi}\gamma^5\chi\bar{f}\gamma^5 f \tag{3.2}$$

$$\mathcal{O}_V = \frac{1}{\Lambda_V^2}\bar{\chi}\gamma^\mu\chi\bar{f}\gamma_\mu f \tag{3.3}$$

$$\mathcal{O}_A = \frac{1}{\Lambda_A^2}\bar{\chi}\gamma^\mu\gamma^5\chi\bar{f}\gamma_\mu\gamma^5 f \tag{3.4}$$

$$\mathcal{O}_T = \frac{m_f}{\Lambda_T^3}\bar{\chi}\sigma^{\mu\nu}\chi\bar{f}\sigma_{\mu\nu}f, \tag{3.5}$$

where Λ_I is the suppression scale for operator $\mathcal{O}_I$. Note that the operators which are chirality-violating are assumed to be proportional to the fermion mass to preserve $SU(2)_L$ and avoid inducing large effects in low-energy flavor observables. The first four operator normalizations are standard within the effective dark matter literature, but previous searches for contact operators have not included the mass suppression for the tensor operator to better make contact with direct detection bounds. We choose to consider the theoretically better motivated normalization of the tensor operator which does include a quark mass suppression, as the operator is chirality-violating and thus would require an insertion of the Higgs field to respect the SM gauge symmetries. Previous analyses have considered the operator without a quark mass dependence to make better contact with direct detection searches, as the unsuppressed tensor induces a coupling to the spin of the quarks composing the nucleon minus the spin of the antiquarks in the nucleon, but it is not clear how a tensor operator with that normalization would be alligned with the mass basis of the quarks so well as to avoid inducing unacceptably large corrections to flavor observables. The choice to include the quark mass suppression of the tensor operator leaves us without collider and direct detection bounds to compare to, and therefore we will only plot the early universe

curves for these operators.

For each operator, we specify which Standard Model fermions the dark matter particle couples to. Generically, leptons are the most significant contributors to keeping the dark matter in kinetic equilibrium with the Standard Model thermal bath, while many of the key experimental searches constrain primarily the couplings to quarks. We choose here to consider explicitly three cases, wherein the dark matter couples only to leptons, only to quarks, or to both with equal suppression scales. For cases including quark couplings we plot the strongest available experimental bounds from LHC searches and direct detection searches, and in cases including lepton couplings we will additionally plot LEP search bounds. In the special case of the lepton-only vector operator we will in addition plot the direct detection bounds induced at one-loop order, as discussed in Ref. [72, 70].

3.2 Results

As discussed above, for each effective operator in Eq. (3.1-3.5) we consider three cases as far as the relevant Standard Model particle class the dark matter couples to:

1. Universal couplings to all SM fermions;

2. Couplings to leptons only;

3. Couplings to quarks only.

Each case presents distinct behaviors in the early as well as in the late universe, and leads to different constraints and conclusions for the effective cutoff scale. Leptonic couplings, when present, tend to dominate the process of kinetic decoupling, as a simple result of the

fact that at the relevant temperatures leptons (especially electron/positron and neutrinos) are in a relativistic state and the number densities are not Boltzmann-suppressed. On the other hand, quark couplings lead to stronger bounds from colliders and direct detection. If lepton couplings are absent then the contributions of quark couplings to kinetic decoupling must be treated with care due to the QCD confinement phase transition. Before the phase transition there is a thermal bath of quarks and the calculation of the scattering rate proceeds analogously with that for the leptonic couplings, but after the phase transition pions are the dominant hadrons and the matrix element of the quark bilinear in the pion must be evaluated. In addition, loop-induced scattering off of leptons arises generically even for vanishing direct couplings to leptons. This effect, which has never been considered in this context before, competes with scattering off of pions, and becomes more and more relevant as pions become less and less abundant at decreasing temperatures due to Boltzmann suppression. We will discuss each operator's coupling to pions individually in presenting our results.

For each case we also present all relevant bounds on effective dark matter interactions from collider searches both at the LHC [73, 74] and at LEP [70]. These constraints are subject to the concerns described in section 3.1 regarding the possibility of probing additional particles at colliders due to the large center of mass energies involved. For all operators which lead to appreciable direct detection cross sections we also plot the current leading bounds from those experiments. For spin-independent scattering the current leading bounds come from the Xenon 100 experiment [75], while for spin-dependent scattering they are set by the SIMPLE [76] and PICASSO [77] experiments.

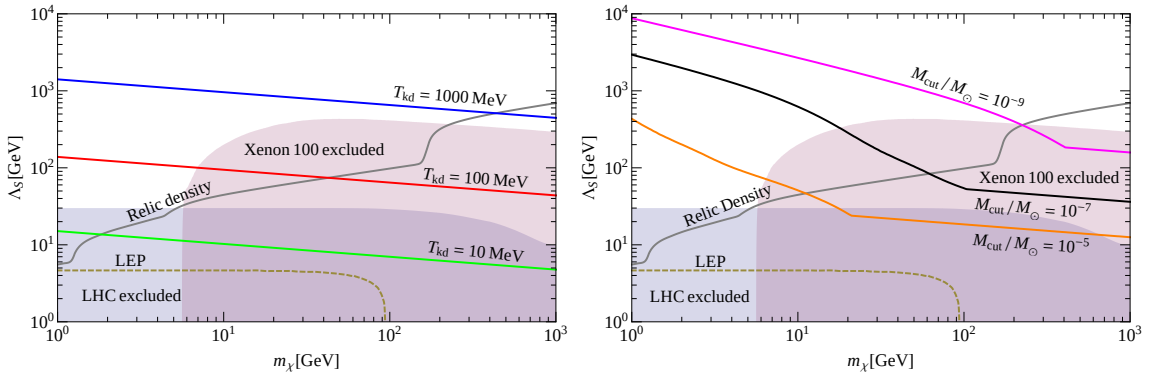

Figure 3.1: *Plots of contours of constant* $T_{\rm kd}$ *(left) and* $M_{\rm cut}$ *(right) for the case of a scalar operator interaction between WIMPs and SM fermions. Here WIMPs couple with the same strength to all SM fermions before the QCD phase transition and leptons and pions after. Shaded regions and the dashed curve represent regions of parameter space excluded by collider and direct detection results, while the solid gray curve represents the correct dark matter relic density.*

For all plots we also present relic density constraints. The line on the plots corresponds to when $\Omega_\chi h^2 = 0.1189$, the best fit value quoted by the Planck collboration [78] when combining their CMB results, WMAP polarization results, high-ℓ CMB data from ground telescopes and baryon acoustic oscillation measurements. For all operators except the tensor case (which has no simple, tree-level UV completion) we use the micrOMEGAs code [79, 80] to calculate the relic density. This was checked analytically to correspond with setting the annihilation cross section to the appropriate value $\langle \sigma v \rangle \approx 3 \times 10^{-26}$ cm^3/s, and this analytical requirement was used to calculate the relic density requirement for the tensor operator case.

3.2.1 Scalar operator

The scalar-type coupling of dark matter to SM fermions contributes to direct detection in the case of quark couplings, and has been constrained by collider searches for both quark and lepton couplings. The collider constraints are relatively weak in this case, however, because of the mass-suppression of this chirality-violating operator. While pair annihilation, direct detection, and scattering responsible for kinetic decoupling all have access to the heavier SM fermion generations, the initial state, for collider studies, is dominated by the lighter states, and therefore collider bounds are weakened relative to the other dark matter probes.

For the case of universal coupling to SM fermions through the scalar operator the results are presented in figure 3.1. We note that for dark matter above approximately 10 GeV in mass the bounds from direct detection, which are strongest in that region, indicate that the kinetic decoupling temperature must be on the order of 1 GeV. The resulting cutoff scale for the smallest protohalos is on the order of the Earth mass (about $10^{-6}\ M_{\odot}$) for WIMP masses above 10 GeV. The relic density matches the observed dark matter only for masses above 200 GeV. Models that possess the right thermal relic density have extremely suppressed cutoff scales, smaller than $10^{-9}\ M_{\odot}$ (see the right panel of figure 3.1).

For the case of lepton-only couplings, the only relevant bound on this operator is from LEP, and the resulting bound is weak enough to not significantly constrain the process of kinetic decoupling. The corresponding results are shown in figure 3.2a, which indicates that kinetic decoupling temperatures below 10 MeV are possible in this case, resulting in small-scale cutoffs exceeding the Earth mass. We estimate in this case that the largest

Figure 3.2: *Plots of contours of constant $T_{\rm kd}$ (left) and $M_{\rm cut}$ (right) for the case of a scalar operator interaction between WIMPs and SM particles in which WIMPs couple directly to only leptons or quarks.. Shaded regions and the dashed curve represent regions of parameter space excluded by collider and direct detection results, while the solid gray curve represents the correct dark matter relic density.*

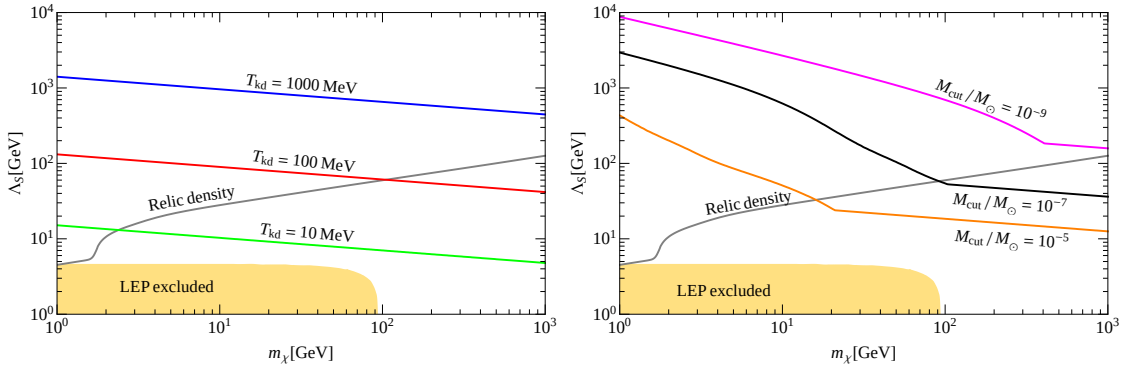

(a) *As in figure 3.1, but for DM scattering off leptons only.*

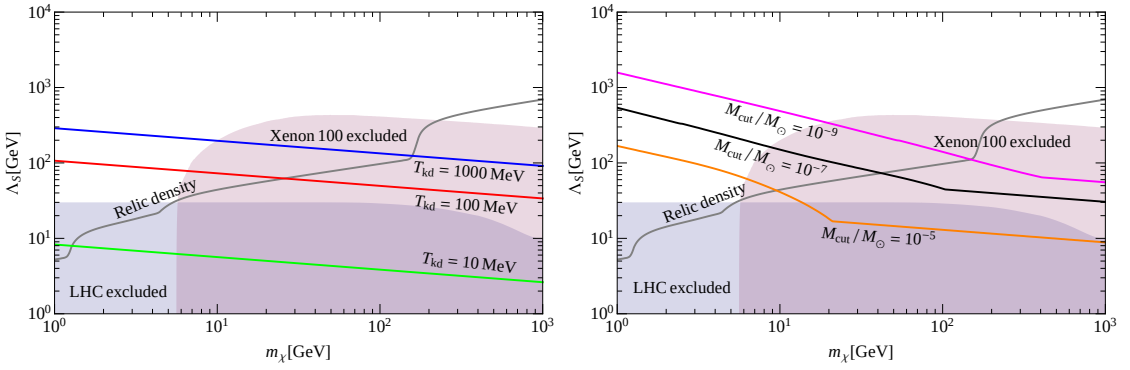

(b) *As in figure 3.1, but DM scatters solely off quarks before the QCD phase transition and pions after.*

possible cutoff mass scale is of about $M_{\rm cut} \sim 10^{-3}\ M_\odot$. We also note that the LEP limits do not impact the cutoff scales Λ_S needed to produce the correct thermal relic density. For WIMP masses of about 10 GeV we find that models that have the correct thermal relic density produce a small scale cutoff of $10^{-5}\ M_\odot$, while those with a mass of 100 GeV of about $10^{-7}\ M_\odot$ and those with a mass of 1 TeV of approximately $10^{-9}\ M_\odot$.

Finally, for quark-only couplings the matrix element $\langle \pi | \bar{q} q | \pi \rangle$, implicitly summed over quark flavors, is needed to evaluate the coupling to pions after the QCD phase transition. This has been evaluated previously in the context of contributions to direct detection by [81] using soft-pion techniques to be

$$\langle \pi^a | \bar{q} q | \pi^a \rangle = \frac{m_\pi^2}{2} \langle \pi^a | \vec{\pi} \cdot \vec{\pi} | \pi^a \rangle, \tag{3.6}$$

where $\vec{\pi}$ is a pion iso-vector, Eq. (A.16). We have implemented this scattering amplitude for interactions after the QCD phase transition with pions, which are the dominant components of the thermal bath at the relevant temperatures. The results for quark-only couplings are shown in figure 3.2b. Direct detection forces in this case the size of the smallest protohalos to values well below $10^{-9}\ M_\odot$ for dark matter particle masses larger than 20 GeV. Models with the correct relic density must have masses above 200 GeV, and small scale cutoff smaller than $10^{-11}\ M_\odot$ in this case.

3.2.2 Vector operator

Vector operators are generically better constrained by collider searches than scalar operators are, but are also very tightly constrained by direct dark matter detection. For universal couplings, direct detection is again the dominant constraint for dark matter masses

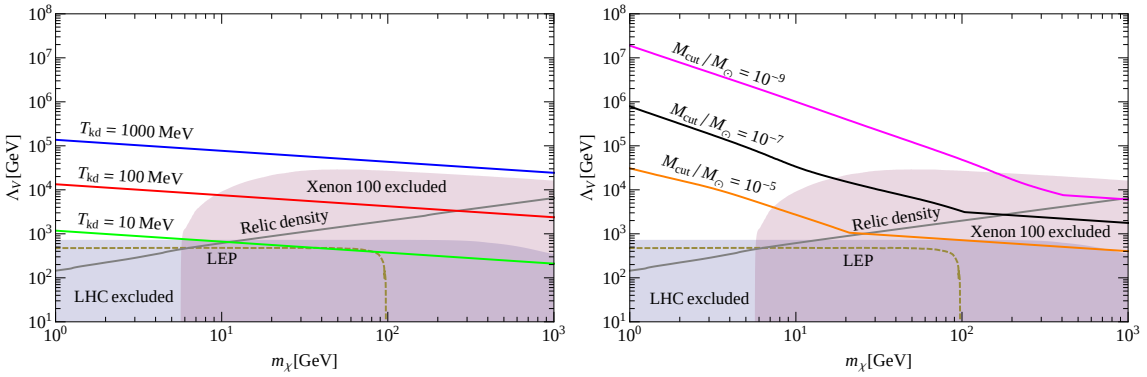

Figure 3.3: *Plots of contours of constant* $T_{\rm kd}$ *(left) and* $M_{\rm cut}$ *(right) for the case of a vector operator interaction between WIMPs and SM fermions in which WIMPs couple with the same strength to all SM fermions. Shaded areas signify the regions of parameter space excluded by LHC and direct detection results, and the dashed line corresponds to a limit on the parameters from an analysis of LEP data. The solid gray curve represents the correct relic density.*

above about 10 GeV, and those constraints again force us to conclude that the kinetic decoupling temperature must be of order 1 GeV. We show our results in figure 3.3. We do not find any sub-TeV WIMP models with a viable thermal relic density, if this operator is the only important contributor to chemical freeze-out. For masses above 100 GeV, we find that the cutoff scale is always smaller than approximately $10^{-9}\ M_\odot$.

Our results for vector interactions only with leptons are shown in figure 3.4. We have plotted bounds from LEP and from direct detection, which arise at one-loop level by effectively inducing a mixing between the integrated-out heavy vector boson and the SM photon. This mechanism was first discussed by Fox et. al. [70], and the bounds we plot are updates of those they derived from the first release of Xenon 100 data to take in to account the full 2012 data set. Even with a loop suppression, direct detection is still the

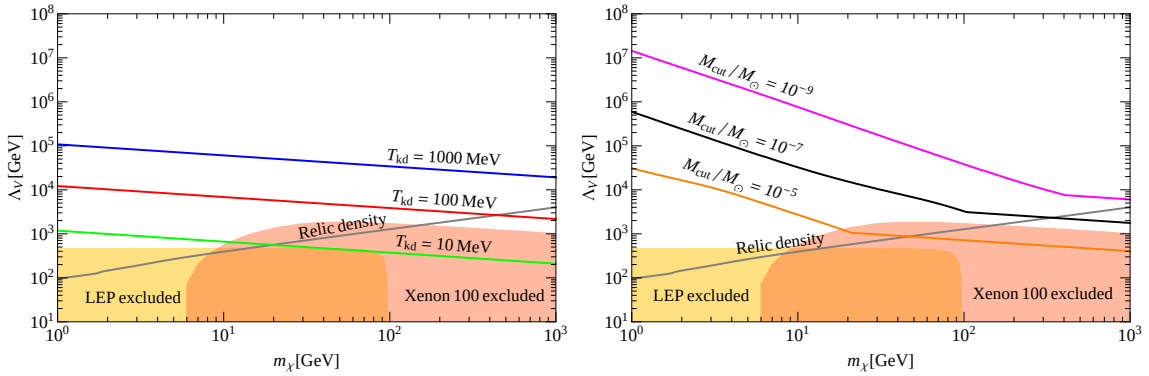

Figure 3.4: *Plots of contours of constant* $T_{\rm kd}$ *(left) and* $M_{\rm cut}$ *(right) for the case of a vector operator interaction between WIMPs and SM fermions in which WIMPs couple directly to leptons only. Shaded areas signify the regions of parameter space excluded by LHC and direct detection results, and the dashed line corresponds to a limit on the parameters from an analysis of LEP data. The solid gray curve represents the correct relic density.*

dominant bound on dark matter models with masses above about 8 GeV, and the decoupling temperature is required to be of order 100 MeV. The resulting smallest possible protohalos are smaller than about $10^{-5}\ M_\odot$ for WIMP masses below 100 GeV, and are generically of order $10^{-7}\ M_\odot$ or smaller for masses above 100 GeV.

Considering couplings to quarks only below the QCD phase transition, we now must evaluate $\langle \pi^a | \bar{q}\gamma^\mu q | \pi^a \rangle$. This also was shown in [81], using the conservation of the vector current, to be

$$\langle \pi^a | \bar{q}\gamma^\mu q | \pi^a \rangle = (a_u - a_d)\, \langle \pi^a | \vec{\pi} \times \partial^\mu \vec{\pi} | \pi^a \rangle, \tag{3.7}$$

where a_q is the coupling to quarks of type q. This clearly vanishes for the coupling structure we have chosen of universal couplings to all quark flavors.

For a vector interaction coupling only to quarks, the induced direct detection

Figure 3.5: *Plots of contours of constant $T_{\rm kd}$ (left) and $M_{\rm cut}$ (right) for the case of a vector operator interaction between WIMPs and SM particles in which WIMPs couple directly to quarks only. Shaded regions represent regions of parameter space excluded by collider and direct detection results, while the solid gray curve represents the correct relic density.*

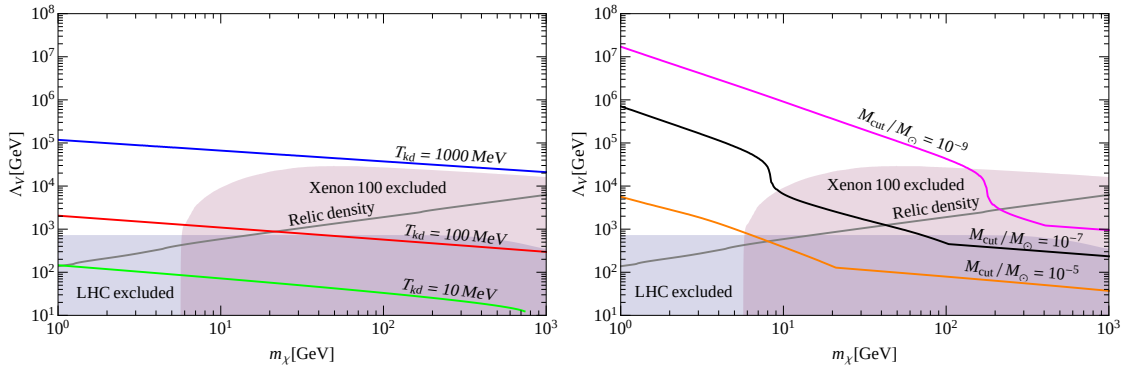

(a) *As in figure 3.3, but for DM coupling directly only to quarks and to leptons via a loop process.*

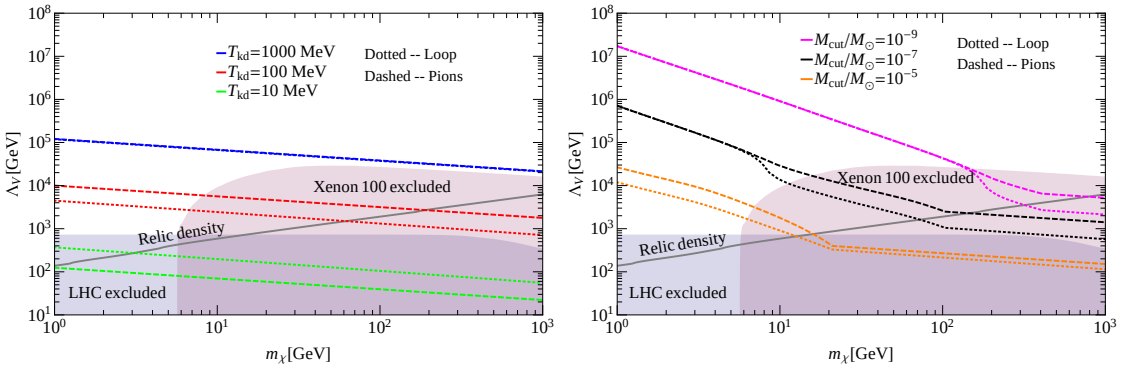

(b) *As in figure 3.3, but for DM coupling directly to quarks and to either leptons via a loop process (dotted lines) or to pions (dashed lines).*

amplitude in the former case can be effectively inverted to give an induced, loop-level coupling to leptons, which can be important as leptons are generically greater contributors to kinetic decoupling than quarks. Since kinetic decoupling is dominated by scatterings at low dark matter velocities, the loop induced coupling to leptons from quarks can be considered as a simple rescaling of the suppression scale involved, and can be calculated in the "leading-log" approximation as discussed in Ref. [72]. The formula for this rescaling in the case where we consider identical couplings to all quark flavors is

$$\Lambda_\ell = \sqrt{\frac{3\pi}{2\alpha}} \frac{\Lambda_q}{\sqrt{\sum_{d,s,b} \ln\left(m_q/\Lambda_q\right) - 2\sum_{u,c,t} \ln\left(m_q/\Lambda_q\right)}}, \tag{3.8}$$

where α is the electromagnetic fine structure constant and all running quantities are evaluated at the renormalization scale of Λ_q, the scale of the effective operator. While this does not minimize the logarithms involved, it does allow us to neglect renormalization running and mixing of different operators, such that it is well-defined to assume one operator is dominant. We enforce perturbativity of this loop expansion by truncating our results when the induced coupling to leptons is not weaker than the initial coupling to quarks. The results for this coupling structure are presented in figure 3.5a. We find, as in fig. 3.3, that no models with sub-TeV masses have the right thermal relic density, and that the predicted cutoff for masses above 10 GeV is always smaller than $10^{-7}\ M_\odot$, while it is smaller than $10^{-9}\ M_\odot$ for masses above 100 GeV.

To explore the relative importance of pion scattering to that of loop-induced lepton scattering, we also consider a quarks-only vector-like operator which couples with opposite sign to up- and down-type quarks. This doesn't change the bounds from colliders or the scattering amplitudes above the QCD phase transition, but it allows for pion scattering below

the QCD phase transition and alters the bounds from direct detection and the loop-induced coupling to leptons by changing the relative sign of the up- and down-type contributions in Eq. (3.8). We have presented the results for this coupling structure in figure 3.5b. This plot only shows results for including the coupling to pions or the loop coupling to leptons, but including both contributions leads to a curve that lies along the curve of larger suppression scale: e.g. for $T_{\rm kd} = 100\,\text{MeV}$ the curve with both effects included would lie along the pion only curve. From this plot, we observe that following the QCD phase transition, pion scattering is the dominant process in setting $T_{\rm kd}$, but as T decreases, the loop coupling to leptons becomes more important as the pions become non-relativistic and their interaction rate with dark matter is Boltzmann suppressed. We thus note that the relative importance of scattering off of pions versus loop-mediated scattering off of leptons below the QCD phase transition is generically comparable, with one process dominating over the other depending upon the kinetic decoupling temperature: for large decoupling temperatures, hence closer to the QCD confinement phase transition, scattering off of pions dominates, while lepton loop-induced scattering dominates as the number density of pions declines at lower temperatures.

3.2.3 Pseudoscalar operator

Pseudoscalar operators present a unique complication among all parity-conserving operators, in that the scattering amplitude vanishes in the limit $t \to 0$ even when the center-of-mass velocity is large. This necessitates a summation over angles which can be neglected in the case of the other operators, as described in section 2.1.3.

Pseudoscalar operators lead to strongly suppressed direct detection scattering, so

the only relevant bounds are from collider searches. Here, when the coupling is universal, the largest possible value for $M_{\rm cut}$ is $10^{-6}M_\odot$ when $m_\chi \geq 20\,\mathrm{MeV}$, as shown in figure 3.6a. Models with the correct relic density have masses of a few GeV and higher and increasingly suppressed cutoff scales as a function of mass: from $10^{-5}M_\odot$ at 5 GeV to $10^{-7}M_\odot$ at 20 GeV, and downward to $10^{-9}M_\odot$ and smaller for any mass larger than 200 GeV.

With lepton only couplings constrained by just LEP data, $M_{\rm cut}$ is again much less constrained, as the next figure, 3.6b, shows. Focusing again on models with the correct relic density, we find kinetic decoupling temperatures from slightly more than 10 MeV at WIMP masses in the GeV range, up to 1 GeV for 400 GeV WIMPs. The inferred cutoff mass scale ranges from $10^{-5}M_\odot$ at 6 GeV to $10^{-7}M_\odot$ at 30 GeV, to $10^{-9}M_\odot$ and smaller for any mass larger than 200 GeV, again for models with the correct thermal relic density.

For quark-only pseudoscalar couplings there exists a minimum value of $T_{\rm kd}$, irrespective of how strongly the dark matter couples, which is the QCD phase transition temperature. After the phase transition the only hadronic state available with cosmologically-relevant number densities are the pions. Since QCD is a parity-conserving theory, we can require that the parity behavior of the quark bilinear match that of the pion state which the dark matter would couple to. However, with only two pions it is impossible to construct any pseudoscalar invariant. This indicates that elastic scattering off of two pions is completely forbidden by the symmetries of the theory for this operator. Other scattering processes are possible, however. Inelastic scatterings, whether changing the number of particles or changing, for example, a pion into a sigma meson, are allowed by the symmetries of the problem. These nonetheless do not contribute efficiently to the continued thermalization of

Figure 3.6: *Plots of contours of constant $T_{\rm kd}$ (left) and $M_{\rm cut}$ (right) for the case of a pseudoscalar operator interaction between WIMPs and SM particles. Shaded regions and the dashed curve represent regions of parameter space excluded by collider results, while the solid gray curve represents the correct relic density.*

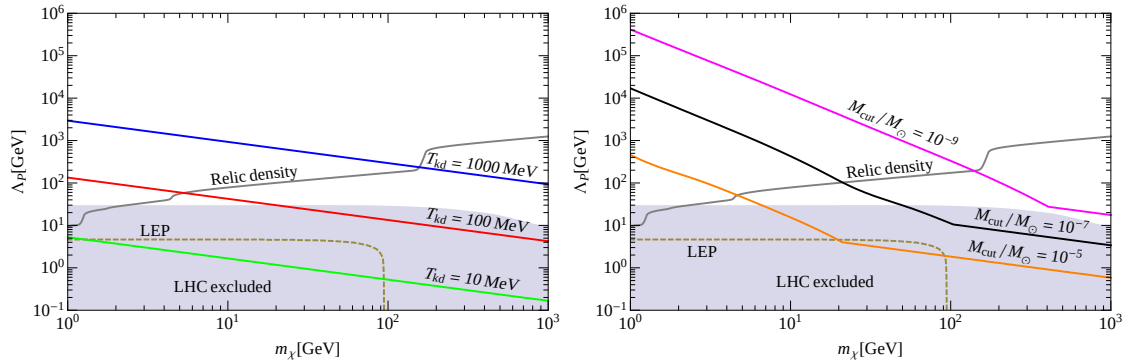

(a) *DM couples to all SM fermions.*

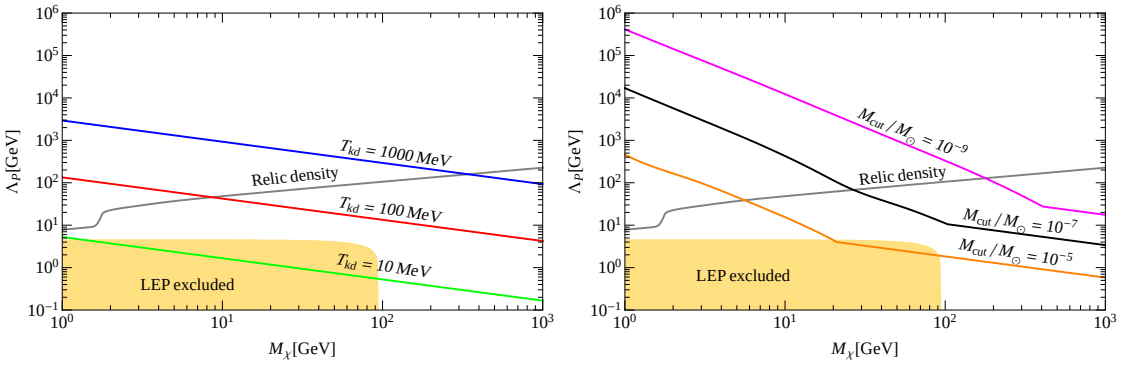

(b) *DM couples only to leptons.*

the dark matter kinematics, because the thermal bath is not energetic enough to produce the more exotic (i.e. higher-mass) QCD states or to provide sufficient energy to produce additional pions in scattering. Thus, the leading contribution is a one-loop-suppressed process requiring two insertions of the operator, which is very strongly suppressed.

3.2.4 Axial-Vector operator

Axial-vector couplings are constrained at levels comparable to vector couplings by colliders, but lead to spin-dependent rather than -independent scattering in direct detection, so the collider bounds are generically stronger than the direct detection bounds for these interactions. Universal couplings to SM fermions are presented in figure 3.7a. We find that with universal couplings existing bounds generically require $T_{\rm kd}$ to be above 10 MeV, and the cutoff is smaller than $10^{-5}\ M_\odot$ for any mass above 20 GeV. This class of operators produces the right thermal relic density for WIMPs above 100 GeV, leading in all cases to cutoff masses smaller than $10^{-5}\ M_\odot$

For couplings to leptons only there are no appreciable direct detection bounds, as any loop-induced scattering akin to that in the vector case would have to proceed through Z-boson exchange, and the additional suppression of t/M_Z^2 makes such contributions negligible. Thus, only LEP bounds are shown along with our results in figure 3.7b. The figure indicates that cutoff scales as small as about $10^{-3}\ M_\odot$ are in principle possible for very light WIMPs. The thermal relic density and LEP bounds put the dark matter mass in the 100 GeV and up range, with cutoff scales at most of $10^{-4}\ M_\odot$, as before suppressed with increasing WIMP mass.

For the same reason that there are no bounds from direct detection on leptonic

Figure 3.7: *Plots of contours of constant $T_{\rm kd}$ (left) and $M_{\rm cut}$ (right) for the case of a axial-vector operator interaction between WIMPs and SM particles. Shaded regions represent regions represent regions excluded by collider results and the non-solid curves represent regions of parameter space excluded by collider and direct detection results. The solid gray curve curve represents the correct relic density.*

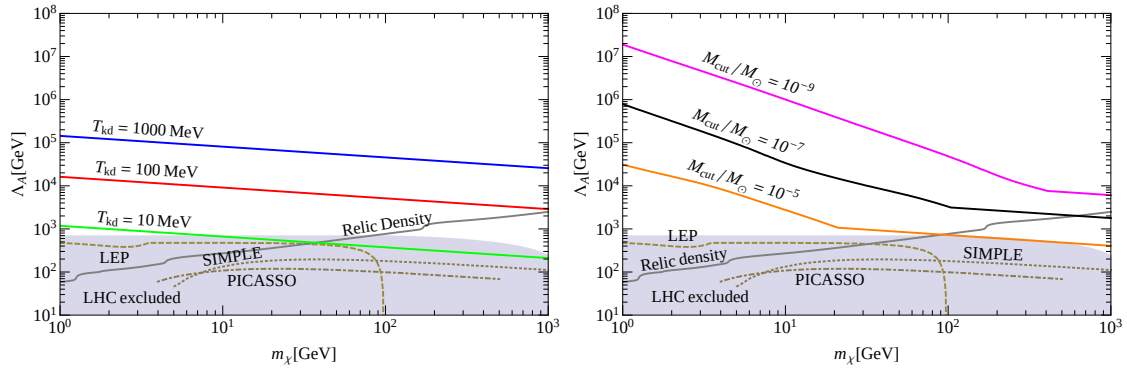

(a) *DM couples to all SM fermions.*

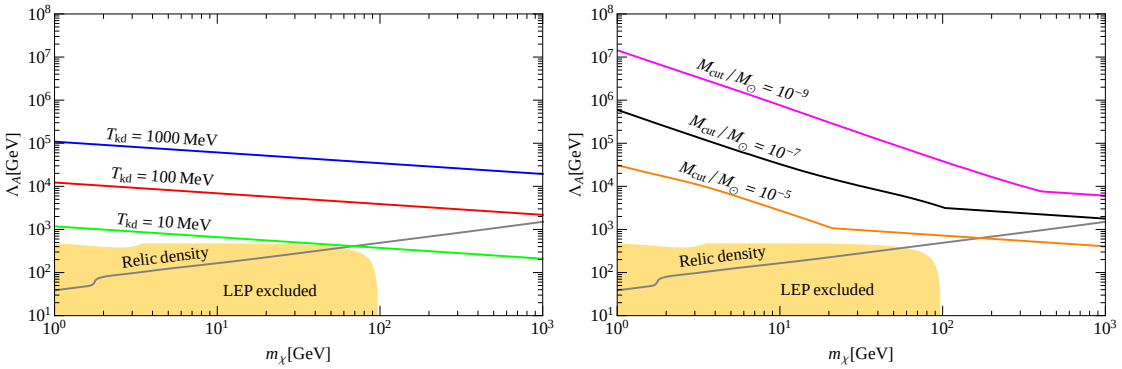

(b) *DM couples only to leptons.*

axial-vector couplings, there is no induced lepton coupling in the case of a quark-only interaction. Additionally, elastic scattering of dark matter off of pions vanishes in this model, as there is no axial invariant which can be constructed from the kinematics of two pions. Once again, inelastic scattering, whether producing or destroying an additional pion or scattering a pion into a different QCD state, is possible, but the low temperature below the QCD phase transition makes these possibilities contribute negligibly to the kinetic decoupling. Thus axial interactions with quarks only also have a minimum $T_{\rm kd} = T_c$, analogously with the case of pseudoscalar couplings.

3.2.5 Tensor operator

The tensor operator normalization which we consider preserves the SM gauge group where other normalizations do not, but is not particularly well studied because it does not correspond to the QCD matrix element which is probed in direct detection. Thus, we cannot present bounds from direct detection on this operator. Additionally, current collider searches have been normalized to correspond to direct detection, so we can't compare directly to those results either. The closest approximation to collider searches which could be considered would be the constraints on the other chirality-suppressed operators, in this work the scalar and pseudoscalar cases. For the direct detection comparison the theoretical picture is a bit more muddled, as the quark mass which appears in this operator should be taken to be related to the yukawa coupling, which will be affected by renormalization running in the strong phase of QCD, and is therefore nontrivial to factor out of the operator and find a meaningful bound. Since neither comparison technique yields a perfect mapping, we will only discuss the early-universe behavior of the operator.

Figure 3.8: *Plots of contours of constant $T_{\rm kd}$ (left) and $M_{\rm cut}$ (right) for the case of a tensor operator interaction between WIMPs and SM particles, where the solid gray curve represents the correct relic density.*

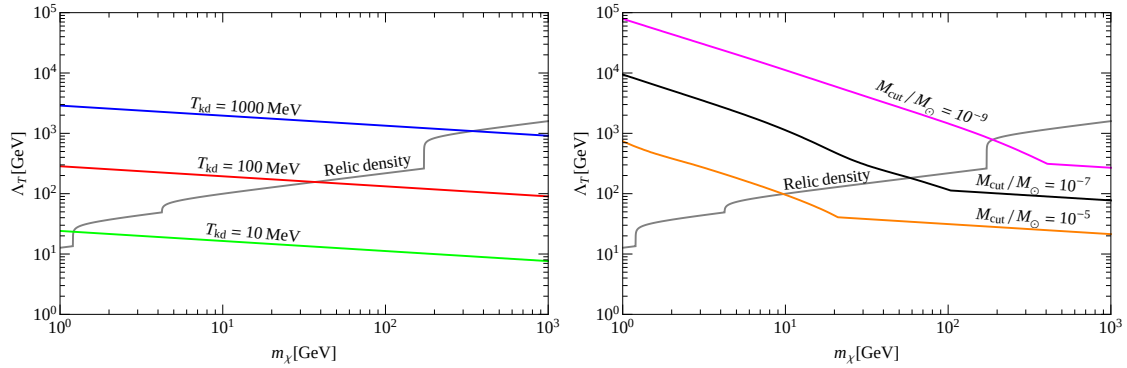

(a) *DM couples to all SM fermions.*

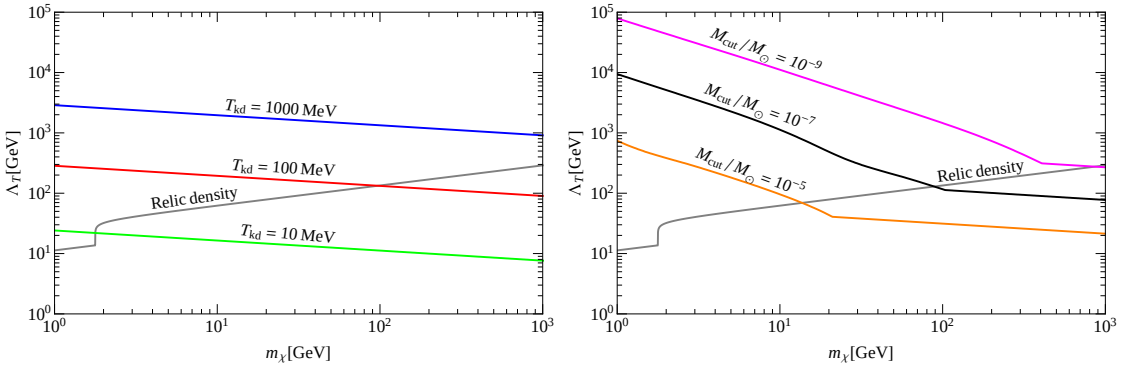

(b) *DM couples only to leptons.*

The results for universal couplings are given in figure 3.8a, while those for leptons only are in figure 3.8b. As a tensor mediated interaction cannot be implemented in CalcHEP, we do not use micrOMEGAs to calculate the relic density, but rather require the velocity averaged cross section to equal the canonical value for s-wave annihilation that gives the correct relic density, i.e

$$\langle \sigma v_{\rm rel} \rangle = \sum_f \frac{9}{2\pi} \frac{m_f^2 m_\chi^2}{\Lambda_T^6} \left(1 - \frac{m_f^2}{m_\chi^2}\right)^{1/2} \approx 3 \times 10^{-26} \, \frac{\rm cm^3}{\rm s} \,, \tag{3.9}$$

where the sum is over all kinematically accessible fermion annihilation products. Once again, after QCD confines in the early universe there is no pion configuration which has the Lorentz transformation properties of a tensor, and thus quark couplings become irrelevant below T_c.

Fig. 3.8a indicates that for good thermal relics, the expected kinetic decoupling temperatures are of 10 MeV in the few GeV mass range, up to 100 MeV for a 30 GeV WIMP, and to 1 GeV for a 300 GeV WIMP. The resulting small-scale cutoff masses are of 10^{-5} $M_\odot$ for a 10 GeV WIMP mass, decreasing to below 10^{-9} $M_\odot$ for masses above 200 GeV. For the exclusively leptonic coupling tensor case, we find a qualitatively similar behavior, with good thermal relics producing slightly lower kinetic decoupling temperatures, and slightly larger cutoff scales.

3.3 Discussion and conclusions

In this study, we addressed the question of establishing the small-scale cutoff of the cosmological matter power spectrum in a variety of particle dark matter models where WIMP coupling to Standard Model fermions is described by effective operators. We included

cases where the dark matter separately couples exclusively to leptons, exclusively to quarks, or universally to both leptons and quarks. We also used collider searches and dark matter direct detection to set model-independent limits on the largest experimentally viable value of the small-scale cutoff resulting from kinetic decoupling for each class of operators, and we calculated the dark matter thermal relic abundance on the same parameter space.

The largest possible cutoffs are found for theories where the dark matter exclusively couples to leptons, as a result of the absence of limits from hadron colliders. For the case of coupling to quarks, in some cases direct dark matter searches squeeze the maximal cutoff scale for protohalos to very small values, in some instances much smaller than the Earth mass. Insisting on setups that produce a thermal relic density in accordance with the observed dark matter density we universally find increasingly suppressed small scale cutoffs with increasing dark matter particle masses.

For theories with quark-only couplings, if the kinetic decoupling falls below the QCD confinement phase transition, two effects exhibit an interesting interplay: scattering off of the lightest available hadronic bound states (pions) and loop-mediated scattering off of leptons, this latter process never having been considered before. We showed that depending on the operator's effective energy scale one or the other effect can dominate the kinetic decoupling process.

While there exist many instances of dark matter models where the effective operator description we adopted here does not apply, the present study has wide applicability to a broad range of WIMP models. In addition, our findings provide a model-independent framework where the relevant range for the small-scale cutoff to the matter power spectrum

can effectively be predicted. Finally, this study highlights the complementarity of collider and direct detection of dark matter with questions pertaining to the cosmology of dark matter and the formation of structure in the universe.

Chapter 4

Earthly Probes of the Smallest Dark Matter Halos

In the present analysis we point out that there might be orthogonal handles to pinpoint the size of primordial dark matter halos, and thus of the effective cutoff scale of structure in the universe. Our main observation is that the same class of processes entering kinetic decoupling – namely, elastic scattering off of light fermions – also enters the cross section for direct dark matter detection, which is determined by elastic scattering off of quarks inside nucleons. Additionally, in a situation of capture-annihilation equilibrium, the rate of high-energy neutrinos expected from the capture and annihilation of WIMPs in celestial bodies such as the Earth or the Sun also depends on the same scattering cross section. We therefore ask, in the present study, whether the mass of dark matter protohalos correlates with quantities that could be measured by experiments on Earth, be it via direct

Adapted from Jonathan M. Cornell and Stefano Profumo. "Earthly probes of the smallest dark matter halos". *JCAP* 1206 (2012), 011. DOI: 10.1088/1475-7516/2012/06/011. arXiv: 1203.1100 [hep-ph]

detection or with neutrino telescopes.

Here, we take a model-dependent view, and focus on two specific and well-defined WIMP scenarios: the lightest neutralino of the minimal supersymmetric extension to the Standard Model (MSSM) [7], and the lightest Kaluza-Klein (KK) excitation of Universal Extra Dimensions [see Ref. 61, for a review] For these two paradigmatic WIMP setups, we study correlations between the dark matter cutoff scale and rates for direct and indirect dark matter detection. We find that strong correlations exist for some quantities, and not for others. We discuss approximations and analytical formulae that help understanding our detailed numerical results, and we conclude that "earthly probes" of the size of the smallest dark matter halos are, in principle and with the model assumptions we detail here, possible.

The ensuing study is articulated as follows: In section 4.1, we explore the correlation that exists between direct detection rates and the cutoff scale for supersymmetric neutralinos. In section 4.1.1 we explore in more detail the reason for this correlation, and in section 4.1.2 we do a similar analysis, but for neutrinos from neutralino annihilation in the sun. In section 4.2, we return to the analysis of 4.1, but for the case of KK dark matter, and finally in section 4.3 we discuss our results and draw our conclusions.

4.1 Neutralino dark matter

We first consider correlations between direct detection rates and protohalo size for MSSM neutralino dark matter. To calculate the dark matter direct detection rates we use the routines in the numerical package DarkSUSY (see Ref. [35]; for an in-depth description of the direct detection calculation see also Ref. [82]), while $T_{\rm kd}$ is calculated numerically as

described in section 2.1.3. We define our MSSM models by 9 parameters given at the weak scale: μ, M_1, M_2, M_3, m_A, $\tan\beta$, $m_{\rm sq}$, A_t and A_b. This is the same parameterization as the "MSSM-7" described in [35] (to which we refer the Reader for further details), with the change that we let M_1, M_2 and M_3 vary freely, while in the MSSM-7 the two parameters M_1 and M_3 are related to M_2 through GUT-scale gaugino mass universality relations. The parameters μ, M_1, M_2, M_3, m_A and $m_{\rm sq}$ are scanned over logarithmically in the range of 50 GeV to 5 TeV, with M_2 and μ allowed to take positive or negative values. $\tan\beta$ is scanned logarithmically over the range 2 to 50, while A_t and A_b are scanned over linearly in the range of -5 to 5.

All of the models we present in are checked against the accelerator and other particle physics constraints contained in the most recent version of DarkSUSY, 5.0.5. They are also checked to see if they satisfy the 5σ bounds on the relic density from the most recent seven year release of WMAP data, in which $\Omega_\chi h$ is constrained to the values $.0840 < \Omega_\chi h < .1400$ [83]. The relic density for each model is calculated with coannihilations using the routines in DarkSUSY [35]. Current (solid line) and future (dashed line) sensitivities from direct detection experiments are also included on many of the the plots. For plots with spin independent scattering cross sections, we present the current sensitivity of the Xenon100 experiment from [84] and the projected sensitivity of the Xenon1T experiment found at [85]. For spin dependent plots, we present the current sensitivity of the 4kg COUPP detector [86] and the expected sensitivity of the future 60 kg COUPP detector [87].

The elastic spin-independent neutralino-nucleon cross section depends, at the microscopic (quark) level, and at tree-level in perturbation theory, on two sets of diagrams:

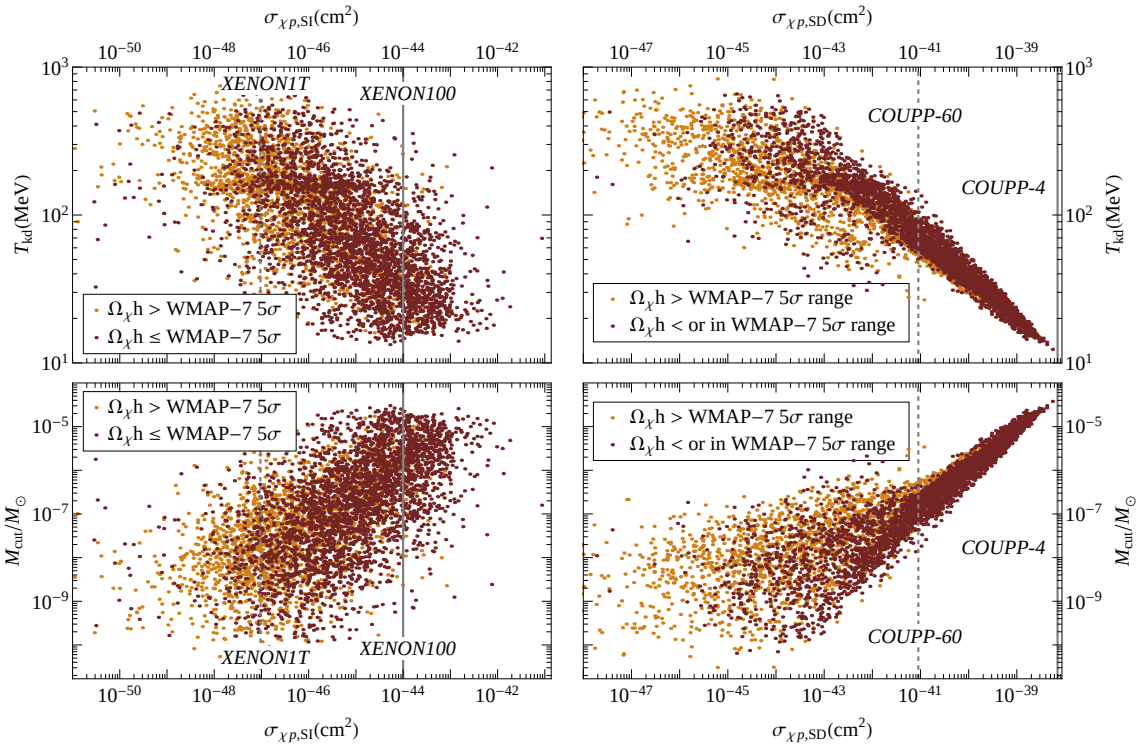

Figure 4.1: *A scatter plot showing the correlation between the neutralino-proton spin-independent (left panels) and spin-dependent (right panels) cross sections with the kinetic decoupling temperature (upper panels) and with the cut-off scale mass (lower panels), for a large sample of supersymmetric models. See the text for details on the definition of the quantities plotted and for details of the scan over the supersymmetric parameter space. All sensitivities presented in this plot are for a 100 GeV WIMP.*

(i) Higgs exchange (including, in absence of CP violation, the two CP-even Higgses) and (ii) squark exchange [7]. Elastic spin-dependent (axial) interactions are also mediated by squark exchange, as well as by Z exchange. Processes relevant to elastic scattering of neutralinos off of light leptons and quarks depend on all scattering processes. Since kinetic decoupling typically occurs at low temperatures, where heavier fermions no longer participate in the thermal bath, Yukawa-suppressed Higgs-exchange processes are generically

subdominant with respect to Z and squark/slepton exchange. This consideration leads us to anticipate that the correlation between kinetic decoupling temperature $T_{\rm kd}$ and the spin-independent elastic neutralino-proton cross section $\sigma_{\rm SI}$ be *weaker* than the correlation with spin-dependent processes, $\sigma_{\rm SD}$.

The theoretical anticipation is in fact confirmed by the results of the extensive scan over MSSM parameters we carried out, shown in Fig. 4.1. The upper panels correlate the scalar and axial cross sections with $T_{\rm kd}$, while the lower panels with $M_{\rm cut}$. As expected, although a general trend is present, we do not find a tight correlation for scalar interactions (panels to the left), while a correlation is definitely present for axial interactions (panels to the right, especially for large and potentially experimentally interesting values of the cross section). The scatter in the correlation between $T_{\rm kd}$ and $\sigma_{\rm SD}$ is within a factor 2 down to $\sigma_{\rm SD} \sim 10^{-40}$ cm^2, and grows for smaller values of the cross section. The correlation has a very small spread at values of the cross section currently probed by the most sensitive detectors (for the most recent results from COUPP, probing cross sections as small as few $\times 10^{-39}$ cm^2 see [86]). We investigate and discuss the origin of this scatter in the following subsections. Note that $\sigma_{\rm SD} \sim 10^{-40}$ cm^2 (for a 100 GeV WIMP) corresponds approximately to the projected reach of a large (1 cubic meter) DMTPC detector with 50 keV threshold operating for one year [88]. This corresponds to a jump of about three orders of magnitude over the current detector performance (this does not include indirect limits from neutrino telescopes) [88, 86].

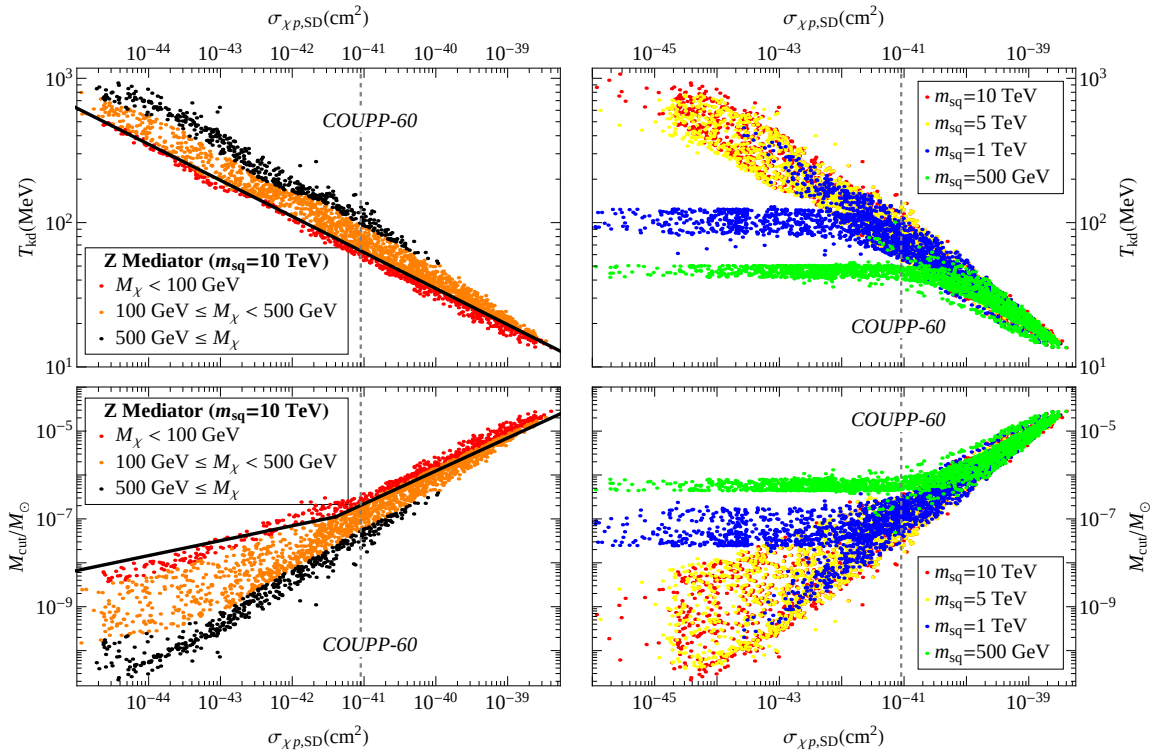

Figure 4.2: *Correlation between the neutralino-proton spin-dependent scattering cross section and the kinetic decoupling temperature (upper panels) or cut-off scale mass (lower panels). The panels to the left assume a common, large value for the squark mass* $m_{\mathrm{sq}} = 10$ *TeV, hence the dominant process for both kinetic decoupling and scattering off of protons is via* Z *exchange. The color coding indicates three ranges for the lightest neutralino mass, while the black line indicates the analytic formula of Eq. (4.4). In the right panels we illustrate the effect of lower squark/slepton masses, with* $m_{\mathrm{sq}} = 0.5,\ 1,\ 5$ *and* 10 *TeV corresponding to the four color codes. See the text for further details on the supersymmetric parameter space scan procedure. All of the models presented in this plot have values of* $\Omega_\chi h$ *within or less than the WMAP-7* 5σ *range. The experimental sensitivities are for a 100 GeV WIMP.*

4.1.1 The role of the neutralino and of the squark mass scale

There are two main sources for the scatter in the correlation found between $T_{\rm kd}$ and $\sigma_{\rm SD}$: the neutralino mass and the squark mass scale.[1] We discuss these effects both analytically and numerically in this section.

In the limit of heavy squark masses, kinetic decoupling and elastic neutralino-nucleon axial scattering are only mediated by Z-exchange, and should thus be tightly correlated. However, at a fixed value of $\sigma_{\rm SD}$, corresponding to a fixed value of the neutralino-Z coupling, $T_{\rm kd}$ inherits a dependence on the neutralino mass scale beyond that produced by the dependence of $\sigma_{\rm SD}$ on M_χ, resulting in a scatter in the values of $T_{\rm kd}$ for a given value of $\sigma_{\rm SD}$. We illustrate this effect (for both $T_{\rm kd}$ and $M_{\rm cut}$) in the left panels of Fig. 4.2. For this scan, we use the set of parameters as before, with the changes that the pseudoscalar Higgs boson mass m_A is set to 1000 GeV, the trilinear couplings $A_t = A_b = 0$, and, most importantly, $m_{\rm sq}$ is set to the high value of 10 TeV. The color-coded dots show models with neutralino masses in the $M_\chi < 100$ GeV (red), 100 GeV $< M_\chi <$ 500 GeV (orange) and $M_\chi > 500$ GeV (black).

The dependence of $T_{\rm kd}$ in the limit of heavy squarks can be understood analytically when we calculate both the neutralino proton scattering cross section and $T_{\rm kd}$ using just the Z exchange tree level diagram, ignoring contributions from slepton and squark exchange diagrams. The cross section of scattering a neutralino off a proton when Z exchange is the only diagram is given by (following, e.g. [7]):

$$\sigma_{\chi p,\rm SD} = \frac{3}{4\pi}\frac{(g_{Z11})^2 M_p^2}{M_Z^4}\left(\sum_{q=u,d,s}(g^L_{Zqq} - g^R_{Zqq})\Delta_q\right)^2 . \tag{4.1}$$

[1] Note that we always assume that squarks and sleptons are degenerate in mass.

To analytically approximate the kinetic decoupling temperature, we use the prescription described in section 2.1.3, which gives us

$$T_{\rm kd} = M_\chi \left(\left(\frac{a}{4} \right)^{1/4} \Gamma \left(\frac{3}{4} \right) \right)^{-1}, \tag{4.2}$$

where

$$a = \frac{31}{84} \sqrt{\frac{5\pi^3}{g_{\rm eff}}} \frac{(g_{Z11})^2 M_\chi^3 M_{\rm Pl}}{M_Z^4} \sum_f g_{SM} \left(\left(g_{Zff}^L \right)^2 + \left(g_{Zff}^R \right)^2 \right). \tag{4.3}$$

Here f is all possible SM scattering partners and $g_{\rm SM}$ is the number of degrees of freedom for the SM partners. Combining these expressions, we find

$$T_{\rm kd} = \frac{1}{\Gamma\left(3/4\right)} \left(\frac{252}{63} \sqrt{\frac{g_{\rm eff}}{5\pi^5}} \frac{M_p^2}{M_{\rm Pl}} \frac{\sum_q \left(\left(g_{Zqq}^L - g_{Zqq}^R \right)^2 \Delta_q \right)}{\sum_f g_{\rm SM} \left(\left(g_{Zff}^L \right)^2 + \left(g_{Zff}^R \right)^2 \right)} \frac{M_\chi}{\sigma_{\chi p,{\rm SD}}} \right)^{1/4}. \tag{4.4}$$

The $T_{\rm kd} \propto (M_\chi/\sigma_{\rm SD})^{1/4}$ behavior can be seen in the left hand side plots in Figure 4.2. To illustrate the validity of this approximation, we plot this expression as the black line in Figure 4.2, with the sum over fermions including all SM leptons except the quarks, and $g_{\rm eff}^{1/2} = 4$, a value which corresponds to $T_{\rm kd} \approx 70$ MeV. M_χ is set to 100 GeV, and from the upper left hand plot, we see that the analytic approximation follows the numerical result well for low $T_{\rm kd}$, with the validity of the approximation becoming less valid at high $T_{\rm kd}$ because of that fact that before the QCD phase transition there is quark scattering which we do not consider and $g_{\rm eff}$ varies significantly from the value we chose.

As squark and slepton masses are lowered, the relative contribution from squark, but especially slepton exchange in the kinetic decoupling process increases. As a result, for sufficiently low squark/slepton masses (which we assume to be at the same scale) the correlation between $T_{\rm kd}$ and $\sigma_{\rm SD}$ is lost. Namely, we expect $T_{\rm kd}$ to be driven by the sfermion

mass, while $\sigma_{\rm SD}$ is tuned by the Z-neutralino coupling and is relatively insensitive to the squark mass scale. We illustrate this numerically, and we assess the importance of this factor in a robust determination of $T_{\rm kd}$ from a measurement of $\sigma_{\rm SD}$, in the right panels of Fig. 4.2. The color-coding shows models where we fix the sfermion mass scale to 10 TeV (red), 5 TeV (yellow), 1 TeV (blue) and 500 GeV (green). The figure shows that deviations from the expected correlation arise at $\sigma_{\rm SD} \lesssim 10^{-44}$ for 5 TeV sfermions, and at $\sigma_{\rm SD} \lesssim 10^{-42}$ for 1 TeV sfermions. For sub-TeV sfermions the correlation can become weaker, although given the negative results on squark and slepton searches from the LHC [89] we expect little effect from light sfermion contributions if $\sigma_{\rm SD}$ is close to the range that could be probed by next generation experiments, $\sigma_{\rm SD} \gtrsim 10^{-40}$.

We also consider the situation in which there is no Z-exchange in scattering processes, corresponding to the limit of a purely bino-like neutralino. To obtain models with such composition, we use a modified version of the original parameter set where we enforce $\mu = M_2 = 10$ TeV, $m_A = 1$ TeV, and $A_t = A_b = 0$. This leaves us with the parameters M_1, M_3 and $m_{\rm sq}$, which are scanned logarithmically over the range 50 GeV to 5 TeV, and $\tan\beta$, which is scanned logarithmically over the range 2 to 50. A plot of $T_{\rm kd}$ and $M_{\rm cut}$ versus $\sigma_{\rm SD}$ for these models is shown in Fig. 4.3. As binolike neutralinos are very weakly interacting, only about 100 of the 2.5×10^3 models in the plot do not produce a relic density greater than the WMAP-7 5σ range.

For such a class of models, we see a correlation between $T_{\rm kd}$, $M_{\rm cut}$, and $\sigma_{\rm SD}$, with, just as before, an additional dependence on the neutralino mass. Unlike in the high $m_{\rm sq}$ case, there is a scatter of large neutralino mass models down into the smaller mass bands.

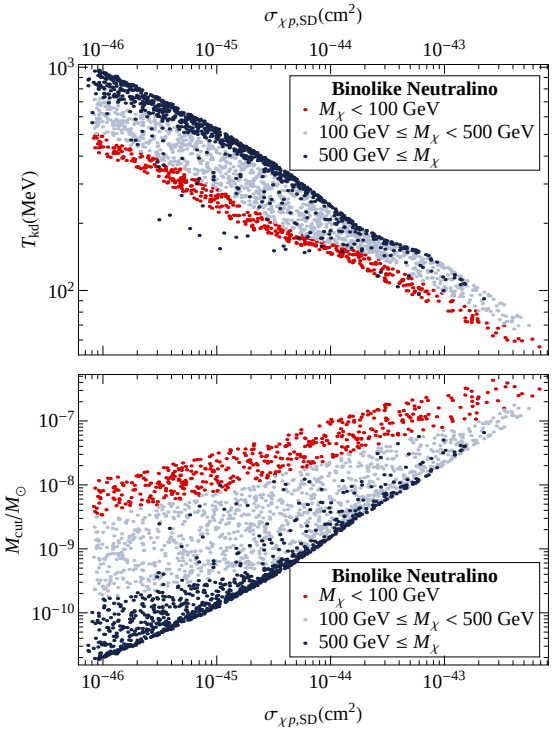

Figure 4.3: *A scatter plot showing the correlation between the neutralino-proton spin-dependent scattering cross section and the kinetic decoupling temperature (upper panel) or cut-off scale mass (lower panel) for supersymmetric models with bino-like lightest neutralinos, hence with suppressed coupling to the Z. The three colors correspond to different ranges of neutralino mass.*

We have identified these models as having a small splitting between M_χ and m_{sq}. In [24], it was shown that for binolike neutralinos, T_{kd} is of the form:

$$T_{\mathrm{kd}} = 7.5 \text{ MeV} \left(\frac{M_{\tilde{l}}^2}{M_\chi^2} - 1 \right)^{1/2} \left(\frac{M_\chi}{100 \text{ GeV}} \right)^{5/4} \tag{4.5}$$

Since in the MSSM-7 parameterization the squark mass scale is the same as the slepton mass scale, when $\left(m_{\mathrm{sq}}^2 - M_\chi^2\right)/M_\chi^2 \ll 1$, T_{kd} is driven to a much smaller value than when the splitting is large, as can be appreciated from Eq. (4.5). When Z-exchange is the only process relevant for the interaction, the mass splitting does not enter into T_{kd}, and we see

no similar effect.

For these models, the highest possible spin dependent cross section is significantly smaller than that of the models from the full parameter space scan as well as that for models where sfermion exchange diagrams are suppressed. As such, these are not models that the current generation of direct detection experiments would explore: this additional source of scatter in the correlation between protohalo size and scattering cross section is thus not worrisome, at a practical level. Furthermore, for general sets of models where one has both Z and sfermion exchange scattering diagrams, these results show that when there is a relatively large scattering cross section, the sfermion exchange contribution to that cross section is subdominant to the contribution from Z exchange: for supersymmetric models that might be detectable with current or future generation detectors it is thus valid to approximate the scattering cross section as being due solely to Z exchange.

4.1.2 Neutrino telescopes

Spin-dependent neutralino-nucleon interactions drive, quantitatively more than spin-independent interactions, the capture rate of neutralinos in the Sun. If the neutralino pair-annihilation rate is large enough so that capture and pair-annihilation in the Sun are in equilibrium (which is typically the case across the MSSM parameter space [90]), the actual rate of neutralino annihilation is governed by the capture rate. We thus expect a correlation of the rate of high-energy neutrinos resulting from neutralino annihilation inside the Sun and $T_{\rm kd}$. Note that effects such as the detector energy threshold are expected to impact the correlation and to potentially disrupt it.

We investigate in Fig. 4.4 the correlation between the flux of neutrinos from the

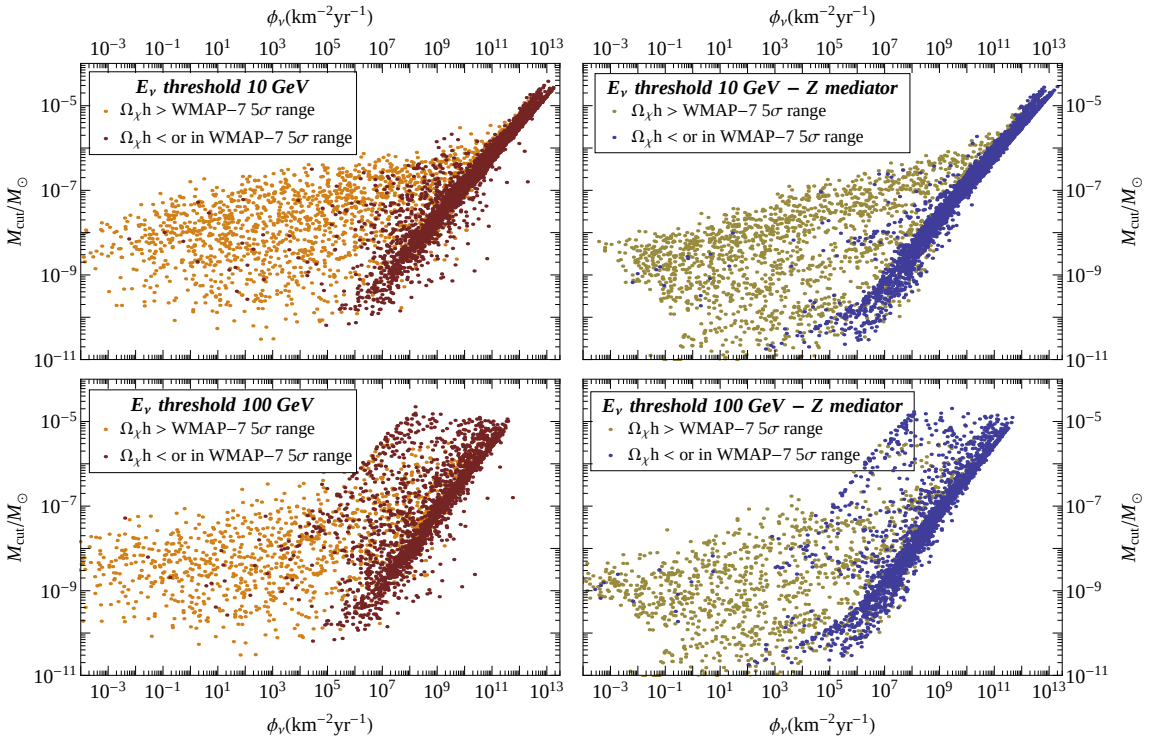

Figure 4.4: *A scatter plot showing the correlation between the flux of neutrinos from the Sun from dark matter annihilation with the cut-off scale mass (lower panels), for a large sample of supersymmetric models. The panels to the right focus on models with large squark masses. The upper panels use a threshold of 10 GeV for the neutrino energy, while the lower ones use 100 GeV. See the text for details on the definition of the quantities plotted, and for details of the scan over the supersymmetric parameter space.*

Sun integrated above two representative energy threshold, namely 10 GeV (upper panels) and 100 GeV (lower panels). Models in the two panels on the right assume heavy squark masses, while those on the left scan over the general MSSM parameter space as before. To calculate the neutrino flux, the routines from DarkSUSY described in [35, 91] are used. We note that a rather tight correlation exists between the neutrino flux from the Sun, ϕ_ν, integrated above 10 GeV and $M_{\rm cut}$, as long as $\phi_\nu > 10^{11}$ km^{-2}yr^{-1}. The most recent IceCube

results looking for neutrinos from solar WIMP annihilation through the W^+W^- channel claim a sensitivity to a total muon flux from this annihilation of about 3×10^2 km^{-2}yr^{-2} for a 1 TeV WIMP [92]. Using the routines from DarkSUSY, we find that this muon flux corresponds to a range of incoming total neutrino fluxes from about $10^{10} - 10^{13}$ km^{-2}yr^{-2} for MSSM models when the neutrino threshold energy is 10 GeV.

Larger energy thresholds tend to loose the desired correlation: a very significant dependence on the neutralino mass is present in the flux above 100 GeV, as, for example, almost no neutrinos with those energies are produced for neutralinos with masses below 200 GeV or so. Therefore, a model with a given $M_{\rm cut}$ can well have a vanishing neutrino flux if the neutralino mass is small enough! Interestingly, with the deployment of the DeepCore detector [93] the effective energy threshold for neutrino detection of the IceCube system has been significantly lowered. Again, for fluxes large enough to be above potentially detectable levels, we find that a tight correlation with $M_{\rm cut}$ is present. The correlation we find is expected to further improve should plans to deploy an additional, even more thickly instrumented section of the detector, PINGU, come to fruition [94].

4.2 Universal extra dimensions

As discussed in section 2.2.2, the particle properties of the lightest KK particle[2] depend in mUED upon three parameters: the effective cut-off scale Λ, the inverse compactification radius $1/R$, and the value of the Standard Model Higgs mass (which at the time this analysis was undertaken was still uncertain). The latter quantity is especially crucial for

[2]We shall use LKP and $B^{(1)}$ interchangeably in what follows.

the calculation of the spin-independent LKP-nucleon scattering cross section. $1/R$, instead, sets the mass scale of the KK levels, including the mass of the LKP, while Λ feeds in the details of the particle spectrum. Here, we consider the range 500 GeV $< 1/R <$ 1400 GeV, $10 < \Lambda R < 40$ for our scans. We also scan over the values of the Higgs mass allowed by current collider constraints [95, 96, 97], with a maximum Higgs mass of 600 GeV. We then find the relic density for all models using the results of [98] and check these against WMAP relic density constraints.

As for neutralinos, the same diagrams contributing to elastic $B^{(1)}$-nucleon scattering contribute to the process of kinetic decoupling. In particular, spin-dependent scattering depends upon KK-quark exchange, while spin-independent scattering is primarily driven by processes mediated by Higgs exchange. As a result, the general expectation for UED is not dissimilar to what we saw in the context of supersymmetry: a tight correlation between spin-dependent elastic processes and kinetic decoupling, and a looser correlation for the scalar cross section. Figures 4.5 and 4.6 accurately confirm these expectation. In Fig. 4.5 we show, for 5000 minimal UED models, the correlation between the elastic spin-dependent cross section and the kinetic decoupling temperature (top panel) and cut-off mass scale (lower panel). All of these models have the same Higgs boson mass, 125 GeV, which does not effect the calculation of $T_{\rm kd}$ or $M_{\rm cut}$, but does have a large effect on the relic density. Here $T_{\rm kd}$ is once again calculated using the numerical method described in section 2.1.3, while the spin dependent cross section is calculated using the approximate formula from Ref. [61, 99]:

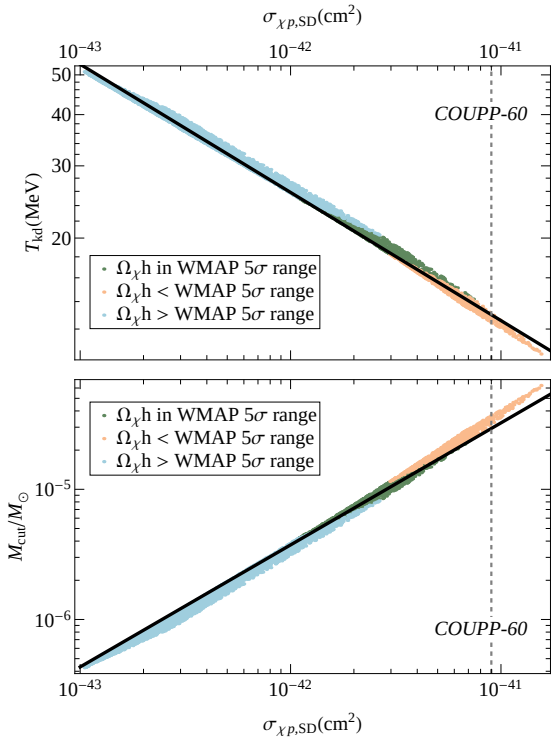

Figure 4.5: *A scatter plot showing the correlation between the $B^{(1)}$-proton spin-dependent cross section with the kinetic decoupling temperature (upper panel) and with the cut-off scale mass (lower panel), for a large sample of universal extra-dimensional models, and the analytic approximation of Eq. (4.8). Plotted sensitivities are for a 1 TeV WIMP. See the text for details on the scan over the UED parameter space.*

$$\sigma_{B^{(1)}p,\mathrm{SD}} \approx 1.8 \times 10^{-42}\ \mathrm{cm}^2 \left(\frac{1\ \mathrm{TeV}}{M_{B^{(1)}}}\right)^4 \left(\frac{0.1}{\Delta_q}\right)^2 . \tag{4.6}$$

In the formula above, Δ_q is the mass splitting between the right handed quarks and the LKP, $\Delta_q = (M_{q_R^{(1)}} - M_{B^{(1)}})/M_{B^{(1)}}$, with all of the KK quarks taken to have the same mass for simplicity. An analytic approximation for T_{kd} was already found in [24], which is

$$T_{\mathrm{kd}} \approx 3 \times 10^2\ \mathrm{MeV} \Delta_e^{1/2} \left(\frac{M_{B^{(1)}}}{1\ \mathrm{TeV}}\right)^{5/4} , \tag{4.7}$$

with $\Delta_e = (M_{e^{(1)}} - M_{B^{(1)}})/M_{B^{(1)}}$. Putting together equations (4.6) and (4.7), we get an analytic approximation relating $T_{\rm kd}$ and $\sigma_{B^{(1)}p,\rm SD}$:

$$T_{\rm kd} \approx 36 \text{ MeV} \left(\frac{\Delta_e}{.01}\right)^{1/2} \left(\frac{.1}{\Delta_q}\right)^{5/8} \left(\frac{10^{-42} \text{ cm}^2}{\sigma_{B^{(1)}p,\rm SD}}\right)^{5/16}. \tag{4.8}$$

There is no dependence on dark matter mass as there was in the SUSY case, rather the kinetic decoupling temperature just goes like $\sigma_{\rm SD}^{-5/16}$, leading to the strong correlation displayed in Figure 4.5. The validity of this approximation is shown by plotting it as the black line in Figure 4.5, with $\Delta_e = .17$ and $\Delta_q = .1$. For the relatively low values of $T_{\rm kd}$ we find for UED models, $M_{\rm cut}$ is always set by the acoustic oscillation cutoff of equation (2.21). In plotting the analytic approximation for $M_{\rm cut}$, we use $g_{\rm eff} = 3.5$, which corresponds to $T_{\rm kd} \approx 30$ MeV.

In the spin-independent case, to find the cross section we use the approximation from [61, 99]:

$$\sigma_{B^{(1)}p,\rm SI} \approx 1.2 \times 10^{-46} \text{ cm}^2 \left(\frac{1 \text{ TeV}}{m_{B^{(1)}}}\right)^2 \left[\left(\frac{100 \text{ GeV}}{M_h}\right)^2 + 0.09 \left(\frac{1 \text{ TeV}}{m_{B^{(1)}}}\right)^2 \left(\frac{0.1}{\Delta_q}\right)^2\right]^2. \tag{4.9}$$

The results of using this formula are shown in Fig. 4.6, where were are now scanning over a full range of Higgs masses. Here the scattering cross section at a given value of $1/R$ depends sensitively on the value of the Standard Model Higgs mass M_h, as shown in the top panel to the left. In the figure, the green points correspond to values allowed before the most recent LHC results on searches for the Standard Model Higgs [95], which are now ruled out (the region without points corresponds to values of M_h already ruled out by searches with the Tevatron and LEP [96, 97]). LHC results have therefore severely constrained the prediction for the scalar $B^{(1)}$-nucleon scattering cross section to a range of about an order

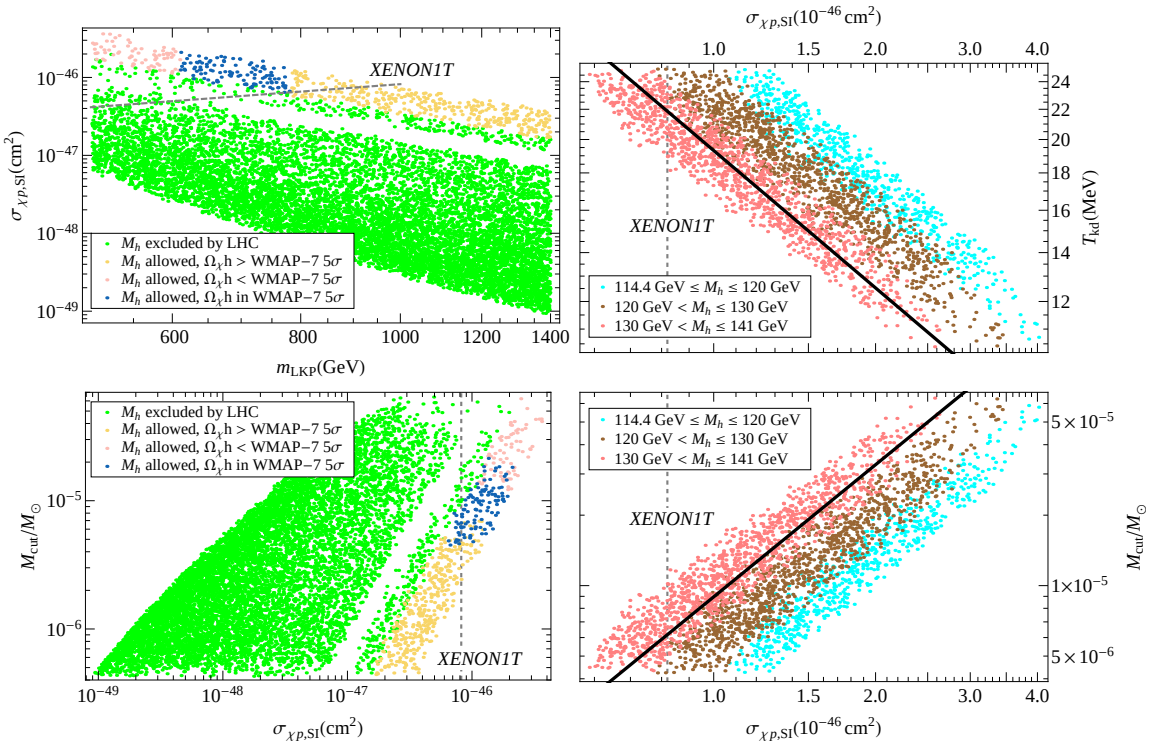

Figure 4.6: *Left: a scatter plot correlating the LKP mass with the LKP-proton spin-independent scattering cross section (upper panel), and correlating the same cross section with the cut-off scale mass (lower panel), for a set of models featuring both LHC-allowed and excluded values for the Higgs mass. Right: a scatter plot correlating the $B^{(1)}$-proton spin-independent cross section with the kinetic decoupling temperature (upper panel) and with the cut-off scale mass (lower panel), for a large sample of universal extra-dimensional models, and for a range of Higgs masses. In all panels except the top left, the plotted sensitivities are for a 1 TeV WIMP. In the right hand panels, all of the models produce a relic density that is within or less than the WMAP-7 constraints on $\Omega_\chi h$.*

of magnitude around 10^{-46} cm^2, along with significantly tightening the correlation between $1/R$ and this cross section. This, in turn, implies a correlation of the latter cross section with the cutoff scale, illustrated in the lower-left panel.

In the future, more accurate measurements of M_h will yield an increasingly tighter

correlation between the spin-independent cross section and the kinetic decoupling temperature and cutoff scales, as we show in the right panels. There, we show with different colors models corresponding to the ranges $114.4 < M_h/\text{GeV} < 120$ (cyan), $120 < M_h/\text{GeV} < 130$ (brown) and $130 < M_h/\text{GeV} < 141$ (red). We also calculate the expected analytic form for the correlation between the quantities shown in the right panels. As Higgs exchange dominates over the KK quark exchange processes in the calculation of the spin independent scattering cross section, we approximate Eq. (4.9) as

$$\sigma_{B^{(1)}p,\text{SI}} \approx 1.2 \times 10^{-46}\ \text{cm}^2 \left(\frac{1\ \text{TeV}}{m_{B^{(1)}}}\right)^2 \left(\frac{100\ \text{GeV}}{M_h}\right)^4. \tag{4.10}$$

Combining equations (4.7) and (4.10), we find

$$T_{\text{kd}} \approx 34\ \text{MeV} \left(\frac{\Delta_e}{.01}\right)^{1/2} \left(\frac{100\ \text{GeV}}{M_h}\right)^{5/2} \left(\frac{10^{-46}\ \text{cm}^2}{\sigma_{B^{(1)}p,\text{SI}}}\right)^{5/8}. \tag{4.11}$$

This approximation for T_{kd} and the corresponding result for M_{cut} are plotted in the right hand side of Fig. 4.6, for $M_h = 125$ GeV and $\Delta_e = .01$. The analytic approximation underestimates T_{kd} slightly, which is due to ignoring the KK quark exchange processes in the expression we use for σ_{SI}. However, the behavior of the numerical and analytic results is the same, with $T_{\text{kd}} \propto (M_h^4 \sigma_{\text{SI}})^{-5/8}$ and with a scatter occurring due to the varying mass splittings.

Finally, we note that we estimated the neutrino flux from the Sun in the case of LKP dark matter, with results that mirror the same behavior and correlation as we found in the case of supersymmetric models, illustrated in Fig. 4.4. It is shown in Ref. [100] that the event rate in neutrino telescopes correlates strongly with $M_{B^{(1)}}$. We have shown that for both the spin dependent and independent cases in UED there is also a correlation

between $M_{B^{(1)}}$ and the scattering cross section. This is shown analytically in Eq. (4.6) for the spin dependent case and numerically in the upper left hand panel of Fig. 4.6 for the spin independent case. Therefore, there is a resulting correlation between the neutrino flux and $\sigma_{\rm SD}$ or $\sigma_{\rm SI}$. The larger mass of LKP with respect to the possibly light neutralino case produces a slightly smaller spread as the one shown in Fig. 4.4, especially with a larger neutrino energy threshold.

4.3 Discussion and conclusions

We addressed the possibility of establishing the small-scale cutoff of the cosmological matter power spectrum in a variety of particle dark matter models via dark matter direct and indirect detection experiments. We argued, and showed with analytical calculations and numerical results, that the kinetic decoupling temperature, which sets the cutoff scale, correlates tightly with the spin-dependent elastic scattering cross section of WIMPs off of nucleons. There also is a generically tight correlation with the flux of high-energy neutrinos from the Sun - whose intensity depends on the capture rate of WIMPs in the Sun, in turn set by the same axial scattering cross section. A weaker correlation is found in the case of scalar WIMP-nucleon interaction. Control over the spectrum and properties of the Higgs sector will dramatically improve this latter correlation, especially in the case of minimal Universal Extra Dimensions. All correlations we found are tightest when the detection rates are largest.

In summary, we find that "earthly" probes of the small-scale cutoff to the cold dark matter power spectrum are possible in the foreseeable future. Multiple measurements,

for example of both scalar and axial scattering cross sections and of a flux of neutrinos from the Sun, would help pinpoint a concordance dark matter model and, in view of the results reported here, its cosmological bearings on structure formation.

Chapter 5

Cosmological and Terrestrial Probes of Dark Matter in mUED

Any model of new physics beyond the standard model is now confronted by a new constraint stemming from the recently discovered Higgs boson [63]. Many models have been designed to explain why the Higgs can be light in spite of quantum corrections which naïvely are expected to push the particle's mass up to high scales; those models generically make predictions for what the Higgs mass would be if the corresponding mechanism is correct. Even models which do not address this hierarchy problem are at least required to match the experimental data pouring in regarding this new particle. For relatively simple models like minimal UED, the decrease in the viable parameter space leads to new predictive power: the parameter space of minimal UED is in fact reduced to being effectively two-dimensional.

Adapted from Jonathan M. Cornell, Stefano Profumo, and William Shepherd. "Dark matter in minimal universal extra dimensions with a stable vacuum and the 'right' Higgs boson". *Phys.Rev.* D89.5 (2014), 056005. DOI: 10.1103/PhysRevD.89.056005. arXiv: 1401.7050 [hep-ph]

The discovery of the Higgs and the measurement of its mass has additional implications for mUED models. In the Standard Model it appears that the electroweak vacuum is only metastable according to the central values of the measured Higgs and top quark masses, but it is actually still possible that the vacuum remains stable up to the Planck scale [101]. This behavior is, of course, modified in the presence of any new physics scenario intervening at some mass scale intermediate between the electroweak and Planck scales. In the context of the UED picture, the vacuum stability is under significant additional stress by the presence of numerous KK fermions strongly coupled to the Higgs, leading to very significant bounds on the parameter space of the model [66].

In this work we focus on the region of parameter space of mUED which is compatible with the Higgs mass and properties, with the requirement of a sufficiently long-lived electroweak vacuum, with direct collider searches for KK particles at the LHC, with the requirement of the lightest KK particle to have the correct thermal relic density and, finally, with such particle be compatible with direct dark matter searches.

In some of the previous studies, the parameter space considered in light of UED dark matter phenomenology had been the KK scale R^{-1} and the Higgs mass M_h, or R^{-1} and the cut-off scale ΛR for putative values of M_h (see e.g. [61] and references therein). Now that the Higgs mass has been experimentally measured, we can consider the complete parameter space in one plot, and at the same time extract interesting implications from the vacuum stability requirement, since the ultra-violet (UV) cutoff of the theory is lowered, which is precisely where vacuum stability concerns force the theory to live. Shortly before this work was released, a compendium of recent UED constraints appeared [102]. Our work

contrasts with this one in our focus on the low values of the cutoff scale favored by the vacuum stability constraint, but our conclusions are qualitatively similar for the parameter space where our studies overlap.

This study is organized as follows. We discuss current bounds from collider searches in section 5.1. We then consider the dark matter physics of the model in section 5.2. Finally, we present our conclusions in section 5.3.

5.1 UED at the LHC

Theories of universal extra dimensions have sometimes been dubbed "bosonic supersymmetry" because of the striking similarities with the phenomenology of supersymmetric models, especially at colliders. It is not surprising, therefore, that searches which are currently placing some of the most stringent constraints on mUED parameter space are typically "re-purposed" supersymmetry (SUSY) searches.

The first KK excitation level contains partners to all SM particles, much like a spectrum of superpartners. Generically, however, mUED predicts a much more compressed particle spectrum than what one would expect from MSSM superpartners, particularly in the region of low ΛR suggested by the properties of the Higgs and by the constraint of vacuum stability. As a result, cascade decays in mUED are much more experimentally challenging than in supersymmetry: all of the SM particles produced are much softer. Nevertheless, interesting bounds can be placed on the mUED parameter space in the simplest searches for squark pairs.

Most of the bounds alluded to above come from initial state radiation (ISR) jets

produced in association with the KK excitations. The ISR jets pass the cuts designed to catch the jets from the squark decay to quark and neutralino, and the momentum of the KK excitation is transferred almost entirely into the DM candidate. Current bounds from these searches are detailed in Ref. [103], and are presented along side our main results in Fig. 5.1. They constrain the UED mass scale R^{-1} to be greater than approximately 825 GeV, and are largely independent of ΛR.

Searches for SUSY which require leptons in the final state can, in principle, have more sensitivity to the cascade decays in mUED than those which use only jets, as soft leptons are much more rare in background than soft jets. The use of such searches to set limits on 6-D UED scenarios was discussed in [104], while the ATLAS experiment itself has recast some of its SUSY searches in this light for mUED [105]. These bounds, also shown in Fig. 5.1, exhibit an interesting behavior with ΛR. They are very weak for the extremely degenerate spectra at very small $\Lambda R \sim 5$, and become most strong at $\Lambda R \sim 10$, where they bound R^{-1} to be greater than about 800 GeV. They then weaken as the colored states become heavier with further increases in ΛR. These bounds are theoretically a bit more robust than those depending on purely hadronic final states as they are less sensitive to possible mis-modelling of the ISR jets crucial to the hadronic signatures. A search which has been specially designed to find mUED may have more reach to the lower values of ΛR, but the backgrounds at low particle momenta will remain very difficult to overcome.

There has been recent interest in attempting to directly bound the second KK excitations of particles [106, 107, 108], as such particles can have loop-level coupling directly to SM fields, and thus may appear as resonances, thus much cleaner to detect than the

soft decay products of the first KK level particles. These searches, however, suffer from the smallness of the loop-induced couplings. As a result, the resulting constraints are generically weaker than those directly searching for the first level KK excitations and we do not include them in our plots. We also note that recent works have shown that current LHC constraints on the loop driven effective coupling of the Higgs to gluons [109] and to W bosons [110] seem to limit $R^{-1} > 1.3$ TeV, but constraints on R^{-1} from the limits on Higgs couplings to other particle species are far less stringent.

5.2 Dark matter in mUED

The relic density of the LKP has been calculated in several previous works, first by [111]. The key issue in this type of calculation is the presence of numerous particles freezing out at similar epochs to the LKP, given the mass-degenerate nature of the mUED spectrum. As a result, the inclusion of a more and more complete set of coannihilating partners [13] has been the name of the game in achieving the highest possible accuracy.

The original calculation of Ref. [111] was extended and refined in Ref. [112, 113], who considered coannihilation processes with all first level KK partners and included all possible tree level (co-)annihilations into 2 SM particles. The next step in complexity arises from the fact that, again due to the nature of the KK ladder, KK level 2 states have a mass comparable to twice the mass of KK level 1 particles, including the LKP. Resonant annihilation (albeit suppressed by small KK level 1-1-2 couplings) is thus a potentially very important effect. This point was addressed in Ref. [114, 115, 98], where it was pointed out that loop induced couplings of second level KK particles to a pair of SM particles

are important for the relic density calculation, as such couplings lead to the mentioned resonantly enhanced annihilation processes.

Finally, it was more recently pointed out, in Ref. [116], that annihilation into second level KK states should be considered in the calculation of the relic density as well, as many of these states will subsequently decay nearly entirely to SM states via a loop process, effectively contributing to the total cross section into SM particles relevant to the freeze-out process.

In this work we include *all the mentioned layers of complexity* in calculating the LKP relic density, and use the "right" Higgs mass [63]. Specifically, we use the most recent mUED CalcHEP model file discussed in [117], modifying it to include all-loop level couplings of second level KK states to SM particles discussed in [116], and use it in connection with version 3.2 of the micrOMEGAs code [80, 118] to calculate the LKP relic density. Our results are shown on the mUED parameter space $(R^{-1}, \Lambda R)$ by the shaded blue band in Fig. 5.1.

As previously discussed, our study focuses on the $(R^{-1}, \Lambda R)$ parameter space, as the Higgs mass is now known to high precision. In the calculation whose results are shown in Fig. 5.1, we have assumed that the second level KK photon and the second level KK Higgs particles and photons decay completely to SM particles. This is driven mainly by the fact that the masses of the second KK excitations are near or below threshold for the decay into the appropriate two first KK excitations, and other decays are loop-suppressed to the same degree as those directly to a SM pair. Including these particles in the final state collects the most important contributions to 3-body SM final states LKP annihilation.

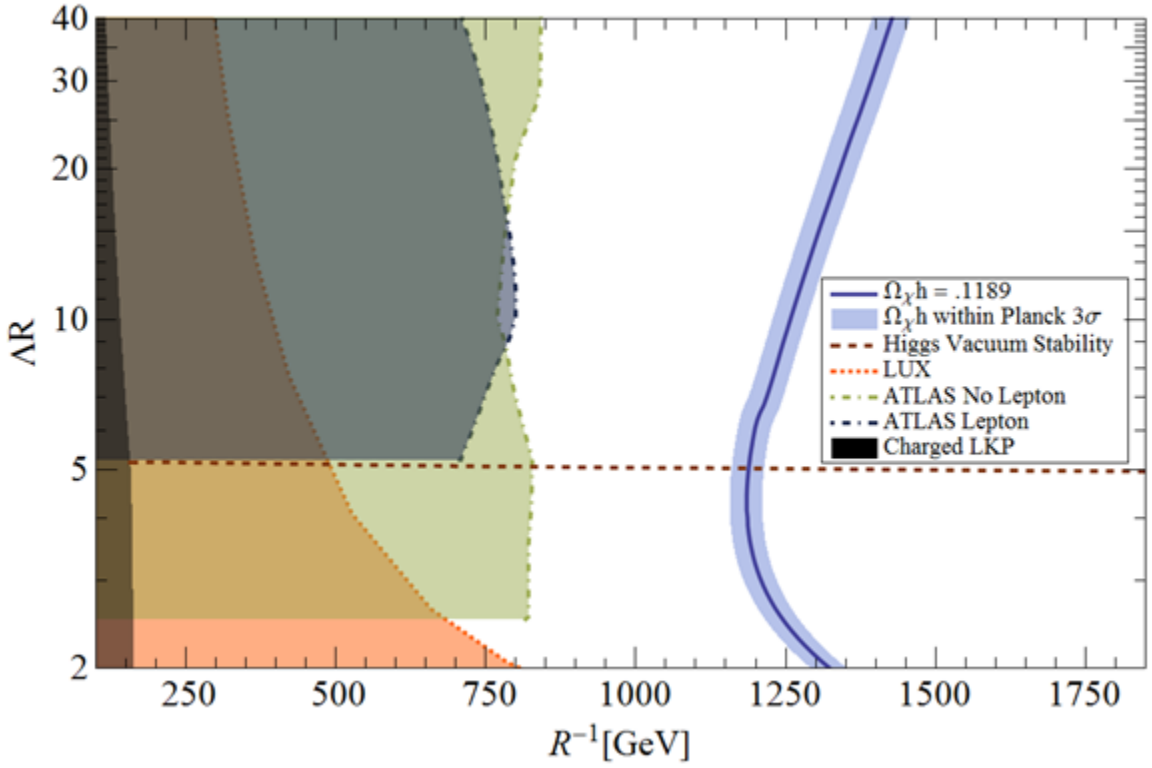

Figure 5.1: *Current collider, direct detection, Higgs vacuum stability, and cosmological limits on the mUED parameter space.*

In Fig. 5.1 the solid blue line corresponds to the best fit value for the dark matter relic density, $\Omega_\chi h = 0.1189$ [78], quoted by the Planck collaboration when including their cosmic microwave background (CMB) results, WMAP polarization results, high-l CMB data from ground telescopes, and baryon acoustic oscillation measurements. The shaded region around this line represents the 3 σ uncertainty on this result, corresponding to a range of values for $\Omega_\chi h$ between 0.1136 and 0.1238. All values of R^{-1} greater than the value traced by this line are forbidden as they lead to over-closure of the universe.

We also include the recent collider limits discussed in the previous section, as well as constraints on the parameter space from direct detection experiments [84]. For the latter, we have utilized spin independent cross sections as calculated with micrOMEGAs [119] and the most recent exclusion limits at 90% confidence level on these cross sections from the Xenon100 [75] and LUX [120] collaborations.

Finally, we have included the limit found by [66], requiring that the universe have a sufficiently stable electroweak vacuum. This is plotted as a dashed brown line in Fig. 5.1, and is approximately a constant upper bound on $\Lambda R < 5$ for all the mass scales of interest for dark matter physics.

One of the key findings of the present investigation is that the cosmologically favored value for the KK scale R^{-1} *increases* at low ΛR (the region of parameter space favored by vacuum stability constraints) as ΛR decreases, while the behavior is the opposite for higher values of ΛR. Inspecting the relevant processes contributing to the LKP freeze-out, we find that this is to be attributed to coannihilation processes between level 1 KK photons and other level 1 KK particles at low values of ΛR, particularly the KK excitations

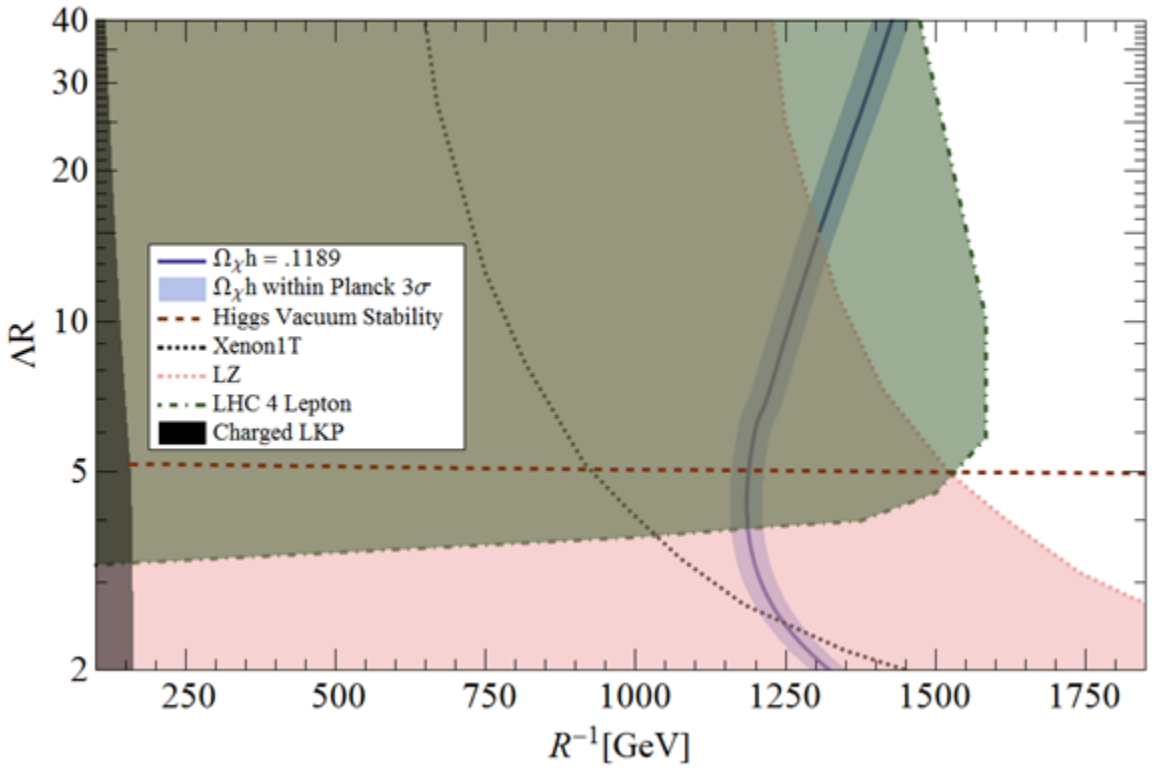

Figure 5.2: *Projected collider and direct detection sensitivities in the mUED parameter space.*

of the gluon and quarks, which quickly become irrelevant as ΛR increases because the splitting between the mass of the level one KK photons and colored KK particles grows rapidly.

In Fig. 5.2, we show the predicted sensitivities of the LHC and of future dark matter direct detection experiments in the mUED parameter space. The projected sensitivity of Xenon 1T is taken from [121], and the future LHC reach is based on a four-lepton search originally presented in [62], which has been updated to account for different possible splittings in [122]. We note that, since this final state requires splittings large enough to detect the leptons produced in cascade decays of KK particles, sensitivity is lost as the

smallest values of ΛR. These future bounds together leave only a small window of viable dark matter parameter space around R^{-1} of 1225 GeV and ΛR of 3. It is possible that future ISR-driven searches may have sensitivity to this region, but no explorations of that sensitivity which include the important systematic errors exist. Future generation-2 experiments such as DarkSide G2 and LZ will conclusively probe the entire range of parameter space, extending the reach of direct dark matter detection well beyond the cosmologically favored blue band [121], as shown by the pink dotted line.

We have also explored the effects on the calculation of the relic density of including the annihilation of the LKP to second-level KK states as well as the effect of including loop-induced vertices of second-level KK particles to SM particles. For a benchmark value of $\Lambda R = 20$, the cosmologically favored valued of $R^{-1} = 1340.8$ GeV when the calculation is done as described in the previous paragraphs. However, the favored value of the compactification scale drops to 1105.0 GeV when we do not take into account the decays of second level KK particles in the final state to SM states in our relic density calculation, and it drops further to $R^{-1} = 1011.9$ GeV when we then remove loop induced couplings of second level KK particles to SM particles from our CalcHEP model file. The effects of including these annihilation processes in the relic density calculation become more pronounced at increasingly higher values of ΛR. Therefore, our results are in agreement with those of Ref. [116]: the inclusion of loop-induced couplings and particularly annihilation processes with second level KK particles in the final state make a substantial difference in the calculation of the relic density pushing the KK scale to up to more than 30% higher, with obvious important phenomenological implications.

5.3 Discussion and conclusions

We explored the parameter space of the minimal Universal Extra Dimensions framework after the Higgs discovery. We outlined and gave an updated overview on the collider and direct dark matter constraints on the relevant parameter space defined, now that the Higgs mass is known, by the inverse compactification scale R^{-1} and the effective theory cutoff scale ΛR. These constraints effectively limit the KK scale R^{-1} to values in excess of 700-800 GeV, depending on the precise value of ΛR, with direct detection searches covering most effectively the low ΛR region where collider searches are less effective due to a highly degenerate mass spectrum.

The requirement that the electroweak vacuum be stable bounds the theory parameter space from above, setting an approximate upper limit to $\Lambda R < 5$ for mass scales that avoid overclosing the universe. We carried out the most accurate to-date calculation of the LKP relic density, and we found that the physics driving the LKP dark matter relic abundance in the low ΛR region is richer than previously thought. Several coannihilation partners for the LKP dark matter particle contribute significantly to the total effective pair-annihilation cross section, and important effects arise also from resonant KK-level 2 modes as well as from pair-annihilation into KK-level 2 particles subsequently decaying into SM particles. The overall result is a significant *increase* in the cosmologically favored R^{-1} range towards larger KK masses, as well as a non-trivial behavior with the cutoff scale ΛR. For intermediate values of ΛR, the benchmark range for R^{-1} is around 1.2 TeV. We note that our results for the relic density constraints differ from [122], because of our inclusion of resonances and annihilations to second level KK states in the calculation, increasing by

as much as 30% the cosmologically favored value of R^{-1}.

Finally, we discussed prospects for the detection of a signal from mUED with both direct detection and collider experiments. We showed that the cosmologically favored parameter space will be entirely exhausted by generation-2 direct dark matter noble gas experiments such as DarkSide G2 and LZ, and LHC searches should also cover much, perhaps all, of the viable parameter space for dark matter in mUED.

Chapter 6

Cosmic Antideuterons from Decaying Gravitino Dark Matter

In supersymmetric theories, R-parity[123, 124] is usually introduced to remove unwanted dimension four operators that would lead to fast proton decay; the renormalizable R-parity violating superpotential is:

$$W_{RPV} = \mu_i L_i \phi_u + \lambda_{ijk} L_i L_j \bar{\ell}_k + \lambda'_{ijk} L_i Q_j \bar{d}_k + \lambda''_{ijk} \bar{u}_i \bar{d}_j \bar{d}_k \,, \tag{6.1}$$

where the indices are generation indices, $i, j, k = 1, \ldots, 3$, and only antisymmetric combinations of i, j (respectively, j, k) are allowed in λ (respectively, λ''). The first three operators violate lepton number while the last violates baryon number, and both types of operators are involved in proton decay. It is then possible for the proton to be stable if only one type of operators is allowed, leaving B (or L) as an accidental symmetry of the theory [125, 126].

This is an aspect of the flavor problems associated with low energy Supersymmetry

Adapted from Angelo Monteux, Eric Carlson, and Jonathan Cornell. "Gravitino Dark Matter and Flavor Symmetries". *JHEP* 1408 (2014), 047. DOI: 10.1007/JHEP08(2014)047. arXiv: 1404.5952 [hep-ph]

(SUSY): generic soft terms give large contributions to flavor-changing neutral currents (FCNCs), which can be suppressed by assuming that flavor symmetries govern the structure of the Minimal Supersymmetric Standard Model (MSSM) Lagrangian. Two particularly well motivated types of flavor symmetries are Abelian horizontal symmetries (*a la* Froggatt-Nielsen [127, 128, 129]) and Minimal Flavor Violation (MFV) [130, 131], according to which the Higgs Yukawa operators are spurions of a $SU(3)^5$ flavor symmetry under which the full MSSM Lagrangian is invariant.

Under the assumption of these flavor symmetries, definite structures of the RPV couplings are predicted:

- with a horizontal $U(1)$ symmetry, the relative structure of the RPV couplings is completely determined by the fermion masses and mixings alone [132, 133, 134, 135]; the baryon number violating (BNV) or lepton number violating (LNV) operators are allowed or forbidden independently. In [132], it was argued that, in order not to disagree with LHC null results, LNV operators should be forbidden altogether when considering sub-TeV SUSY. The BNV couplings λ''_{ijk} are written in terms of an overall scale λ''_{323} and depend on the horizontal charges (we denote the charge of a field by the field symbol itself, $\Phi \equiv q_\Phi$, and the inter-generational difference between two fields as $\Phi_{ij} \equiv q_{\Phi_i} - q_{\Phi_j}$):

$$\lambda''_{ijk} = \lambda''_{323}\varepsilon^{u_{i3}+d_{j2}+d_{k3}}, \qquad \left(\text{where } \varepsilon \equiv V_{12}^{CKM} \simeq \sin\theta_C\right), \tag{6.2}$$

$$\begin{pmatrix} \lambda''_{112} & \lambda''_{212} & \lambda''_{312} \\ \lambda''_{113} & \lambda''_{213} & \lambda''_{313} \\ \lambda''_{123} & \lambda''_{223} & \lambda''_{323} \end{pmatrix} = \lambda''_{323} \begin{pmatrix} 3\times10^{-5} & 3\times10^{-3} & 5\times10^{-2} \\ 1\times10^{-4} & 1\times10^{-2} & 2\times10^{-1} \\ 6\times10^{-4} & 5\times10^{-2} & 1 \end{pmatrix}. \tag{6.3}$$

- in the MFV framework [130, 131], the baryon number violating couplings depend just on $\tan\beta$ and an overall scale factor w'', while the lepton number violating operators are naturally suppressed. For $\tan\beta \gtrsim 1$ we have:

$$\lambda''_{ijk} = w'' \tan^2\beta \, m_i^{(u)} m_j^{(d)} m_k^{(d)} \epsilon_{jkl} V_{il}^* / v^3, \tag{6.4}$$

$$\begin{pmatrix} \lambda''_{112} & \lambda''_{212} & \lambda''_{312} \\ \lambda''_{113} & \lambda''_{213} & \lambda''_{313} \\ \lambda''_{123} & \lambda''_{223} & \lambda''_{323} \end{pmatrix} = w'' \tan^2\beta \begin{pmatrix} 3\times10^{-12} & 1\times10^{-8} & 4\times10^{-5} \\ 6\times10^{-9} & 1\times10^{-5} & 6\times10^{-5} \\ 5\times10^{-7} & 4\times10^{-5} & 2\times10^{-4} \end{pmatrix}. \tag{6.5}$$

  The coefficient w'' is not constrained by the flavor structure and should be an $\mathcal{O}(1)$ number.

We take these examples as a justification to consider scenarios in which only Baryonic R-parity violation (BRPV) is allowed, while lepton number is conserved (at least to a good approximation). This is the scenario that will be studied in the rest of this study. It should be noted that in both models (eqs. (6.3) and (6.5)), λ''_{223} is the largest coupling that does not involve a top in the final state.

Implicit in R-parity scenarios is stability of the lightest supersymmetric particle (LSP) which can provide a viable relic Dark Matter (DM) candidate. With a neutralino LSP, this is the usual SUSY WIMP scenario, and problems can arise from late time gravitino decays to the LSP [136], disturbing the predictions of Big Bang Nucleosynthesis (BBN). Alternatively, for a gravitino LSP, it is the NLSP decay to the gravitino that is suppressed by the Planck scale M_P and can interfere with BBN. In contrast, R-parity violation allows

superpartners to decay directly and quickly into SM particles,[1] solving this problem but at the same time eliminating dark matter candidates from the theory. If, however, the gravitino is the LSP, its decay (see Figure 6.1) is suppressed by the SUSY breaking scale F (or equivalently, by M_P),[2] by the R-parity violating couplings, and by the superpartner scale $\tilde{m}$. This naturally allows for lifetimes longer than the age of the universe [137]. Because the gravitino is unstable, its decays will generate cosmic-rays and high-energy γ-ray emission which can potentially be detected by modern indirect-detection experiments. Given the non-observation of gravitino decay products, we will proceed to set limits on RPV couplings and will compare them to bounds coming from low-energy baryon-number-violating processes (which are especially weak for couplings involving third generation fields). Although this has been studied in the literature, many groups have focused only on the bilinear RPV coupling $\mu_i L_i \phi_u$ [137, 138, 139, 140, 141] with just Refs. [142, 143, 144, 145] discussing the trilinear interactions; weak scale supersymmetry was also frequently assumed. Here, we do not set the superpartner scale, we discuss the connection to models with flavor symmetries, which has been unexplored so far, and we show that the limits can be stronger than those from low-energy flavor physics.

Following Ref. [146], the decay rate of Figure 6.1 can be written as

$$\Gamma_{3/2} \simeq \frac{19}{60 \cdot 768\pi^3} \lambda''^2_{ijk} \frac{m_{3/2}^3}{M_P^2} \left(\frac{m_{3/2}}{\tilde{m}}\right)^4 \tag{6.6}$$

in the limit of vanishing masses for the final state particles and at leading order in $m_{3/2}/\tilde{m}$.

[1] As noted above, we consider only baryonic RPV in this study. Then, late NLSP decays are not a problem for a neutralino or squark NLSPs, but they can be for a stau NLSP. In the second case, heavy superapartners and/or light gravitinos would be needed.

[2] For a comprehensive review of gravitino interactions, see Ref. [56].

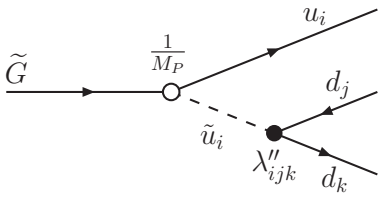

Figure 6.1: *Gravitino RPV decay; the white vertex marks the $1/M_P$-suppressed interaction, while the RPV interaction $\lambda''_{ijk}\tilde{\bar{u}}_i\bar{d}_j\bar{d}_k$ is marked by a black dot.*

The lifetime is

$$\tau_{\tilde{G}\to u_i d_j d_k} = 2.9\times 10^{14}\text{sec}\left(\frac{10\text{ GeV}}{m_{3/2}}\right)^3 \frac{1}{\lambda''^2_{ijk}}\left(\frac{\tilde{m}}{m_{3/2}}\right)^4. \tag{6.7}$$

In this equation $\tilde{m}$ is the common mass scale of the squarks which participate in the process; it is slightly modified in presence of a large hierarchy between different squarks. In particular, the detailed dependence on the squark masses is recovered by substituting the factor $19m^4_{3/2}/\tilde{m}^4$ in (6.6) with

$$\frac{m^2_{3/2}}{m^4_{\tilde{u}_i}}\left(3+2n_d\frac{m^2_{\tilde{u}_i}}{m^2_{\tilde{d}_j}}+3n_d^2\frac{m^4_{\tilde{u}_i}}{m^4_{\tilde{d}_j}}\right), \tag{6.8}$$

where we have denoted by $\tilde{d}_j$ the lightest down squark, and n_d is the number of down squarks participating in the process, $n=\begin{cases} 1,\ m_{\tilde{d}_j}\ll m_{\tilde{d}_k} \\ 2,\ m_{\tilde{d}_j}\sim m_{\tilde{d}_k}\end{cases}$.

With the pre-inflationary gravitino abundance washed out during inflation, gravitinos are produced by thermal scattering at reheating and by decays of other fields (such as moduli, or the inflaton). We will show overclosure limits coming from the overproduction of gravitinos, and in the following we will assume $T_R > \tilde{m} > m_{3/2}$ for the reheating temperature. As a conservative choice, we will assume that the full DM relic abundance is

generated *in toto* at reheating;[3] the second class of processes will just strengthen the over-closure bounds that we are considering.[4] The thermal scattering, with a cross section of order $\sigma \approx g_3^2 \frac{\tilde{m}^2}{M_P^2 m_{3/2}^2}$, overcloses the universe unless (see [56, 55] for the precise expression)

$$10^{-3} \frac{T_R \tilde{m}^2}{m_{3/2}} \lesssim M_P T_{eq}. \tag{6.9}$$

where the equality holds if the gravitino forms all of the dark matter, as we will assume in the following, and $T_{eq} \sim 1.5$ eV is the temperature of matter-radiation equality.

This chapter is organized as follows: in Section 6.1, we review the importance of antideuterons for the indirect detection of dark matter candidates and the coalescence model of antideuteron formation. We then compute and discuss the antideuteron injection spectrum. In Section 6.2 we derive the upper limits on the RPV coupling λ''_{223} from the lack of antideuterons and discuss the dependence on the SUSY and SUSY mediation scales. We apply these limits in Section 6.3, where we discuss the implications for models with flavor symmetries. Finally, we conclude in Section 6.4.

6.1 Antideuterons from gravitino decays

Measurements of the cosmic-ray antiproton spectrum by BESS [147, 148, 149] and PAMELA [150] have provided important constraints on cosmic-ray transport in the galaxy, as well as placed limits on exotic source models such as dark matter annihilations or decays and primordial black hole emission. In the near future, data from the AMS-02 experiment on-board the international space-station will provide the most precise measurements to date.

[3] If the universe reheats below $\tilde{m}$, gravitinos are not produced thermally. Still, a gravitino relic abundance might be produced by moduli or inflaton decay.

[4] On the other hand, these limits can be relaxed with a late entropy injection diluting the relic abundance.

While indirect detection limits on antiprotons currently provide the leading constraints on R-parity violating λ''_{ijk} couplings, the production of secondary antiprotons through cosmic-ray spallation processes provides an astrophysical background with considerable uncertainty.

In 2000, Donato et al. [151] proposed new physics searches, specifically neutralino annihilations, using heavier anti-nuclei such as antideuterons, antihelium-3, or antitritium. In contrast to antiprotons, the secondary background for antideuterons is highly suppressed at low energies while gravitino decays produce a peaked spectrum. This happens for three reasons: first, the scattering of cosmic-ray protons with interstellar gas produces (secondary) antiprotons only if the cosmic-ray proton has a total energy above the production threshold $E_{\rm p} = 7m_p$ in the galactic rest frame. At these energies, the density of Galactic cosmic-rays is substantial, and the antiproton spectrum below ≈ 5 GeV becomes heavily populated by the astrophysical background. In the case of antideuterons, this threshold is increased to $E_{\rm p} = 17m_p$, where a rapid decrease in the Galactic proton spectrum heavily suppresses the astrophysical background.[5] Second, astrophysical production occurs in a center of mass frame which is highly boosted with respect to the rest of the galaxy, whereas dark matter decays occur at rest. This results in the background spectrum peaking at higher energies than that of dark matter decays, which typically peaks in the non-relativistic regime. Finally, the small binding energy of antideuterons causes them to disintegrate rather than lose energy through inelastic scattering, unlike antiprotons for which such collisions lead to an increased abundance at lower energies. These low-energy antideuteron astrophysical backgrounds are 10-50 times less in magnitude than the primary signals expected from naive thermal dark matter models [152, 153], so searches for low energy antideuterons can

[5]The proton spectrum peaks at approximately 10 GeV and subsequently falls off proportionally to $E^{-2.82}$.

provide a promising discovery channel for new physics. Heavier elements such as antihelium are even cleaner [154], although the expected signals are too small to be observed with the current generation of experiments as shown by one of the authors (EC) [155] and later independently [156]. For the Baryonic R-parity violating operators under consideration here, constraints on the couplings are currently competitive with those from antiprotons and are expected to improve substantially with the results of AMS-02.

The detection of antinuclei from dark matter decay has been thoroughly investigated in the literature with an emphasis on simple two-body final states such as $b\bar{b}$ or W^+W^- (see e.g. [151, 160, 157, 159, 158, 152, 153] for antideuterons and [155, 156] for antihelium). Recently, Ref. [145] provided the first antideuteron constraints for gravitinos decaying through a variety of R-parity violating operators. One novel feature of their analysis is the detailed treatment of the Monte Carlo parameters controlling the hadronization model which are tuned to reproduce a wider array of experimental antideuteron production rates. In this study, much of the same production and propagation framework is used, but we do not vary the hadronization model in order to extract the model-*dependent* features of gravitino decay, and compare them to standard treatments of decaying dark matter. In doing so, we can provide simple scaling relations which allow BRPV coupling constraints to be easily adapted from future updated measurements and more sophisticated propagation schemes that are presented in the context of two-body decays to heavy quark pairs.

In any process producing antinucleons, it is possible for antiprotons and antineutrons to bind together into a nucleus and produce antideuterons. The traditional formation model, known as the 'coalescence mechanism', was designed to empirically describe nuclei

production in heavy-ion collisions based on the phase-space distributions of the constituent nucleons. It possesses a single energy-independent parameter, the coalescence momenta p_0, and assumes that if any antineutron and antiproton pair have relative invariant 4-momenta $(k_n - k_p)^2 = (\Delta\vec{k})^2 - (\Delta E)^2 \leq p_0^2$, they will fuse and form an antideuteron. The parameter p_0 is then tuned to match collider measurements of $\overline{\mathrm{d}}$ production.

It has long been known that this model cannot accommodate the available data for a single value of the coalescence momenta to better than a factor of ~ 3. Despite this simplistic model, an improved prescription is largely hindered by limited collider data for production of antideuterons from e^+e^- collisions at high energies, as well as a lacking understanding of the underlying nuclear formation dynamics. However, recently renewed interest in antideuteron searches have led to at least two important improvements. First, it was pointed out in Ref. [158] that the isotropic nucleon distribution functions used in analytic estimates of formation rates led to an artificial suppression of the $\overline{\mathrm{d}}$ production rate at large center of mass energies. In particular, the jet structure of high-energy showers introduces significant angular correlations between nucleons. One must therefore run Monte Carlo simulations and apply the coalescence mechanism on an event-by-event basis using the simulated phase space distributions of protons and neutrons. Second, it was realized that the antideuteron wave-function is spatially localized to ≈ 2 fm and contributions to the nucleon population from long-lived baryons should be omitted, as they decay at large relative distances from the other particles in the shower. In practice, weakly decaying baryons are then excluded by stabilizing particles with a lifetime $\tau > 2\mathrm{fm/c}$ with a negligible dependence on this parameter due to the large gap between weak and hadronic timescales.

For our study, we first use `Feynrules v2.0` package [161] (using a modified version of the `gld-grv` [162] and `RPV-MSSM` [163] model files) to translate our R-parity violating Lagrangian into a UFO format readable by matrix element generators. The matrix elements and phase space for the hard process $\tilde{G} \to \bar{u}_i \bar{d}_j \bar{d}_k$ are then generated using `MadGraph v5.0` and `MadEvent` [164]. Finally, these parton level distributions are fed into `Pythia 8.1` [165] for showering and hadronization.

In order to fix the coalescence parameter we must choose a value which reproduces a measured rate. As previous studies have noted, a single value of the coalescence momentum cannot simultaneously reproduce rates from different underlying processes such as pp vs e^+e^-. While this can be slightly improved by tuning the hadronization parameters, we follow previous studies which use electron-positron collisions more likely to resemble a dark matter scenario – i.e. color singlets that are not composite. Following the approach of Refs. [153, 152, 157], we use $e^+e^- \to \overline{\mathrm{d}}$ measurements from ALEPH at the Z^0 resonance, finding $(5.9 \pm 1.8 \pm .5) \times 10^{-6}$ antideuterons per hadronic Z^0-decay with $\overline{\mathrm{d}}$ momenta 0.62-1.03 GeV/c and polar angle $|\cos\theta| < 0.95$ ([166]). We find a value $p_0^{A=2} = 0.192 \pm .030$ GeV/c consistent with Refs. [153, 152].

In Figure 6.2 we show the typical antideuteron injection spectra for a gravitino decay of mass $m_{3/2}$ =10 GeV, 30 GeV, 100 GeV, 1 TeV, and 10 TeV. In solid lines, we show the spectra from the heaviest accessible channel, which is expected to dominate the decay rate in scenarios with flavor symmetries, while dashed lines show the second heaviest contribution[6]. For comparison, we also show the spectra for a standard dark-matter decay to $b\bar{b}$ in dotted lines. Shaded bands show the acceptance energies for BESS (red), GAPS

[6] In the case of the *cbs* channel at 10 GeV we observe no events.

(green), the low-energy band of AMS-02 (blue), and the high energy band of AMS-02 (gray). Here we assume that the spectra will be shifted to lower energies as the antideuterons propagate through the heliosphere and shift each band upward in energy due to the Fisk potential $\phi_f = 500$ MV acting on a unit electric charge in accordance with the Gleeson & Axford Force Field approximation [167]. The vertical normalization of each energy band is arbitrary and we have slightly offset the BESS band in order to keep the others visible. We note that while the energy range of each experiment is fixed, they are rescaled by a factor $m_{3/2}^{-1}$ in these dimensionless coordinates. With the injection spectra now in hand, several observations can be made:

1. Comparing between decay channels, we see that the second lightest quark mass channels have a significantly harder spectrum than the heaviest. For $m_{3/2}$ less than a few hundred GeV, these low mass final state channels yield slightly more detectable antideuterons. Such behavior is also evidenced in Ref. [145] where the light quark channels provide the best limits on the trilinear BRPV coupling. Interestingly, this behavior reverses for $m_{3/2} \gtrsim 1$ TeV, where the heaviest quark channel dominates by a factor $\sim 20 - 30\%$ over the detectable low energies. One explanation may be the following: Increased jet multiplicity as the 2nd and 3rd generation quarks cascade down to u and d type quarks will divide the gravitino's energy. For low masses, this could sufficiently raise the threshold where heavy channels can consistently form the requisite number of protons and neutrons. When the gravitino mass is very high, each jet will contain energy $E \gg m_p$, and the 3-tiered decay of the top-quark will effectively soften the otherwise harder spectrum.

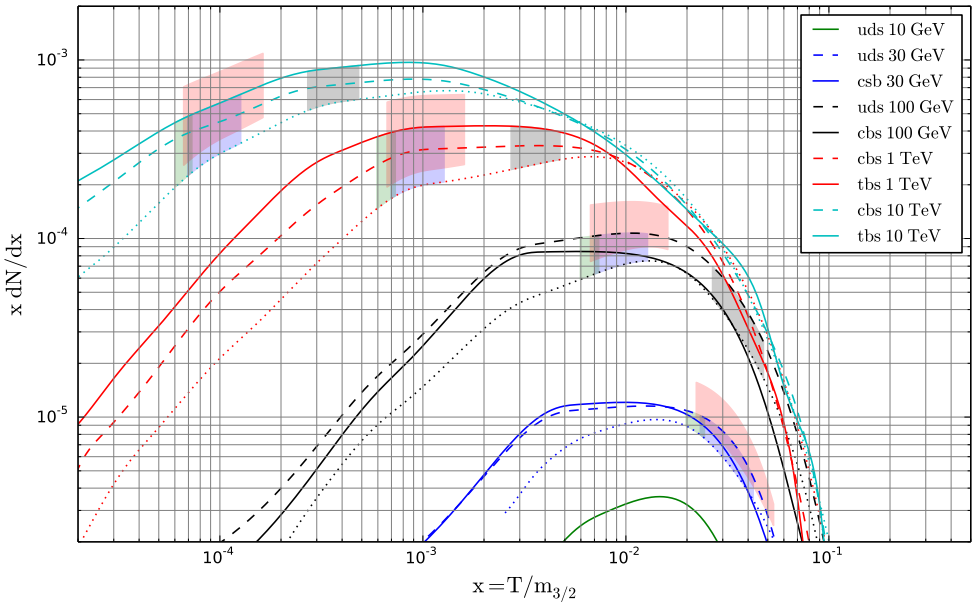

Figure 6.2: *Antideuteron injection spectra for different operators involved and different gravitino masses, as displayed in the legend. dN is the average number of antideuterons with energy dT generated in the decay of a single gravitino. In particular, we display spectra generated by the operators* $\bar{u}_1\bar{d}_1\bar{d}_2$ *(uds),* $\bar{u}_2\bar{d}_2\bar{d}_3$ *(cbs),* $\bar{u}_3\bar{d}_2\bar{d}_3$ *(tbs). Solid lines represent the heaviest accessible channel while dashed lines show the second heaviest. Dotted lines represent the case of a 2-body decay to b-quarks, which is often presented in antideuteron analyses. In shaded bands, we show the ranges of experimental detectability after accounting for solar modulation effects. The bands are for BESS (red), GAPS (green), AMS-02-L (blue), and AMS-02-H (gray). We have vertically offset the BESS band for readability (vertical normalizations for these bands are arbitrary). The energy range of the bands is identical for different gravitino masses, but in these coordinates the horizontal locations scale as a function of* $m_{3/2}^{-1}$.

2. Compared with the 2-body decay to $b\bar{b}$, we see a significantly softer spectrum for our gravitino decay in all cases. This results in a mild enhancement in detectable antideuterons of $\mathcal{O}(50\%)$ for $m_{3/2} \approx 50$ GeV increasing to a significant factor $\approx$ 3 above 1 TeV. This is mostly attributed to the higher initial multiplicity of quarks in the final state of the hard process which splits the initial gravitino energy into three final states rather than two. In addition to this, the 3-body phase-space allows the hard jets to occasionally align, and thus increase the probability of a neutron and proton coalescing. In the 2-body case, jets are forced back-to-back for a decay at rest, and are therefore less likely to have cross-jet correlations.

3. The formation model used here is distinct from Ref. [145]. Notably, we use `Pythia` for hadronization (based on the string fragmentation model) while in Ref. [145], `Herwig++` (based on the cluster hadronization model) is used. It has been shown in Ref. [168] that differences between the two different models can lead to substantially different preferred values of the coalescence momentum and variances in the spectrum of anti-deuterons produced. Furthermore, our coalescence momentum is fit to a single data-point at the Z^0-resonance while the Ref. [145] varies the parameters of the hadronization model in order to reproduce results from e^+e^- and pp collisions at 50 GeV-7 TeV. We therefore expect to see some level of disagreement at higher gravitino masses. In fact, we do find a significant enhancement in our yield (integrated over the low-energy experimental bands) of around 30% at 50 GeV up to 300% at 1 TeV. As this is an artifact of the underlying hadronization and coalescence model, it occurs independent of the two results enumerated above for which the comparison is based

on a common framework.

In order to translate the injection spectra into the observable astrophysical fluxes, one must propagate the $\overline{\mathrm{d}}$ nuclei through two stages: interstellar transport from the position of production to the solar system and modulation of the spectra during through the heliosphere. Interstellar transport of antiprotons and light-nuclei is very well studied but unfortunately still suffers from considerable uncertainties. Our implementation of interstellar propagation follows the standard semi-analytical treatment using the 'two-zone diffusion model' which provides a simplified but good approximation by neglecting energy losses and diffusive reacceleration. The neglect of tertiary processes – i.e. non-annihilating inelastic scatters are treated as annihilations – is well justified and in particular does not redistribute the spectrum of antideuterons toward lower energies. In other words, the Green's function which solves the simplified transport equation is proportional to a δ-function and as a result, the injection spectrum can be factored out of propagation. Similarly, propagation through the solar system in the Force-Field model [167] only introduces an energy dependent scaling and a global shift of the spectrum to 500 MeV lower energy. This implies that event-rates and observable fluxes can be readily compared by computing the ratio of the injection spectra, integrated over the experimental acceptance range. As AMS-02 and GAPS results become available, propagation uncertainties are likely to be reduced based on upper limits on the antiproton spectrum. Recent analyses have already incorporated sophisticated numerical treatments of interstellar and heliospheric propagation and present their findings in terms of annihilation or decay to heavy quarks [152]. Conversion of these rates to case of gravitino dark matter is therefore a simple rescaling according to the integrated ratios

of injection read from Figure 6.2. Our treatment of propagation and conversion of the flux to event rates is completely identical to that presented in Section 3 of Ref. [145] and we therefore omit our own details, pointing the interested reader to the discussion presented there[7]. In the next section we will discuss how the differences between our injection spectra and that of Ref. [145] lead to different limits on the BRPV couplings.

6.2 Model-independent limits on RPV couplings

In this section, we will show the model-independent limits on the RPV couplings coming from null observation of antideuterons at the BESS experiment [170] and the future reach of the AMS-02 experiment; as a starting point, we take the limits on λ'' due to lack of observation of cosmic antideuterons from Ref. [145], where the full gravitino decay $\tilde{G} \to \bar{u}_i \bar{d}_j \bar{d}_k \to \bar{D} + \ldots$ was studied. There, no flavor symmetry was assumed, and the strongest limits were set on the coupling λ''_{112} (uds channel) in the range 10 GeV $\leq m_{3/2} \lesssim 1$ TeV, for $\tilde{m} = 1$ TeV.

In Figure 6.2, we showed the spectra generated by decays of a gravitino in the uds, cbs, and tbs channels for different choices of the gravitino mass: compared to Ref. [145], we find that the number of antideuterons produced in the uds channel in the BESS energy sensitivity range is about 50% higher at low gravitino masses ($m_{3/2} = 50$ GeV), and about a factor of 3 higher at $m_{3/2} = 800$ GeV. The local flux of antideuterons scales as λ''^2. A change in the injection spectra by a factor A therefore strengthens the bounds on λ'' by a

[7]Here, and in Ref. [145], the halo model chosen is a standard NFW profile and the Fisk potential is taken to be $\phi_F = 500MV$. In the next section, our results use the 'MED' propagation model to compute the flux, although it should be kept in mind that these propagation uncertainties span 2-3 orders of magnitude. See also Ref. [169] or a recent review of indirect detection of decaying dark matter.

factor of $\sqrt{A}$ assuming we are in the signal dominated regime (i.e. low relative background flux). We then rescale the 95% confidence level limits on the coupling λ''_{112} from Figures 7 and 8 of [145] in order to self-consistently employ our injection spectra.

As previously mentioned the number of antideuterons produced in the *uds* and *cbs* channels differs only by 20-30% in the energy range accessible by the BESS and AMS-02 experiments. This implies that the limits on the respective couplings differ only by 10-15%. We are particularly interested in the coupling λ''_{223}, which, according to both eqs. (6.3) and (6.5), is the largest coupling that does not involve a top in the final state. As such, the decay process will proceed through the *cbs* channel for gravitino masses between the *b*-quark mass and about 1 TeV. At high gravitino masses (above 1 TeV), the decay involving the coupling λ''_{323} and a top quark will also be relevant. For such high masses, the *tbs* channel gives a slightly higher number of antideuterons when compared to the *cbs* channel, so that the 95% CL limit on λ''_{323} will be slightly stronger than the limit on λ''_{223} at the same scale. As the resulting antideuteron spectrum flattens at the low energies relevant experimentally, we can extend the bounds from Ref. [145] to gravitino masses above 1 TeV and expect no qualitative change in behavior. As we will see in Section 6.3, because both flavor models predict $\lambda''_{323} > \lambda''_{223}$, λ''_{323} will be the most constrained in this regime. At lower masses, the constraints are strongest for λ''_{223}.

In Figure 6.3 we compare the limits from Ref. [145] with the ones that will be used in the following. We plot the bounds on the individual couplings $\lambda''_{112}, \lambda''_{323}$ (λ''_{223} is degenerate with λ''_{112}) as a function of the gravitino mass, with a reference superpartner scale $\tilde{m} = 1$ TeV.

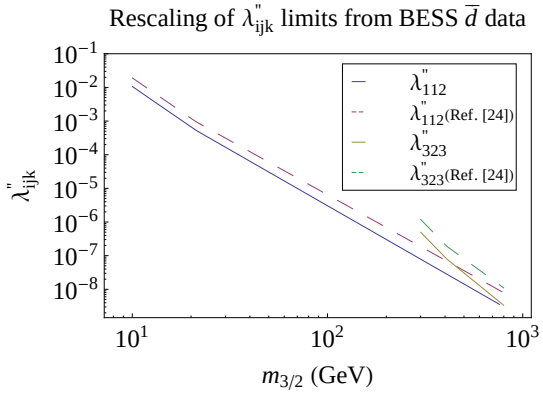

Figure 6.3: *95% CL upper limits on different couplings λ''_{ijk} from antideuteron data, compared to the values in Ref. [145]. The region above the lines is excluded. In this graph, $\tilde{m}$ is set at 1 TeV.*

Provided that the gravitino is the LSP, the injection spectra are independent of the mass of the superpartner involved in the process. Thus, the only dependence on the superpartner scale $\tilde{m}$ is in the hard process that determines the decay rate, as shown in Eq. (6.6). In Figure 6.4, we show how the limits on λ''_{223} depend on the superpartner scale: the dot-dashed diagonal lines show the upper limits on λ''_{223} for given values of $\tilde{m} = 1, 10, 100$ TeV. The parameter space above each line is ruled out. Alternatively, we fix the ratio $\tilde{m}/m_{3/2}$ to approximately $1, 10, 10^2, 10^3$ and show the allowed parameter space. Here the vertical black dashed lines show the upper bounds on the gravitino mass coming from overproduction during reheating. Setting the ratio $\tilde{m}/m_{3/2}$ corresponds to setting the SUSY mediation scale M: if the gravitino mass is $m_{3/2} \approx \frac{F}{M_P}$ and the squark masses are $\tilde{m} \sim \frac{F}{M}$, we have $\tilde{m}/m_{3/2} = M_P/M$. The limits on λ''_{223} presented in Figure 6.4 are independent of the flavor structure. As stressed above, for $m_{3/2} \gtrsim 1$ TeV, similar limits apply to λ''_{323}.

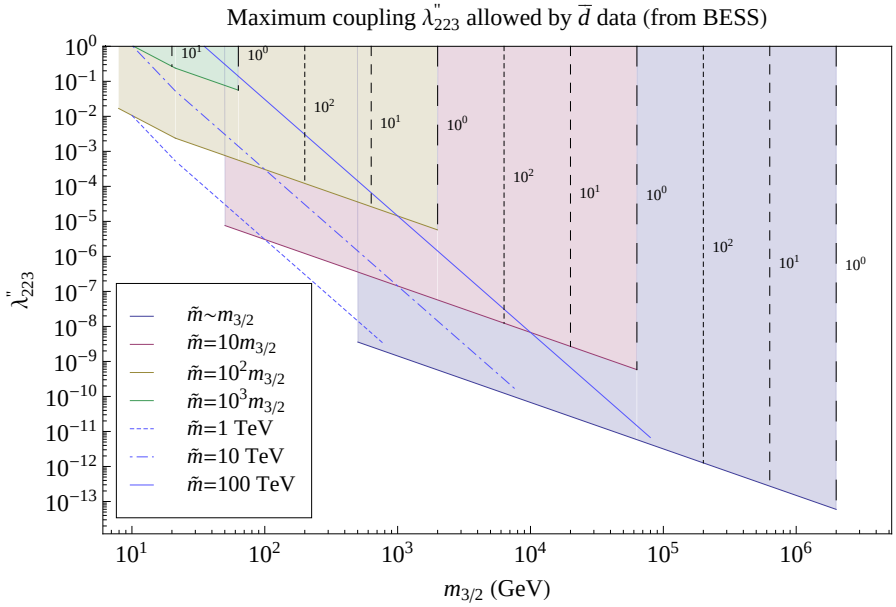

Figure 6.4: *Maximum coupling λ''_{223} allowed by the non-observation of antideuterons at BESS, for different values of $m_{3/2}/\tilde{m}$; the shaded region above each continuous line is excluded. The blue lines correspond to fixed values of $\tilde{m} = 1, 10, 100$ TeV (repectively dotted, dashed and solid line). The vertical dashed lines are the upper limits on the gravitino mass coming from overproduction of gravitinos at reheating, with the labels indicating the respective values of $T_R/\tilde{m}$; the regions to the right of these lines are excluded for each given value of $m_{3/2}/\tilde{m}$.*

It should be noted that the relevant squarks in this process are $\tilde{s}_R, \tilde{c}_R, \tilde{b}_R$; limits from R-parity conserving LHC searches for first and second generation squarks are above 1 TeV, while for $\tilde{b}_1$ they are at ≈ 650 GeV [171, 172]; without R-parity it is *in principle* possible for squarks to be significantly lighter than the R-parity conserving constraints. However, we find it a plausible assumption that the superpartners are not hiding at extremely low masses. Allowing for a little hierarchy between $\tilde{b}$ and $\tilde{c}, \tilde{s}$, we require that $\tilde{m} \geq 500$ GeV for simplicity.

6.3 Constraints on models with flavor symmetries

As seen in eqs. (6.3) and (6.5), flavor symmetries constrain the structure of the unknown RPV couplings; limits on one coupling (as λ''_{223}) directly translate into limits on all the other couplings (in particular, the largest one, λ''_{323}).

6.3.1 Horizontal symmetries

In models with a horizontal symmetry, as λ''_{223} is smaller than λ''_{323} by a factor of 20, the conversion is straightforward: for $m_{3/2}$ between 10 GeV and 200 GeV, the *cbs* channel is predominant in creating antideuterons. Above the top mass, from about 200 GeV to about 1 TeV, the *tbs* channel contribution grows until it eventually outweighs the *cbs* channel due to its larger coupling. For $m_{3/2} \gtrsim 1$ TeV, the *tbs* channel gives approximately 20-30% more antideuterons per decaying gravitino than the *cbs* channel (see Figure 6.2), with *tbs* dominating the decays given the larger coupling.

In Figure 6.5, we present the limits on the largest allowed RPV coupling, λ''_{323}, which is likely to be the most relevant for LHC phenomenology. On the left, we show limits on λ''_{323} for given values of $\tilde{m}$, while on the right we fix the ratio $m_{3/2}/\tilde{m}$. We also show the future reach of the AMS-02 experiment. An improvement of a factor of 10 is expected across the entire range of gravitino masses.

These limits on RPV couplings can be compared to those found when requiring RPV gives a small contribution to low-energy flavor changing processes, in particular neutron-antineutron oscillation or the neutron decay $n \to \Xi$. In [132], one of the authors (AM) showed that the largest RPV coupling is bound to be less than about $10^{-2} - 10^{-3}$,

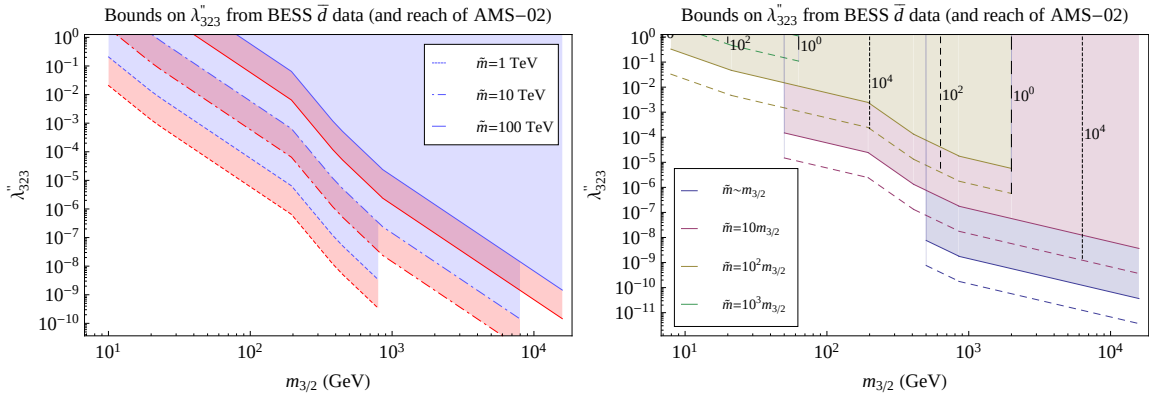

Figure 6.5: *Maximum coupling λ''_{323} allowed by the non-observation of antideuterons at BESS, and the reach of AMS-02, in the context of horizontal symmetries. The region above each line is excluded. Left: the blue lines indicate current upper bounds on λ''_{323} for fixed values of $\tilde{m} = 1, 10, 100$ TeV, while the red lines and red shaded area correspond to the parameter space which will be probed by AMS-02. Right: for different values of $m_{3/2}/\tilde{m}$, solid lines show the upper bound on λ''_{323} from BESS, while dashed lines show the future reach of AMS-02. The vertical dashed lines are the upper limits on the gravitino mass coming from overproduction at reheating, with the labels indicating the respective values of $T_R/\tilde{m}$; the regions to the right of these lines are excluded for each given value of $m_{3/2}/\tilde{m}$.*

depending on the dominant process and the superpartner scale, and independent of the gravitino mass. We see that, apart from $m_{3/2} \lesssim 30 - 50$ GeV, the antideuteron limits from a decaying gravitino DM *are stronger than those from low-energy experiments.*

Some reference scales should be kept in mind while discussing these limits:

- $\lambda''_{323} = 10^{-7}$; in Ref. [173], it was discussed how large R-parity violation would have washed out baryon number in the early universe if the B-violating processes were in equilibrium at a temperature of order $\tilde{m}$, and how RPV SUSY at colliders would most

likely involve displaced vertices (this was also pointed out in [132] in the context of horizontal symmetries, and in [174]). In Figure 6.5, the requirement $\lambda''_{323} < 10^{-7}$ is automatically satisfied for $m_{3/2} \gtrsim 500$ GeV for TeV-scale SUSY. For heavier superpartners, or split spectra, it is true for $m_{3/2} \gtrsim 2 - 5$ TeV. In other words, for large splittings between the gravitino and the superpartners, the cosmic ray flux from gravitino DM is more constraining than the requirements of having baryogenesis with a large reheating temperature. It should be noted that in baryogenesis scenarios with low reheating temperature [175, 176], this bound does not apply as the baryon asymmetry is created after the BNV processes has fallen out of equilibrium (An alternative setting in which baryogenesis is generated by the decay of a meta-stable WIMP was presented in [177].).

- $\lambda''_{323} = 10^{-9}$: in [132] one of the authors (AM) showed that, in order to evade collider signatures for subTeV SUSY, the lower limit $\lambda''_{323} > 10^{-9}$ should hold for either a neutralino NLSP (in which case the missing energy signature of R-parity conserving SUSY reappears) or a stop NLSP (for which the the long lived stop hadronizes into R-hadrons and heavy stable charged particle searches would apply). From Figure 6.5 we can conclude that heavy gravitinos with $m_{3/2} \sim \tilde{m} > 1$ TeV imply $\lambda''_{323} \lesssim 10^{-9}$ and either give standard R-parity conserving LHC phenomenology or long-lived particles.

- $\lambda''_{323} = 10^{-13}$: the lowest scale for which the RPV decay of the NLSP happens before BBN is 10^{-13}. We see that this scale is not particularly constrained by Figure 6.5.

For collider-accessible superpartners, we can conclude that if the coupling λ''_{323} was measured to be large, it would imply a small gravitino mass.

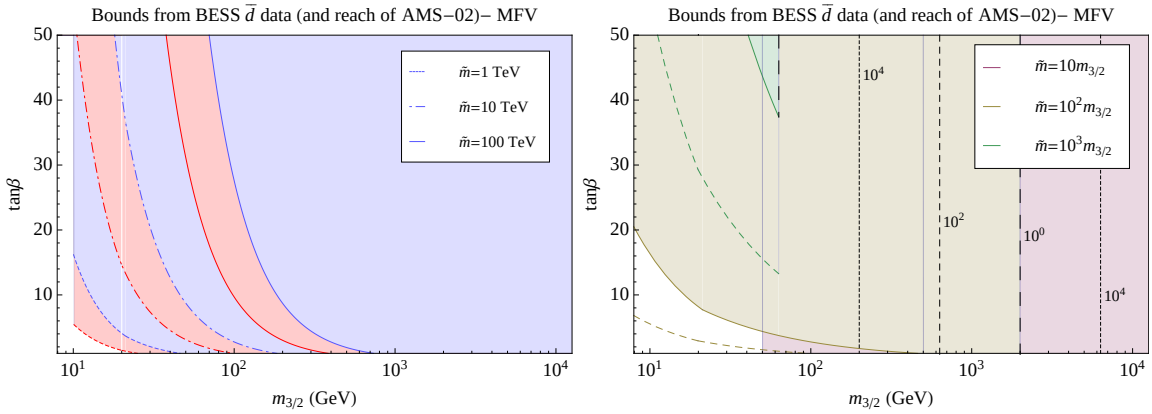

Figure 6.6: *Constraints in the $m_{3/2} - \tan\beta$ plane when the RPV couplings have a MFV flavor structure; the shaded region above each continuous line is excluded in that case. The region above each line is excluded.. Left: the blue lines indicate current upper bounds on λ''_{323} for fixed values of $\tilde{m} = 1, 10, 100$ TeV, while the red lines and red shaded area corresponds to the parameter space which will be probed by AMS-02. Right: for different values of $m_{3/2}/\tilde{m}$, solid lines show the upper bound on λ''_{323} from BESS, while dashed lines show the future reach of AMS-02. The vertical dashed lines are the upper limits on the gravitino mass coming from overproduction at reheating, with the labels indicating the respective values of $\frac{T_R}{\tilde{m}}$. We set $w'' \sim 1$; the limits scale as $1/\sqrt{w''}$.*

6.3.2 MFV: A gravitino on the edge

In models with a minimal flavor violating structure [130, 131], the only free parameters are the overall scale w'', $\tan\beta$ and $m_{3/2}$. The *cbs* coupling λ''_{223} is set to

$$\lambda''_{223} = 4 \times 10^{-5} \tan^2\beta w'' \tag{6.10}$$

As we will see, we do not need to consider the larger *tbs* coefficient $\lambda''_{323} \simeq 5\lambda''_{223}$ as the limits from the *cbs* channel are already enough to rule out the large gravitino mass range where the *tbs* channel (with a top quark in the final state) would dominate.

Setting $w'' \sim 1$, the resulting limits on $m_{3/2}$ and $\tan\beta$ are shown in Figure 6.6. For fixed values of $\tilde{m}$, we are forced into a corner with small $\tan\beta$ and/or small $m_{3/2}$. In particular, for LHC-accessible superpartners, the gravitino must be lighter than 50 GeV if $\tan\beta \sim 1$, and $\tan\beta$ can be as large as 20 for $m_{3/2} = 10$ GeV. We also note that it is possible to accommodate a 125 GeV Higgs mass in the case of large $\tan\beta$ and $\tilde{m} = 10$ TeV, as well as in the case of $\tilde{m} = 100$ TeV. The AMS-02 experiment will remove a large fraction of this parameter space: for $\tilde{m} = 1$ TeV the limits will be $m_{3/2} \lesssim 10$ GeV, with $\tan\beta \lesssim 5$ for $\tilde{m} \sim 10$ GeV.

For given values of $m_{3/2}/\tilde{m}$, the only viable options are $\tilde{m} = 10^2 m_{3/2}$ and $\tilde{m} = 10^3 m_{3/2}$. In the first case, the gravitino mass should be lower than ~ 200 GeV for low $\tan\beta$ and below a few tens GeV for larger $\tan\beta$; in the second case, a larger zone of the parameter space will be explored by AMS-02, but the gravitino is easily overproduced.

If the overall scale factor w'' was allowed to be $\ll 1$ a larger region of the parameter space would survive. Given that some couplings are larger than $\mathcal{O}(10^{-7})$, the MFV structure is consistent with high temperature baryogenesis only if $w'' \ll 1$. In this case, the limits would scale as $\sqrt{w''}$ and can be relaxed. Still, w'' cannot be infinitely small, and using the expression (6.5) for the RPV couplings, we avoid the previously discussed limit of $\lambda''_{323} \gtrsim 10^{-9}$ with $w'' \gtrsim 10^{-5}$. If allowed, a small w'' should be considered as a tuning of the model.

6.4 Conclusions

In this work, we studied how the non-observation of antideuterons cosmic rays places significant constraints on gravitino dark matter in baryonic R-parity violating models with flavor symmetries. We studied a selected number of decay channels and presented limits on the RPV couplings λ''_{223} and λ''_{323}, which are almost everywhere stronger than bounds from baryon-number-violating low-energy processes. If flavor symmetries can be used as guides, these are the largest couplings and severe bounds can be cast. While the limits on horizontal flavor symmetries are not as strong, in the minimal flavor violating case the gravitino mass is forced to $m_{3/2} \lesssim 20$ GeV for TeV-scale SUSY. The AMS-02 experiment will be able to reduce this bound below 10 GeV. A suggestive implication (which could hold at least for the MFV scenario) is that the gravitino might be effectively stable, not because of a discrete symmetry such as R-parity, but because decays are not kinematically allowed.[8] Further studies, especially at gravitino masses between 1 and 10 GeV, are needed. In this range, the best constraints on the RPV coupling will come from antiprotons, positrons and gamma rays. This would also imply a somewhat suppressed mediation scale for SUSY breaking, lower than M_P or M_{GUT}, providing a suggestive hint for more new physics at intermediate energies. In a forthcoming publication [180], we are comprehensively exploring all the different decay and detection channels, the uncertainties related to propagation and

[8] If the gravitino is lighter than the proton, the proton can decay to it $p \to K^+ \tilde{G}$. This was considered in Refs. [178, 179]), with the most relevant bounds being:

$$\lambda''_{112} \leq 5 \times 10^{-16} \left(\frac{\tilde{m}}{300\ \text{GeV}}\right)^2 \left(\frac{m_{3/2}}{1\ \text{eV}}\right), \qquad \lambda''_{323} \leq 5 \times 10^{-8} \left(\frac{\tilde{m}}{300\ \text{GeV}}\right)^2 \left(\frac{m_{3/2}}{1\ \text{eV}}\right) \tag{6.11}$$

For models with a horizontal symmetry, this corresponds to $\lambda''_{323} \lesssim 10^{-2} \left(\frac{\tilde{m}}{300\ \text{GeV}}\right)^2 \left(\frac{m_{3/2}}{100\ \text{MeV}}\right)$, which should be compared to the limits in figure 6.5. In the MFV scenario, the gravitino mass has to be above $\mathcal{O}(100\ \text{keV}) \times \tan^2\beta$ (a similar bound was also studied in ref. [131], resulting in a dependence on $\tan^4\beta$).

DM halo profile, as well as the full dependence on the SUSY spectrum.

Note Added While the write-up of the paper this chapter is based on was being completed, reference [181] was submitted to the arXiv, which puts similar limits on gravitino DM in the MFV framework by analyzing the antiproton and γ fluxes and has no mention of the SUSY scale. In the present work, the source of the bounds is the lack of observation of antideuterons, which is less sensitive to astrophysical uncertainties. In addition to analyzing other types of flavor symmetries and a larger range of gravitino masses, we extensively discuss sensitivity to the superpartner scale and limits from overclosure.

Chapter 7

Conclusion

In this thesis, I have presented studies of four dark matter candidates: a generic WIMP which interacts via four-fermion interactions, the neutralino and gravitino of supersymmetry, and the KK photon of minimal UED. For these candidates, I have explored how they can be probed via their cosmological properties, their astrophysical signatures, and the signals they are expected to produce in terrestrial searches at both direct detection experiments and the LHC. A summary of the results follows:

- In chapter 3, we calculated the kinetic decoupling temperature for WIMPs that interact via various effective operators with SM particles. These limits were then cross correlated with constraints from null searches in direct detection experiments and colliders. Also considered were limits from overclosure. In general, the limits on the couplings are quite constraining, leading to cut-offs of the matter power spectrum that are at mass scales below an Earth mass, too small to be easily observable. However, the major exception to this conclusion was in the case where dark matter couples

only to leptons. As limits from the LHC and direct detection in general do not apply in this case (or at the very least are much weaker), for some operators we do not constrain the cutoff scale at all for masses above 100 GeV. It is also interesting to note that when we assume that direct detection rates and annihilation rates in the early universe which set the relic density are related to one another via a crossing symmetry, many operators are excluded entirely at DM masses of 100 GeV or less. However, this assumption is often not true, as the rate for each of these processes can be set by different operators in more complicated models.

- In chapter 4, we again considered the matter power spectrum cutoff, but in this case we calculated the matter spectrum cutoff for two specific dark matter candidates: neutralinos and KK photons. Here we showed that for these models there is a direct correlation between the direct detection scattering rates and the power spectrum cutoff, as would be expected as it is scattering processes which determine each of these. However, in the case of the neutralino, the correlations are only valid in the case of *spin-dependent* scattering rates, as spin-independent scattering is dominated by Higgs exchange, which is of minimal importance in the early universe. The correlation is strong for KK photons in mUED for both types of direct detection mainly due to the limited parameter space of the theory. For neutralinos, we also showed that there is a strong correlation between the rate of neutrinos from DM annihilation in the sun and the power spectrum cutoff. While the results we presented are for specific models, it should be noted that for any model in which couplings of DM to quarks and leptons are related, such a correlation would generically be expected. These correlations are

useful because they allow us to make statements about the halo mass cutoff, which is often quite small and hard to observe directly, from direct detection results and observations of the solar neutrino flux.

- In chapter 5, we continued our study of KK photons considering the case where the mUED cutoff is quite low. This was motivated by the measurement of the Higgs mass, which implies that the cutoff of the theory must be low in order to assure the stability of the electroweak vacuum. The low cutoff leads to increased degeneracy in the masses of the various KK particles at each mode. Therefore, in determining the relic density, there are important co-annihilations which had not been previously considered, particularly annihilations of KK gluons. By combining direct detection constraints, LHC limits, and limits from universe overclosure, we showed that currently the KK photon is still allowed to be within the mass range of 800 to 1250 GeV. However, the next generation of direct detection experiments should probe all of the remaining viable mUED parameter space.

- Finally, in chapter 6, we considered a last dark matter candidate: the gravitino of supersymmetry. This gravitino was allowed to decay through R-parity violating operators which violate baryon number. Furthermore, we considered the situation where the relative strengths of these R-parity violating operators are set by flavor symmetries. We constrained the strength of these operators by considering the decays of gravitinos to anti-deuterons, showing that in the minimal flavor violating scenario with TeV-scale SUSY, the gravitino mass is currently constrained to be below 20 GeV from searches for this species of cosmic ray. While there have been many studies of

cosmic rays from dark matter decays, this one is unique because it is a probe of flavor physics as well, albeit indirect.

To truly understand the particle nature of dark matter, multiple complementary probes such as the ones that I have considered in this dissertation are necessary. To believe that one has truly discovered dark matter, it will almost certainly be necessary for a discovery to be made both at the LHC and at a direct detection experiment or through an astrophysical search. Any new particle discovered at the LHC must correspond to a signature from a cosmic source, for without such a signal how can we be sure that this particle is the dark matter? Likewise, any direct or indirect detection signal would likely be the result of a theory which would lead to observable interactions at the LHC. While these are the most direct ways to constrain particle dark matter models, my work has shown that there are others that can be useful as well, such as measurements of small scale structure.

The next few years will put the WIMP paradigm to the test. The LHC is running again, the Fermi Gamma Ray Space Telescope continues to take data, AMS-02 is measuring cosmic ray fluxes, and a wide range of direct detection experiments are either already online or in the works. If these searches do not discover signals that can be conclusively associated with dark matter, a large region of the theoretical parameter space where the WIMP is a thermal relic will be excluded. We could be either on the verge of a discovery or a recognition that we need to move beyond the WIMP model, however compelling it may be.

Appendix A

EFT Scattering Matrix Elements

A.1 Standard model fermions

A.1.1 Scalar

For the effective operator describing the scalar interaction between a SM fermion f and a Dirac fermion χ

$$\mathcal{O}_S = \frac{m_f}{\Lambda_S^3}\bar{\chi}\chi\bar{f}f\,, \tag{A.1}$$

the matrix element for the scattering process between f and χ squared and summed over initial spin states and averaged over final spin states is of the form

$$\frac{1}{4}\sum_{\text{Spin States}}|\mathcal{M}|^2 = 4\frac{m_f^2}{\Lambda_S^6}\left(\mathbf{p}\cdot\mathbf{p}' + m_\chi^2\right)\left(\mathbf{k}\cdot\mathbf{k}' + m_f^2\right)\,, \tag{A.2}$$

where $\mathbf{p}$ and $\mathbf{p}'$ are the incoming and outgoing 4-momentum of the χ particle respectively and $\mathbf{f}$ and $\mathbf{f}'$ are the same for the SM fermion. Setting $t = 0$, this becomes

$$\frac{1}{4}\sum_{\text{Spin States}}|\mathcal{M}| = 16\frac{m_f^4 m_\chi^2}{\Lambda_S^6}\,. \tag{A.3}$$

A.1.2 Psuedoscalar

We now consider the effective operator describing pseudoscalar interactions,

$$\mathcal{O}_P = \frac{m_f}{\Lambda_P^3}\bar{\chi}\gamma^5\chi\bar{f}\gamma^5 f\,. \tag{A.4}$$

For a scattering process when the interaction is described by this operator, we find

$$\frac{1}{4}\sum_{\text{Spin States}}|\mathcal{M}|^2 = 4\frac{m_f^2}{\Lambda_P^6}\left(m_\chi^2 - \mathbf{p}\cdot\mathbf{p}'\right)\left(m_f^2 - \mathbf{f}\cdot\mathbf{f}'\right) = \frac{m_f^2}{\Lambda_P^6}t^2\,. \tag{A.5}$$

A.1.3 Vector

Now considering the operator

$$\mathcal{O}_V = \frac{1}{\Lambda_V^2}\bar{\chi}\gamma^\mu\chi\bar{f}\gamma_\mu f\,, \tag{A.6}$$

$$\frac{1}{4}\sum_{\text{Spin States}}|\mathcal{M}|^2 = \frac{8}{\Lambda_V^4}\left[\left(\mathbf{p}\cdot\mathbf{k}\right)\left(\mathbf{p}'\cdot\mathbf{k}'\right) + \left(\mathbf{p}\cdot\mathbf{k}'\right)\left(\mathbf{p}'\cdot\mathbf{k}\right)\right.$$
$$\left. - \left(\mathbf{p}\cdot\mathbf{p}'\right)m_f^2 - \left(\mathbf{k}\cdot\mathbf{k}'\right)m_\chi^2 + 2m_\chi^2 m_f^2\right]\,. \tag{A.7}$$

As before, we consider only forward scattering, so $t = 0$. Working in the frame where the dark matter particle is stationary, $s = m_\chi^2 + 2m_\chi\omega + m_f^2$ and the matrix element becomes:

$$\frac{1}{4}\sum_{\text{Spin States}}|\mathcal{M}|^2 = 16\frac{m_\chi^2}{\Lambda_V^4}\omega^2\,. \tag{A.8}$$

A.1.4 Pseudovector

The axial vector operator is of the form

$$\mathcal{O}_A = \frac{1}{\Lambda_V^2}\bar{\chi}\gamma^\mu\gamma^5\chi\bar{f}\gamma_\mu\gamma^5 f\,, \tag{A.9}$$

$$\frac{1}{4}\sum_{\text{Spin States}}|\mathcal{M}|^2 = \frac{8}{\Lambda_A^4}\left[(\mathbf{p}\cdot\mathbf{k})\left(\mathbf{p}'\cdot\mathbf{k}'\right) + \left(\mathbf{p}\cdot\mathbf{k}'\right)\left(\mathbf{p}'\cdot\mathbf{k}\right)\right.$$
$$\left. + \left(\mathbf{p}\cdot\mathbf{p}'\right)m_f^2 + \left(\mathbf{k}\cdot\mathbf{k}'\right)m_\chi^2 + 2m_\chi^2 m_f^2\right] . \quad \text{(A.10)}$$

Once again, taking the two limits $t = 0$ and $s = m_\chi^2 + 2m_\chi\omega + m_f^2$, this becomes

$$\frac{1}{4}\sum_{\text{Spin States}}|\mathcal{M}|^2 = 16\frac{m_\chi^2}{\Lambda_A^4}\left(\omega^2 + 2m_f^2\right) . \quad \text{(A.11)}$$

As $m_f \approx 0$ for relativistic fermions, this is essentially the same as the result for the vector operator.

A.1.5 Tensor

Finally, the tensor operator takes the form

$$\mathcal{O}_T = \frac{m_f}{\Lambda_T^3}\bar{\chi}\sigma^{\mu\nu}\chi\bar{f}\sigma_{\mu\nu}f \quad \text{(A.12)}$$

where $\sigma^{\mu\nu} = (i/2)[\gamma^\mu, \gamma^\nu]$.

$$\frac{1}{4}\sum_{\text{Spin States}}|\mathcal{M}|^2 = 32\frac{m_f^2}{\Lambda_T^6}\left(2\left(\mathbf{p}'\cdot\mathbf{k}\right)\left(\mathbf{p}\cdot\mathbf{k}'\right) - \left(\mathbf{p}\cdot\mathbf{p}'\right)\left(\mathbf{k}\cdot\mathbf{k}'\right) + 2\left(\mathbf{p}\cdot\mathbf{k}\right)\left(\mathbf{p}'\cdot\mathbf{k}'\right)\right.$$
$$\left. + 3m_\chi^2 m_f^2\right) , \quad \text{(A.13)}$$

and then when $t = 0$ and $s = m_\chi^2 + 2m_\chi\omega + m_f^2$, this becomes

$$\frac{1}{4}\sum_{\text{Spin States}}|\mathcal{M}|^2 = 64\frac{m_f^2 m_\chi^2}{\Lambda_T^6}\left(2\omega^2 + m_f^2\right) . \quad \text{(A.14)}$$

A.2 Pions

A.2.1 Scalar

For the scalar pion coupling we have a Lagrangian term [81]

$$\mathcal{L} \supset \frac{m_\pi^2}{2\Lambda_S^3}\bar{\chi}\chi\vec{\pi}\cdot\vec{\pi}\,, \tag{A.15}$$

where

$$\vec{\pi} = \begin{pmatrix} \frac{1}{\sqrt{2}}\left(\pi^+ + \pi^-\right) \\ \frac{i}{\sqrt{2}}\left(\pi^+ - \pi^-\right) \\ \pi^0 \end{pmatrix}. \tag{A.16}$$

Simplifying the dot product, this gives

$$\mathcal{L} \supset \frac{m_\pi^2}{2\Lambda^3}\bar{\chi}\chi\left(\pi^0\pi^0 + 2\pi^+\pi^-\right). \tag{A.17}$$

Note that this leads to a Feynman rule which is identical for all pion charges, and the scattering amplitude which we calculate is

$$i\mathcal{M} = \frac{m_\pi^2}{\Lambda_S^3}\bar{\chi}\chi\,. \tag{A.18}$$

Squaring and averaging over initial spins, then choosing the zero relative velocity limit, gives the final result

$$\frac{1}{2}\sum_{\text{Spin States}}|\mathcal{M}|^2 = \frac{4m_\pi^4 m_\chi^2}{\Lambda_S^6}\,. \tag{A.19}$$

A.2.2 Vector

The coupling from the vector operator has the form [81]

$$\mathcal{L} \supset \frac{2i}{\Lambda_V^2}\bar{\chi}\gamma_\mu\chi\left(\vec{\pi}\times\partial^\mu\vec{\pi}\right)_3 \tag{A.20}$$

when we introduce a negative sign in front of the operator in Eq. A.6 for down type quark interactions, as otherwise this term is zero. The relevant component of the cross product is $\pi_1\partial^\mu\pi_2 - \pi_2\partial^\mu\pi_1$, which can be rewritten in terms of the physical fields to give

$$\mathcal{L} \supset \frac{2i}{\Lambda_V^2}\bar{\chi}\gamma_\mu\chi\left(\pi^+\partial^\mu\pi^- - \pi^-\partial^\mu\pi^+\right) . \tag{A.21}$$

Thus, this operator does not couple to neutral pions, and the scattering amplitude off of a charged pion is equal to

$$i\mathcal{M} = \frac{2}{\Lambda_V^2}\bar{\chi}\gamma_\mu\chi\left(\mathbf{k}+\mathbf{k}'\right)^\mu . \tag{A.22}$$

Squaring and averaging over incoming spins, we have

$$\frac{1}{2}\sum_{\text{Spin States}}|\mathcal{M}|^2 = \frac{8}{\Lambda_V^4}\left(\left(\mathbf{k}+\mathbf{k}'\right)^2\left(m_\chi^2 - \mathbf{p}\cdot\mathbf{p}'\right) + 2\mathbf{p}\cdot\left(\mathbf{k}+\mathbf{k}'\right)\mathbf{p}'\cdot\left(\mathbf{k}+\mathbf{k}'\right)\right) . \tag{A.23}$$

Simplifying this in terms of Mandelstam variables we find

$$\frac{1}{2}\sum_{\text{Spin States}}|\mathcal{M}|^2 = \frac{4}{\Lambda_V^4}\left(4m_\pi^2 t - t^2 + s^2 + u^2 - 2su\right) , \tag{A.24}$$

and working in the limit where $t \to 0$, this becomes

$$\frac{1}{2}\sum_{\text{Spin States}}|\mathcal{M}|^2 = \frac{64m_\chi^2\omega^2}{\Lambda_V^4} . \tag{A.25}$$

Bibliography

[1] Jonathan M. Cornell and Stefano Profumo. "Earthly probes of the smallest dark matter halos". *JCAP* 1206 (2012), 011. DOI: 10.1088/1475-7516/2012/06/011. arXiv: 1203.1100 [hep-ph].

[2] Jonathan M. Cornell, Stefano Profumo, and William Shepherd. "Kinetic Decoupling and Small-Scale Structure in Effective Theories of Dark Matter". *Phys.Rev.* D88.1 (2013), 015027. DOI: 10.1103/PhysRevD.88.015027. arXiv: 1305.4676 [hep-ph].

[3] Jonathan M. Cornell, Stefano Profumo, and William Shepherd. "Dark matter in minimal universal extra dimensions with a stable vacuum and the 'right' Higgs boson". *Phys.Rev.* D89.5 (2014), 056005. DOI: 10.1103/PhysRevD.89.056005. arXiv: 1401.7050 [hep-ph].

[4] Angelo Monteux, Eric Carlson, and Jonathan Cornell. "Gravitino Dark Matter and Flavor Symmetries". *JHEP* 1408 (2014), 047. DOI: 10.1007/JHEP08(2014)047. arXiv: 1404.5952 [hep-ph].

[5] P.A.R. Ade et al. *Planck 2015 results. XIII. Cosmological parameters*. 2015. arXiv: 1502.01589 [astro-ph.CO].

[6] Gianfranco Bertone, Dan Hooper, and Joseph Silk. "Particle dark matter: Evidence, candidates and constraints". *Phys.Rept.* 405 (2005), 279–390. DOI: 10.1016/j.physrep.2004.08.031. arXiv: hep-ph/0404175 [hep-ph].

[7] Gerard Jungman, Marc Kamionkowski, and Kim Griest. "Supersymmetric dark matter". *Phys.Rept.* 267 (1996), 195–373. DOI: 10.1016/0370-1573(95)00058-5. arXiv: hep-ph/9506380 [hep-ph].

[8] K.G. Begeman, A.H. Broeils, and R.H. Sanders. "Extended rotation curves of spiral galaxies: Dark haloes and modified dynamics". *Mon.Not.Roy.Astron.Soc.* 249 (1991), 523.

[9] Simon D.M. White et al. "The Baryon content of galaxy clusters: A Challenge to cosmological orthodoxy". *Nature* 366 (1993), 429–433. DOI: 10.1038/366429a0.

[10] Wayne Hu and Scott Dodelson. "Cosmic microwave background anisotropies". *Ann.Rev.Astron.Astrophys.* 40 (2002), 171–216. DOI: 10.1146/annurev.astro.40.060401.093926. arXiv: astro-ph/0110414 [astro-ph].

[11] Edward W. Kolb and Michael S. Turner. "The Early Universe". *Front.Phys.* 69 (1990), 1–547.

[12] Lawrence J. Hall et al. "Freeze-In Production of FIMP Dark Matter". *JHEP* 1003 (2010), 080. DOI: 10.1007/JHEP03(2010)080. arXiv: 0911.1120 [hep-ph].

[13] Kim Griest and David Seckel. "Three exceptions in the calculation of relic abundances". *Phys.Rev.* D43 (1991), 3191–3203. DOI: 10.1103/PhysRevD.43.3191.

[14] Torsten Bringmann. "Particle Models and the Small-Scale Structure of Dark Matter". *New J.Phys.* 11 (2009), 105027. DOI: 10.1088/1367-2630/11/10/105027. arXiv: 0903.0189 [astro-ph.CO].

[15] J.E. Gunn et al. "Some Astrophysical Consequences of the Existence of a Heavy Stable Neutral Lepton". *Astrophys.J.* 223 (1978), 1015–1031. DOI: 10.1086/156335.

[16] Christoph Schmid, Dominik J. Schwarz, and Peter Widerin. "Amplification of cosmological inhomogeneities from the QCD transition". *Phys.Rev.* D59 (1999), 043517. DOI: 10.1103/PhysRevD.59.043517. arXiv: astro-ph/9807257 [astro-ph].

[17] C. Boehm, Pierre Fayet, and R. Schaeffer. "Constraining dark matter candidates from structure formation". *Phys.Lett.* B518 (2001), 8–14. DOI: 10.1016/S0370-2693(01)01060-7. arXiv: astro-ph/0012504 [astro-ph].

[18] Louis E. Strigari et al. "Redefining the Missing Satellites Problem". *Astrophys.J.* 669 (2007), 676–683. DOI: 10.1086/521914. arXiv: 0704.1817 [astro-ph].

[19] Xue-lei Chen, Marc Kamionkowski, and Xin-min Zhang. "Kinetic decoupling of neutralino dark matter". *Phys.Rev.* D64 (2001), 021302. DOI: 10.1103/PhysRevD.64.021302. arXiv: astro-ph/0103452 [astro-ph].

[20] Anne M. Green, Stefan Hofmann, and Dominik J. Schwarz. "The power spectrum of SUSY - CDM on sub-galactic scales". *Mon.Not.Roy.Astron.Soc.* 353 (2004), L23. DOI: 10.1111/j.1365-2966.2004.08232.x. arXiv: astro-ph/0309621 [astro-ph].

[21] Stefano Profumo, Kris Sigurdson, and Marc Kamionkowski. "What mass are the smallest protohalos?" *Phys.Rev.Lett.* 97 (2006), 031301. DOI: 10.1103/PhysRevLett.97.031301. arXiv: astro-ph/0603373 [astro-ph].

[22] Anne M. Green, Stefan Hofmann, and Dominik J. Schwarz. "The First wimpy halos". *JCAP* 0508 (2005), 003. DOI: 10.1088/1475-7516/2005/08/003. arXiv: astro-ph/0503387 [astro-ph].

[23] Edmund Bertschinger. "The Effects of Cold Dark Matter Decoupling and Pair Annihilation on Cosmological Perturbations". *Phys.Rev.* D74 (2006), 063509. DOI: 10.1103/PhysRevD.74.063509. arXiv: astro-ph/0607319 [astro-ph].

[24] Torsten Bringmann and Stefan Hofmann. "Thermal decoupling of WIMPs from first principles". *JCAP* 0407 (2007), 016. DOI: 10.1088/1475-7516/2007/04/016. arXiv: hep-ph/0612238 [hep-ph].

[25] Abraham Loeb and Matias Zaldarriaga. "The Small-scale power spectrum of cold dark matter". *Phys.Rev.* D71 (2005), 103520. DOI: 10.1103/PhysRevD.71.103520. arXiv: astro-ph/0504112 [astro-ph].

[26] Jurg Diemand, Michael Kuhlen, and Piero Madau. "Early supersymmetric cold dark matter substructure". *Astrophys.J.* 649 (2006), 1–13. DOI: 10.1086/506377. arXiv: astro-ph/0603250 [astro-ph].

[27] Hong-Sheng Zhao et al. *Earth-mass mini-halos are tidally disrupted by close encounters with stars*. 2005. arXiv: astro-ph/0502049 [astro-ph].

[28] Ben Moore et al. *On the survival and disruption of Earth mass CDM micro-haloes*. 2005. arXiv: astro-ph/0502213 [astro-ph].

[29] Tobias Goerdt et al. "The survival and disruption of CDM micro-haloes: Implications for direct and indirect detection experiments". *Mon.Not.Roy.Astron.Soc.* 375 (2007),

191–198. DOI: 10.1111/j.1365-2966.2006.11281.x. arXiv: astro-ph/0608495 [astro-ph].

[30] Jurg Diemand, Michael Kuhlen, and Piero Madau. "Dark matter substructure and gamma-ray annihilation in the Milky Way halo". *Astrophys.J.* 657 (2007), 262–270. DOI: 10.1086/510736. arXiv: astro-ph/0611370 [astro-ph].

[31] J. Diemand et al. "Clumps and streams in the local dark matter distribution". *Nature* 454 (2008), 735–738. DOI: 10.1038/nature07153. arXiv: 0805.1244 [astro-ph]; Michael Kuhlen et al. "Dark Matter Direct Detection with Non-Maxwellian Velocity Structure". *JCAP* 1002 (2010), 030. DOI: 10.1088/1475-7516/2010/02/030. arXiv: 0912.2358 [astro-ph.GA].

[32] Leonidas A. Moustakas et al. *Strong gravitational lensing probes of the particle nature of dark matter*. 2009. arXiv: 0902.3219 [astro-ph.CO].

[33] Shant Baghram, Niayesh Afshordi, and Kathryn M. Zurek. "Prospects for Detecting Dark Matter Halo Substructure with Pulsar Timing". *Phys.Rev.* D84 (2011), 043511. DOI: 10.1103/PhysRevD.84.043511. arXiv: 1101.5487 [astro-ph.CO].

[34] Joel R. Primack. "Cosmology: small scale issues revisited". *New J.Phys.* 11 (2009), 105029. DOI: 10.1088/1367-2630/11/10/105029. arXiv: 0909.2247 [astro-ph.CO].

[35] P. Gondolo et al. "DarkSUSY: Computing supersymmetric dark matter properties numerically". *JCAP* 0407 (2004), 008. DOI: 10.1088/1475-7516/2004/07/008. arXiv: astro-ph/0406204 [astro-ph].

[36] Paolo Gondolo, Junji Hisano, and Kenji Kadota. "The Effect of quark interactions on dark matter kinetic decoupling and the mass of the smallest dark halos". *Phys.Rev.* D86 (2012), 083523. DOI: 10.1103/PhysRevD.86.083523. arXiv: 1205.1914 [hep-ph].

[37] Stefan Hofmann, Dominik J. Schwarz, and Horst Stoecker. "Damping scales of neutralino cold dark matter". *Phys.Rev.* D64 (2001), 083507. DOI: 10.1103/PhysRevD.64.083507. arXiv: astro-ph/0104173 [astro-ph].

[38] Savvas M. Koushiappas. "The detection of sub-solar mass dark matter halos". *New J.Phys.* 11 (2009), 105012. DOI: 10.1088/1367-2630/11/10/105012. arXiv: 0905.1998 [astro-ph.CO].

[39] Argyro Tasitsiomi and A.V. Olinto. "The Detectability of neutralino clumps via atmospheric Cherenkov telescopes". *Phys.Rev.* D66 (2002), 083006. DOI: 10.1103/PhysRevD.66.083006. arXiv: astro-ph/0206040 [astro-ph].

[40] Savvas M. Koushiappas, Andrew R. Zentner, and Terrence P. Walker. "The observability of gamma-rays from neutralino annihilations in Milky Way substructure". *Phys.Rev.* D69 (2004), 043501. DOI: 10.1103/PhysRevD.69.043501. arXiv: astro-ph/0309464 [astro-ph].

[41] Edward A. Baltz, James E. Taylor, and Lawrence L. Wai. "Can Astrophysical Gamma Ray Sources Mimic Dark Matter Annihilation in Galactic Satellites?" *Astrophys.J.* 659 (2007), L125–L128. DOI: 10.1086/517882. arXiv: astro-ph/0610731 [astro-ph].

[42] L. Pieri, G. Bertone, and E Branchini. "Dark Matter Annihilation in Substructures Revised". *Mon.Not.Roy.Astron.Soc.* 384 (2008), 1627. DOI: 10.1111/j.1365-2966.2007.12828.x. arXiv: 0706.2101 [astro-ph].

[43] Michael Kuhlen, Jurg Diemand, and Piero Madau. "The Dark Matter Annihilation Signal from Galactic Substructure: Predictions for GLAST". *Astrophys.J.* 686 (2008), 262. arXiv: 0805.4416 [astro-ph].

[44] Tomoaki Ishiyama, Junichiro Makino, and Toshikazu Ebisuzaki. "Gamma-ray Signal from Earth-mass Dark Matter Microhalos". *Astrophys.J.* 723 (2010), L195. DOI: 10.1088/2041-8205/723/2/L195. arXiv: 1006.3392 [astro-ph.CO].

[45] Brandon Anderson et al. "Fermi-LAT Sensitivity to Dark Matter Annihilation in Via Lactea II Substructure". *Astrophys.J.* 718 (2010), 899–904. DOI: 10.1088/0004-637X/718/2/899. arXiv: 1006.1628 [astro-ph.HE].

[46] Pierre Brun et al. "The cosmic ray lepton puzzle in the light of cosmological N-body simulations". *Phys.Rev.* D80 (2009), 035023. DOI: 10.1103/PhysRevD.80.035023. arXiv: 0904.0812 [astro-ph.HE].

[47] Timur Delahaye et al. "Astrophysical boost factor and dark matter indirect detection". *J.Phys.Conf.Ser.* 203 (2010), 012050. DOI: 10.1088/1742-6596/203/1/012050.

[48] Savvas M. Koushiappas. "Proper motion of gamma-rays from microhalo sources". *Phys.Rev.Lett.* 97 (2006), 191301. DOI: 10.1103/PhysRevLett.97.191301. arXiv: astro-ph/0606208 [astro-ph].

[49] Shin'ichiro Ando et al. "Can proper motions of dark-matter subhalos be detected?" *Phys.Rev.* D78 (2008), 101301. DOI: 10.1103/PhysRevD.78.101301. arXiv: 0809.0886 [astro-ph].

[50] Samuel K. Lee, Shin'ichiro Ando, and Marc Kamionkowski. "The Gamma-Ray-Flux Probability Distribution Function from Galactic Halo Substructure". *JCAP* 0907 (2009), 007. DOI: 10.1088/1475-7516/2009/07/007. arXiv: 0810.1284 [astro-ph].

[51] M. Ackermann et al. "Search for Dark Matter Satellites using the FERMI-LAT". *Astrophys.J.* 747 (2012), 121. DOI: 10.1088/0004-637X/747/2/121. arXiv: 1201.2691 [astro-ph.HE].

[52] Marc Kamionkowski and Savvas M. Koushiappas. "Galactic substructure and direct detection of dark matter". *Phys.Rev.* D77 (2008), 103509. DOI: 10.1103/PhysRevD.77.103509. arXiv: 0801.3269 [astro-ph].

[53] Jacqueline Chen and Savvas M. Koushiappas. "Gravitational Nanolensing from Subsolar Mass Dark Matter Halos". *Astrophys.J.* 724 (2010), 400–410. DOI: 10.1088/0004-637X/724/1/400. arXiv: 1008.2385 [astro-ph.CO].

[54] Stephen P. Martin. "A Supersymmetry primer". *Adv.Ser.Direct.High Energy Phys.* 21 (2010), 1–153. DOI: 10.1142/9789814307505_0001. arXiv: hep-ph/9709356 [hep-ph].

[55] Lawrence J. Hall, Joshua T. Ruderman, and Tomer Volansky. "A Cosmological Upper Bound on Superpartner Masses". *JHEP* 1502 (2015), 094. DOI: 10.1007/JHEP02(2015)094. arXiv: 1302.2620.

[56] Takeo Moroi. "Effects of the gravitino on the inflationary universe". PhD thesis. 1995. arXiv: hep-ph/9503210 [hep-ph].

[57] Theodor Kaluza. "On the Problem of Unity in Physics". *Sitzungsber. Preuss. Akad. Wiss. Berlin (Math.Phys.)* 1921 (1921), 966–972.

[58] Oskar Klein. "Quantum Theory and Five-Dimensional Theory of Relativity. (In German and English)". *Z.Phys.* 37 (1926), 895–906. DOI: 10.1007/BF01397481.

[59] Thomas Appelquist, Hsin-Chia Cheng, and Bogdan A. Dobrescu. "Bounds on universal extra dimensions". *Phys.Rev.* D64 (2001), 035002. DOI: 10.1103/PhysRevD.64.035002. arXiv: hep-ph/0012100 [hep-ph].

[60] Nima Arkani-Hamed, Savas Dimopoulos, and G.R. Dvali. "The Hierarchy problem and new dimensions at a millimeter". *Phys.Lett.* B429 (1998), 263–272. DOI: 10.1016/S0370-2693(98)00466-3. arXiv: hep-ph/9803315 [hep-ph].

[61] Dan Hooper and Stefano Profumo. "Dark matter and collider phenomenology of universal extra dimensions". *Phys.Rept.* 453 (2007), 29–115. DOI: 10.1016/j.physrep.2007.09.003. arXiv: hep-ph/0701197 [hep-ph].

[62] Hsin-Chia Cheng, Konstantin T. Matchev, and Martin Schmaltz. "Bosonic supersymmetry? Getting fooled at the CERN LHC". *Phys.Rev.* D66 (2002), 056006. DOI: 10.1103/PhysRevD.66.056006. arXiv: hep-ph/0205314 [hep-ph].

[63] Serguei Chatrchyan et al. "Observation of a new boson at a mass of 125 GeV with the CMS experiment at the LHC". *Phys.Lett.* B716 (2012), 30–61. DOI: 10.1016/j.physletb.2012.08.021. arXiv: 1207.7235 [hep-ex]; Georges Aad et al. "Observation of a new particle in the search for the Standard Model Higgs boson with

the ATLAS detector at the LHC". *Phys.Lett.* B716 (2012), 1–29. DOI: 10.1016/j.physletb.2012.08.020. arXiv: 1207.7214 [hep-ex].

[64] Hsin-Chia Cheng, Konstantin T. Matchev, and Martin Schmaltz. "Radiative corrections to Kaluza-Klein masses". *Phys.Rev.* D66 (2002), 036005. DOI: 10.1103/PhysRevD.66.036005. arXiv: hep-ph/0204342 [hep-ph].

[65] Cosmin Macesanu. "The Phenomenology of universal extra dimensions at hadron colliders". *Int. J. Mod. Phys.* A21 (2006), 2259–2296. DOI: 10.1142/S0217751X06030886. arXiv: hep-ph/0510418 [hep-ph].

[66] Mattias Blennow et al. "RG running in a minimal UED model in light of recent LHC Higgs mass bounds". *Phys.Lett.* B712 (2012), 419–424. DOI: 10.1016/j.physletb.2012.05.029. arXiv: 1112.5339 [hep-ph]; Takuya Kakuda et al. "Universal extra dimensions after Higgs discovery". *Phys.Rev.* D88 (2013), 035007. DOI: 10.1103/PhysRevD.88.035007. arXiv: 1305.1686 [hep-ph].

[67] Laura G. van den Aarssen, Torsten Bringmann, and Yasar C Goedecke. "Thermal decoupling and the smallest subhalo mass in dark matter models with Sommerfeld-enhanced annihilation rates". *Phys.Rev.* D85 (2012), 123512. DOI: 10.1103/PhysRevD.85.123512. arXiv: 1202.5456 [hep-ph].

[68] Laura G. van den Aarssen, Torsten Bringmann, and Christoph Pfrommer. "Is dark matter with long-range interactions a solution to all small-scale problems of Λ CDM cosmology?" *Phys.Rev.Lett.* 109 (2012), 231301. DOI: 10.1103/PhysRevLett.109.231301. arXiv: 1205.5809 [astro-ph.CO].

[69] Ian M. Shoemaker. "Constraints on Dark Matter Protohalos in Effective Theories and Neutrinophilic Dark Matter". *Phys.Dark Univ.* 2.3 (2013), 157–162. DOI: 10.1016/j.dark.2013.07.002. arXiv: 1305.1936 [hep-ph].

[70] Patrick J. Fox et al. "LEP Shines Light on Dark Matter". *Phys.Rev.* D84 (2011), 014028. DOI: 10.1103/PhysRevD.84.014028. arXiv: 1103.0240 [hep-ph].

[71] Patrick J. Fox et al. "Taking a Razor to Dark Matter Parameter Space at the LHC". *Phys.Rev.* D86 (2012), 015010. DOI: 10.1103/PhysRevD.86.015010. arXiv: 1203.1662 [hep-ph]; Arvind Rajaraman et al. "LHC Bounds on Interactions of Dark Matter". *Phys.Rev.* D84 (2011), 095013. DOI: 10.1103/PhysRevD.84.095013. arXiv: 1108.1196 [hep-ph]; Patrick J. Fox et al. "Missing Energy Signatures of Dark Matter at the LHC". *Phys.Rev.* D85 (2012), 056011. DOI: 10.1103/PhysRevD.85.056011. arXiv: 1109.4398 [hep-ph]; Jessica Goodman et al. "Constraints on Dark Matter from Colliders". *Phys.Rev.* D82 (2010), 116010. DOI: 10.1103/PhysRevD.82.116010. arXiv: 1008.1783 [hep-ph]; Yang Bai, Patrick J. Fox, and Roni Harnik. "The Tevatron at the Frontier of Dark Matter Direct Detection". *JHEP* 1012 (2010), 048. DOI: 10.1007/JHEP12(2010)048. arXiv: 1005.3797 [hep-ph]; Jessica Goodman et al. "Constraints on Light Majorana dark Matter from Colliders". *Phys.Lett.* B695 (2011), 185–188. DOI: 10.1016/j.physletb.2010.11.009. arXiv: 1005.1286 [hep-ph].

[72] Joachim Kopp et al. "DAMA/LIBRA and leptonically interacting Dark Matter". *Phys.Rev.* D80 (2009), 083502. DOI: 10.1103/PhysRevD.80.083502. arXiv: 0907.3159 [hep-ph].

[73] ATLAS Collaboration. *Search for New Phenomena in Monojet plus Missing Transverse Momentum Final States using 10fb-1 of pp Collisions at sqrts=8 TeV with the ATLAS detector at the LHC*. ATLAS-CONF-2012-147, ATLAS-COM-CONF-2012-190. 2012.

[74] CMS Collaboration. *Search for new physics in monojet events in pp collisions at sqrt(s)= 8 TeV*. CMS-PAS-EXO-12-048. 2013.

[75] E. Aprile et al. "Dark Matter Results from 225 Live Days of XENON100 Data". *Phys.Rev.Lett.* 109 (2012), 181301. DOI: 10.1103/PhysRevLett.109.181301. arXiv: 1207.5988 [astro-ph.CO].

[76] M. Felizardo et al. "Final Analysis and Results of the Phase II SIMPLE Dark Matter Search". *Phys.Rev.Lett.* 108 (2012), 201302. DOI: 10.1103/PhysRevLett.108.201302. arXiv: 1106.3014 [astro-ph.CO].

[77] S. Archambault et al. "Constraints on Low-Mass WIMP Interactions on ^{19}F from PICASSO". *Phys.Lett.* B711 (2012), 153–161. DOI: 10.1016/j.physletb.2012.03.078. arXiv: 1202.1240 [hep-ex].

[78] P.A.R. Ade et al. "Planck 2013 results. XVI. Cosmological parameters". *Astron.Astrophys.* 571 (2014), A16. DOI: 10.1051/0004-6361/201321591. arXiv: 1303.5076 [astro-ph.CO].

[79] G. Belanger et al. "micrOMEGAs: A Tool for dark matter studies". *Nuovo Cim.* C033N2 (2010), 111–116. DOI: 10.1393/ncc/i2010-10591-3. arXiv: 1005.4133 [hep-ph].

[80] G. Belanger et al. "MicrOMEGAs 2.0: A Program to calculate the relic density of dark matter in a generic model". *Comput.Phys.Commun.* 176 (2007), 367–382. DOI: 10.1016/j.cpc.2006.11.008. arXiv: hep-ph/0607059 [hep-ph].

[81] Gary Prezeau et al. "New contribution to wimp-nucleus scattering". *Phys. Rev. Lett.* 91 (2003), 231301. DOI: 10.1103/PhysRevLett.91.231301. arXiv: astro-ph/0309115 [astro-ph].

[82] Lars Bergstrom and Paolo Gondolo. "Limits on direct detection of neutralino dark matter from b $\rightarrow$ s gamma decays". *Astropart.Phys.* 5 (1996), 263–278. DOI: 10.1016/0927-6505(96)00027-8. arXiv: hep-ph/9510252 [hep-ph].

[83] E. Komatsu et al. "Seven-Year Wilkinson Microwave Anisotropy Probe (WMAP) Observations: Cosmological Interpretation". *Astrophys.J.Suppl.* 192 (2011), 18. DOI: 10.1088/0067-0049/192/2/18. arXiv: 1001.4538 [astro-ph.CO].

[84] E. Aprile et al. "Dark Matter Results from 100 Live Days of XENON100 Data". *Phys.Rev.Lett.* 107 (2011), 131302. DOI: 10.1103/PhysRevLett.107.131302. arXiv: 1104.2549 [astro-ph.CO].

[85] *DM Tools*. URL: http://dmtools.brown.edu/.

[86] Jeter Hall. *COUPP Updates*. URL: https://hepconf.physics.ucla.edu/dm12/talks/hall.pdf.

[87] COUPP Collaboration. *A Proposal for a Ton Scale Bubble Chamber for Dark Matter Detection*. Oct. 7, 2010. URL: http://www-coupp.fnal.gov/public/500kg%20PAC%20Proposal.pdf.

[88] G. Sciolla et al. "The DMTPC project". *J.Phys.Conf.Ser.* 179 (2009), 012009. DOI: 10.1088/1742-6596/179/1/012009. arXiv: 0903.3895 [astro-ph.IM].

[89] Vardan Khachatryan et al. "Search for Supersymmetry in pp Collisions at 7 TeV in Events with Jets and Missing Transverse Energy". *Phys.Lett.* B698 (2011), 196–218. DOI: 10.1016/j.physletb.2011.03.021. arXiv: 1101.1628 [hep-ex]; Georges Aad et al. "Search for supersymmetry using final states with one lepton, jets, and missing transverse momentum with the ATLAS detector in $\sqrt{s} = 7$ TeV pp". *Phys.Rev.Lett.* 106 (2011), 131802. DOI: 10.1103/PhysRevLett.106.131802. arXiv: 1102.2357 [hep-ex].

[90] Francis Halzen and Dan Hooper. "The Indirect Search for Dark Matter with IceCube". *New J.Phys.* 11 (2009), 105019. DOI: 10.1088/1367-2630/11/10/105019. arXiv: 0910.4513 [astro-ph.HE].

[91] Lars Bergstrom, Joakim Edsjo, and Paolo Gondolo. "Indirect detection of dark matter in km size neutrino telescopes". *Phys.Rev.* D58 (1998), 103519. DOI: 10.1103/PhysRevD.58.103519. arXiv: hep-ph/9806293 [hep-ph].

[92] Carlos de los Heros. "Dark matter searches with IceCube". *PoS* IDM2010 (2011), 064. arXiv: 1012.0184 [astro-ph.HE].

[93] Christopher Wiebusch. *Physics Capabilities of the IceCube DeepCore Detector*. 2009. arXiv: 0907.2263 [astro-ph.IM].

[94] D. Jason Koskinen. "IceCube-DeepCore-PINGU: Fundamental neutrino and dark matter physics at the South Pole". *Mod.Phys.Lett.* A26 (2011), 2899–2915. DOI: 10.1142/S021773231103725X.

[95] ATLAS Collaboration. *Combination of Higgs Boson Searches with up to 4.9 fb-1 of pp Collisions Data Taken at a center-of-mass energy of 7 TeV with the ATLAS Experiment at the LHC*. ATLAS-CONF-2011-163, ATLAS-COM-CONF-2011-195. 2011; ATLAS Collaboration. *Combined Standard Model Higgs boson searches with up to 2.3 fb-1 of pp collisions at sqrts=7 TeV at the LHC*. ATLAS-CONF-2011-157, ATLAS-COM-CONF-2011-181. 2011; CMS Collaboration. *Combined Standard Model Higgs boson searches with up to 2.3 inverse femtobarns of pp collision data at sqrt(s)=7 TeV at the LHC*. CMS-PAS-HIG-11-023. 2011.

[96] TEVNPH Working Group. *Combined CDF and D0 Upper Limits on Standard Model Higgs Boson Production with up to 8.6 fb^{-1} of Data*. FERMILAB-CONF-11-354-E. 2011. arXiv: 1107.5518 [hep-ex].

[97] R. Barate et al. "Search for the standard model Higgs boson at LEP". *Phys.Lett.* B565 (2003), 61–75. DOI: 10.1016/S0370-2693(03)00614-2. arXiv: hep-ex/0306033 [hep-ex].

[98] Mitsuru Kakizaki, Shigeki Matsumoto, and Masato Senami. "Relic abundance of dark matter in the minimal universal extra dimension model". *Phys.Rev.* D74 (2006), 023504. DOI: 10.1103/PhysRevD.74.023504. arXiv: hep-ph/0605280 [hep-ph].

[99] Geraldine Servant and Timothy M.P. Tait. "Elastic scattering and direct detection of Kaluza-Klein dark matter". *New J.Phys.* 4 (2002), 99. DOI: 10.1088/1367-2630/4/1/399. arXiv: hep-ph/0209262 [hep-ph].

[100] Dan Hooper and Graham D. Kribs. "Probing Kaluza-Klein dark matter with neutrino telescopes". *Phys.Rev.* D67 (2003), 055003. DOI: 10.1103/PhysRevD.67.055003. arXiv: hep-ph/0208261 [hep-ph].

[101] Giuseppe Degrassi et al. "Higgs mass and vacuum stability in the Standard Model at NNLO". *JHEP* 1208 (2012), 098. DOI: 10.1007/JHEP08(2012)098. arXiv: 1205.6497 [hep-ph].

[102] Geraldine Servant. *Status Report on Universal Extra Dimensions After LHC8*. 2014. arXiv: 1401.4176 [hep-ph].

[103] The ATLAS Collaboration. *Search for squarks and gluinos with the ATLAS detector in final states with jets and missing transverse momentum and 20.3 fb^{-1} of $\sqrt{s} = 8$ TeV proton-proton collision data*. ATLAS-CONF-2013-047, ATLAS-COM-CONF-2013-049. 2013.

[104] Giacomo Cacciapaglia et al. "LHC Missing-Transverse-Energy Constraints on Models with Universal Extra Dimensions". *Phys.Rev.* D87.7 (2013), 075006. DOI: 10.1103/PhysRevD.87.075006. arXiv: 1302.4750 [hep-ph].

[105] The ATLAS Collaboration. *Search for squarks and gluinos in events with isolated leptons, jets and missing transverse momentum at $\sqrt{s} = 8$ TeV with the ATLAS detector*. ATLAS-CONF-2013-062, ATLAS-COM-CONF-2013-039. 2013.

[106] Lisa Edelhuser, Thomas Flacke, and Michael Krmer. "Constraints on models with universal extra dimensions from dilepton searches at the LHC". *JHEP* 1308 (2013), 091. DOI: 10.1007/JHEP08(2013)091. arXiv: 1302.6076.

[107] Shigeki Matsumoto et al. "Productions of second Kaluza-Klein gauge bosons in the minimal universal extra dimension model at LHC". *Phys.Rev.* D80 (2009), 056006. DOI: 10.1103/PhysRevD.80.056006. arXiv: 0903.3255 [hep-ph].

[108] Sanghyeon Chang et al. "Direct bound on the minimal Universal Extra Dimension model from the $t\bar{t}$ resonance search at the Tevatron". *Phys.Rev.* D86 (2012), 117503. DOI: 10.1103/PhysRevD.86.117503. arXiv: 1207.6876 [hep-ph].

[109] Ujjal Kumar Dey and Tirtha Sankar Ray. "Constraining minimal and nonminimal universal extra dimension models with Higgs couplings". *Phys.Rev.* D88.5 (2013), 056016. DOI: 10.1103/PhysRevD.88.056016. arXiv: 1305.1016 [hep-ph].

[110] Anindya Datta, Ayon Patra, and Sreerup Raychaudhuri. "Higgs Boson Decay Constraints on a Model with a Universal Extra Dimension". *Phys.Rev.* D89.9 (2014), 093008. DOI: 10.1103/PhysRevD.89.093008. arXiv: 1311.0926 [hep-ph].

[111] Geraldine Servant and Timothy M.P. Tait. "Is the lightest Kaluza-Klein particle a viable dark matter candidate?" *Nucl.Phys.* B650 (2003), 391–419. DOI: 10.1016/S0550-3213(02)01012-X. arXiv: hep-ph/0206071 [hep-ph].

[112] Kyoungchul Kong and Konstantin T. Matchev. "Precise calculation of the relic density of Kaluza-Klein dark matter in universal extra dimensions". *JHEP* 0601 (2006), 038. DOI: 10.1088/1126-6708/2006/01/038. arXiv: hep-ph/0509119 [hep-ph].

[113] Fiona Burnell and Graham D. Kribs. "The Abundance of Kaluza-Klein dark matter with coannihilation". *Phys.Rev.* D73 (2006), 015001. DOI: 10.1103/PhysRevD.73.015001. arXiv: hep-ph/0509118 [hep-ph].

[114] Mitsuru Kakizaki et al. "Significant effects of second KK particles on LKP dark matter physics". *Phys.Rev.* D71 (2005), 123522. DOI: 10.1103/PhysRevD.71.123522. arXiv: hep-ph/0502059 [hep-ph].

[115] Mitsuru Kakizaki et al. "Relic abundance of LKP dark matter in UED model including effects of second KK resonances". *Nucl.Phys.* B735 (2006), 84–95. DOI: 10.1016/j.nuclphysb.2005.11.022. arXiv: hep-ph/0508283 [hep-ph].

[116] G. Belanger, M. Kakizaki, and A. Pukhov. "Dark matter in UED: The Role of the second KK level". *JCAP* 1102 (2011), 009. DOI: 10.1088/1475-7516/2011/02/009. arXiv: 1012.2577 [hep-ph].

[117] Alexander Belyaev et al. "Discovering Minimal Universal Extra Dimensions (MUED) at the LHC". *JHEP* 1306 (2013), 080. DOI: 10.1007/JHEP06(2013)080. arXiv: 1212.4858.

[118] G. Belanger et al. "micrOMEGAs_3: A program for calculating dark matter observables". *Comput.Phys.Commun.* 185 (2014), 960–985. DOI: 10.1016/j.cpc.2013.10.016. arXiv: 1305.0237 [hep-ph].

[119] G. Belanger et al. "Dark matter direct detection rate in a generic model with micrOMEGAs 2.2". *Comput.Phys.Commun.* 180 (2009), 747–767. DOI: 10.1016/j.cpc.2008.11.019. arXiv: 0803.2360 [hep-ph].

[120] D.S. Akerib et al. "First results from the LUX dark matter experiment at the Sanford Underground Research Facility". *Phys.Rev.Lett.* 112 (2014), 091303. DOI: 10.1103/PhysRevLett.112.091303. arXiv: 1310.8214 [astro-ph.CO].

[121] P. Cushman et al. *Working Group Report: WIMP Dark Matter Direct Detection.* 2013. arXiv: 1310.8327 [hep-ex].

[122] Sebastian Arrenberg et al. *Kaluza-Klein Dark Matter: Direct Detection vis-a-vis LHC (2013 update).* 2013. arXiv: 1307.6581.

[123] Glennys R. Farrar and Pierre Fayet. "Phenomenology of the Production, Decay, and Detection of New Hadronic States Associated with Supersymmetry". *Phys.Lett.* B76 (1978), 575–579. DOI: 10.1016/0370-2693(78)90858-4.

[124] M.C. Bento, Lawrence J. Hall, and Graham G. Ross. "Generalized Matter Parities from the Superstring". *Nucl.Phys.* B292 (1987), 400. DOI: 10.1016/0550-3213(87)90652-3.

[125] Luis E. Ibanez and Graham G. Ross. "Fermion masses and mixing angles from gauge symmetries". *Phys.Lett.* B332 (1994), 100–110. DOI: 10.1016/0370-2693(94)90865-6. arXiv: hep-ph/9403338 [hep-ph].

[126] Herbi K. Dreiner, Christoph Luhn, and Marc Thormeier. "What is the discrete gauge symmetry of the MSSM?" *Phys.Rev.* D73 (2006), 075007. DOI: 10.1103/PhysRevD.73.075007. arXiv: hep-ph/0512163 [hep-ph].

[127] C.D. Froggatt and Holger Bech Nielsen. "Hierarchy of Quark Masses, Cabibbo Angles and CP Violation". *Nucl.Phys.* B147 (1979), 277. DOI: 10.1016/0550-3213(79)90316-X.

[128] Miriam Leurer, Yosef Nir, and Nathan Seiberg. "Mass matrix models". *Nucl.Phys.* B398 (1993), 319–342. DOI: 10.1016/0550-3213(93)90112-3. arXiv: hep-ph/9212278 [hep-ph].

[129] Yosef Nir and Nathan Seiberg. "Should squarks be degenerate?" *Phys.Lett.* B309 (1993), 337–343. DOI: 10.1016/0370-2693(93)90942-B. arXiv: hep-ph/9304307 [hep-ph].

[130] Emanuel Nikolidakis and Christopher Smith. "Minimal Flavor Violation, Seesaw, and R-parity". *Phys.Rev.* D77 (2008), 015021. DOI: 10.1103/PhysRevD.77.015021. arXiv: 0710.3129 [hep-ph].

[131] Csaba Csaki, Yuval Grossman, and Ben Heidenreich. "MFV SUSY: A Natural Theory for R-Parity Violation". *Phys.Rev.* D85 (2012), 095009. DOI: 10.1103/PhysRevD.85.095009. arXiv: 1111.1239 [hep-ph].

[132] Angelo Monteux. "Natural, R-parity violating supersymmetry and horizontal flavor symmetries". *Phys.Rev.* D88 (2013), 045029. DOI: 10.1103/PhysRevD.88.045029. arXiv: 1305.2921 [hep-ph].

[133] Anjan S. Joshipura, Rishikesh D. Vaidya, and Sudhir K. Vempati. "U(1) symmetry and R-parity violation". *Phys.Rev.* D62 (2000), 093020. DOI: 10.1103/PhysRevD.62.093020. arXiv: hep-ph/0006138 [hep-ph].

[134] Andres Florez et al. "Baryonic violation of R parity from anomalous $U(1)_H$". *Phys.Rev.* D87.9 (2013), 095010. DOI: 10.1103/PhysRevD.87.095010. arXiv: 1303.0278 [hep-ph].

[135] D. Aristizabal Sierra, Diego Restrepo, and Oscar Zapata. "Decaying Neutralino Dark Matter in Anomalous U(1)(H) Models". *Phys.Rev.* D80 (2009), 055010. DOI: 10.1103/PhysRevD.80.055010. arXiv: 0907.0682 [hep-ph].

[136] M. Yu. Khlopov and Andrei D. Linde. "Is It Easy to Save the Gravitino?" *Phys.Lett.* B138 (1984), 265–268. DOI: 10.1016/0370-2693(84)91656-3.

[137] Fumihiro Takayama and Masahiro Yamaguchi. "Gravitino dark matter without R-parity". *Phys.Lett.* B485 (2000), 388–392. DOI: 10.1016/S0370-2693(00)00726-7. arXiv: hep-ph/0005214 [hep-ph].

[138] Koji Ishiwata, Shigeki Matsumoto, and Takeo Moroi. "High Energy Cosmic Rays from the Decay of Gravitino Dark Matter". *Phys.Rev.* D78 (2008), 063505. DOI: 10.1103/PhysRevD.78.063505. arXiv: 0805.1133 [hep-ph].

[139] Michael Grefe and Timur Delahaye. "Antiproton Limits on Decaying Gravitino Dark Matter". *Phys.Procedia* 61 (2015), 85–90. DOI: 10.1016/j.phpro.2014.12.015. arXiv: 1401.2564 [hep-ph].

[140] Sergei Bobrovskyi et al. "Broken R-Parity in the Sky and at the LHC". *JHEP* 1010 (2010), 061. DOI: 10.1007/JHEP10(2010)061. arXiv: 1007.5007 [hep-ph].

[141] Gianfranco Bertone et al. "Gamma-Rays from Decaying Dark Matter". *JCAP* 0711 (2007), 003. DOI: 10.1088/1475-7516/2007/11/003. arXiv: 0709.2299 [astro-ph].

[142] S. Lola, P. Osland, and A.R. Raklev. "Radiative gravitino decays from R-parity violation". *Phys.Lett.* B656 (2007), 83–90. DOI: 10.1016/j.physletb.2007.09.048. arXiv: 0707.2510 [hep-ph].

[143] N.-E. Bomark et al. "Gravitino Dark Matter and the Flavour Structure of R-violating Operators". *Phys.Lett.* B677 (2009), 62–70. DOI: 10.1016/j.physletb.2009.05.011. arXiv: 0811.2969 [hep-ph].

[144] N.-E. Bomark et al. "Photon, Neutrino and Charged Particle Spectra from R-violating Gravitino Decays". *Phys.Lett.* B686 (2010), 152–161. DOI: 10.1016/j.physletb.2010.02.050. arXiv: 0911.3376 [hep-ph].

[145] L.A. Dal and A.R. Raklev. "Antideuteron Limits on Decaying Dark Matter with a Tuned Formation Model". *Phys.Rev.* D89.10 (2014), 103504. DOI: 10.1103/PhysRevD.89.103504. arXiv: 1402.6259 [hep-ph].

[146] G. Moreau and M. Chemtob. "R-parity violation and the cosmological gravitino problem". *Phys.Rev.* D65 (2002), 024033. DOI: 10.1103/PhysRevD.65.024033. arXiv: hep-ph/0107286 [hep-ph].

[147] S. Orito et al. "Precision measurement of cosmic ray anti-proton spectrum". *Phys.Rev.Lett.* 84 (2000), 1078–1081. DOI: 10.1103/PhysRevLett.84.1078. arXiv: astro-ph/9906426 [astro-ph].

[148] T. Maeno et al. "Successive measurements of cosmic ray anti-proton spectrum in a positive phase of the solar cycle". *Astropart.Phys.* 16 (2001), 121–128. DOI: 10.1016/S0927-6505(01)00107-4. arXiv: astro-ph/0010381 [astro-ph].

[149] Sadakazu Haino et al. "Measurements of primary and atmospheric cosmic - ray spectra with the BESS-TeV spectrometer". *Phys.Lett.* B594 (2004), 35–46. DOI: 10.1016/j.physletb.2004.05.019. arXiv: astro-ph/0403704 [astro-ph].

[150] O. Adriani et al. "A new measurement of the antiproton-to-proton flux ratio up to 100 GeV in the cosmic radiation". *Phys.Rev.Lett.* 102 (2009), 051101. DOI: 10.1103/PhysRevLett.102.051101. arXiv: 0810.4994 [astro-ph].

[151] Fiorenza Donato, Nicolao Fornengo, and Pierre Salati. "Anti-deuterons as a signature of supersymmetric dark matter". *Phys.Rev.* D62 (2000), 043003. DOI: 10.1103/PhysRevD.62.043003. arXiv: hep-ph/9904481 [hep-ph].

[152] N. Fornengo, L. Maccione, and A. Vittino. "Dark matter searches with cosmic antideuterons: status and perspectives". *JCAP* 1309 (2013), 031. DOI: 10.1088/1475-7516/2013/09/031. arXiv: 1306.4171 [hep-ph].

[153] Alejandro Ibarra and Sebastian Wild. "Prospects of antideuteron detection from dark matter annihilations or decays at AMS-02 and GAPS". *JCAP* 1302 (2013), 021. DOI: 10.1088/1475-7516/2013/02/021. arXiv: 1209.5539 [hep-ph].

[154] R. Duperray et al. "Flux of light antimatter nuclei near Earth, induced by cosmic rays in the Galaxy and in the atmosphere". *Phys.Rev.* D71 (2005), 083013. DOI: 10.1103/PhysRevD.71.083013. arXiv: astro-ph/0503544 [astro-ph].

[155] Eric Carlson et al. "Antihelium from Dark Matter". *Phys.Rev.* D89.7 (2014), 076005. DOI: 10.1103/PhysRevD.89.076005. arXiv: 1401.2461 [hep-ph].

[156] Marco Cirelli et al. "Anti-helium from Dark Matter annihilations". *JHEP* 1408 (2014), 009. DOI: 10.1007/JHEP08(2014)009. arXiv: 1401.4017 [hep-ph].

[157] Yanou Cui, John D. Mason, and Lisa Randall. "General Analysis of Antideuteron Searches for Dark Matter". *JHEP* 1011 (2010), 017. DOI: 10.1007/JHEP11(2010)017. arXiv: 1006.0983 [hep-ph].

[158] Mario Kadastik, Martti Raidal, and Alessandro Strumia. "Enhanced anti-deuteron Dark Matter signal and the implications of PAMELA". *Phys.Lett.* B683 (2010), 248–254. DOI: 10.1016/j.physletb.2009.12.005. arXiv: 0908.1578 [hep-ph].

[159] Alejandro Ibarra and Sebastian Wild. "Determination of the Cosmic Antideuteron Flux in a Monte Carlo approach". *Phys.Rev.* D88 (2013), 023014. DOI: 10.1103/PhysRevD.88.023014. arXiv: 1301.3820 [astro-ph.HE].

[160] Howard Baer and Stefano Profumo. "Low energy antideuterons: shedding light on dark matter". *JCAP* 0512 (2005), 008. DOI: 10.1088/1475-7516/2005/12/008. arXiv: astro-ph/0510722 [astro-ph].

[161] Adam Alloul et al. "FeynRules 2.0 - A complete toolbox for tree-level phenomenology". *Comput.Phys.Commun.* 185 (2014), 2250–2300. DOI: 10.1016/j.cpc.2014.04.012. arXiv: 1310.1921 [hep-ph].

[162] Neil D. Christensen et al. "Simulating spin-$\frac{3}{2}$ particles at colliders". *Eur.Phys.J.* C73.10 (2013), 2580. DOI: 10.1140/epjc/s10052-013-2580-x. arXiv: 1308.1668 [hep-ph].

[163] Benjamin Fuks. "Beyond the Minimal Supersymmetric Standard Model: from theory to phenomenology". *Int.J.Mod.Phys.* A27 (2012), 1230007. DOI: 10.1142/S0217751X12300074. arXiv: 1202.4769 [hep-ph].

[164] Johan Alwall et al. "MadGraph 5 : Going Beyond". *JHEP* 1106 (2011), 128. DOI: 10.1007/JHEP06(2011)128. arXiv: 1106.0522 [hep-ph].

[165] Torbjorn Sjostrand, Stephen Mrenna, and Peter Z. Skands. "A Brief Introduction to PYTHIA 8.1". *Comput.Phys.Commun.* 178 (2008), 852–867. DOI: 10.1016/j.cpc.2008.01.036. arXiv: 0710.3820 [hep-ph].

[166] S. Schael et al. "Deuteron and anti-deuteron production in e+ e- collisions at the Z resonance". *Phys.Lett.* B639 (2006), 192–201. DOI: 10.1016/j.physletb.2006.06.043. arXiv: hep-ex/0604023 [hep-ex].

[167] L.J. Gleeson and W.I. Axford. "Solar Modulation of Galactic Cosmic Rays". *Astrophys.J.* 154 (1968), 1011. DOI: 10.1086/149822.

[168] L.A. Dal and M. Kachelriess. "Antideuterons from dark matter annihilations and hadronization model dependence". *Phys.Rev.* D86 (2012), 103536. DOI: 10.1103/PhysRevD.86.103536. arXiv: 1207.4560 [hep-ph].

[169] Alejandro Ibarra, David Tran, and Christoph Weniger. "Indirect Searches for Decaying Dark Matter". *Int.J.Mod.Phys.* A28 (2013), 1330040. DOI: 10.1142/S0217751X13300408. arXiv: 1307.6434 [hep-ph].

[170] Hideyuki Fuke et al. "Search for cosmic-ray antideuterons". *Phys.Rev.Lett.* 95 (2005), 081101. DOI: 10.1103/PhysRevLett.95.081101. arXiv: astro-ph/0504361 [astro-ph].

[171] Georges Aad et al. "Search for direct third-generation squark pair production in final states with missing transverse momentum and two b-jets in $\sqrt{s} = 8$ TeV pp collisions with the ATLAS detector". *JHEP* 1310 (2013), 189. DOI: 10.1007/JHEP10(2013)189. arXiv: 1308.2631 [hep-ex].

[172] Serguei Chatrchyan et al. "Search for supersymmetry in hadronic final states with missing transverse energy using the variables α_T and b-quark multiplicity in pp collisions at $\sqrt{s} = 8$ TeV". *Eur.Phys.J.* C73.9 (2013), 2568. DOI: 10.1140/epjc/s10052-013-2568-6. arXiv: 1303.2985 [hep-ex].

[173] Kurt Barry, Peter W. Graham, and Surjeet Rajendran. "Displaced vertices from R -parity violation and baryogenesis". *Phys.Rev.* D89.5 (2014), 054003. DOI: 10.1103/PhysRevD.89.054003. arXiv: 1310.3853 [hep-ph].

[174] Gordan Krnjaic and Yuhsin Tsai. "Soft RPV Through the Baryon Portal". *JHEP* 1403 (2014), 104. DOI: 10.1007/JHEP03(2014)104. arXiv: 1304.7004 [hep-ph].

[175] Ian Affleck and Michael Dine. "A New Mechanism for Baryogenesis". *Nucl.Phys.* B249 (1985), 361. DOI: 10.1016/0550-3213(85)90021-5.

[176] Savas Dimopoulos and Lawrence J. Hall. "Baryogenesis at the MeV Era". *Phys.Lett.* B196 (1987), 135. DOI: 10.1016/0370-2693(87)90593-4.

[177] Yanou Cui and Raman Sundrum. "Baryogenesis for weakly interacting massive particles". *Phys.Rev.* D87.11 (2013), 116013. DOI: 10.1103/PhysRevD.87.116013. arXiv: 1212.2973 [hep-ph].

[178] Kiwoon Choi, Eung Jin Chun, and Jae Sik Lee. "Proton decay with a light gravitino or axino". *Phys.Rev.* D55 (1997), 3924–3926. DOI: 10.1103/PhysRevD.55.3924. arXiv: hep-ph/9611285 [hep-ph].

[179] Kiwoon Choi, Kyuwan Hwang, and Jae Sik Lee. "Constraints on R-parity and B violating couplings in gauge mediated supersymmetry breaking models". *Phys.Lett.* B428 (1998), 129–135. DOI: 10.1016/S0370-2693(98)00371-2. arXiv: hep-ph/9802323 [hep-ph].

[180] Eric Carlson, Jonathan Cornell, and Angelo Monteux. *In preparation.*

[181] Michael Savastio. "Cosmological Constraints on MFV SUSY". *JHEP* 1407 (2014), 025. DOI: 10.1007/JHEP07(2014)025. arXiv: 1404.3710 [hep-ph].